UNIVERSITY OF Southampton

University of Southampton Research Repository
ePrints Soton

Copyright © and Moral Rights for this thesis are retained by the author and/or other copyright owners. A copy can be downloaded for personal non-commercial research or study, without prior permission or charge. This thesis cannot be reproduced or quoted extensively from without first obtaining permission in writing from the copyright holder/s. The content must not be changed in any way or sold commercially in any format or medium without the formal permission of the copyright holders.

When referring to this work, full bibliographic details including the author, title, awarding institution and date of the thesis must be given e.g.

AUTHOR (year of submission) "Full thesis title", University of Southampton, name of the University School or Department, PhD Thesis, pagination

http://eprints.soton.ac.uk

UNIVERSITY OF SOUTHAMPTON

FACULTY OF PHYSICAL SCIENCES AND ENGINEERING

Droplet microfluidics for biomolecule separation and detection

by

Yan Zhao

Thesis for the degree of Doctor of Philosophy

April 2015

UNIVERSITY OF SOUTHAMPTON

ABSTRACT

FACULTY OF PHYSICAL SCIENCES AND ENGINEERING

Thesis for the degree of Doctor of Philosophy

Droplet microfluidics for biomolecule separation and detection

By Yan Zhao

Droplet microfluidics is a new approach for chemical and biological analysis. Discrete nano-litre droplets ensure chemical reactions occur quickly without cross-talk, allowing samples to be processed without dispersion. Droplet microfluidics is effectively a digital sample processing platform enabling sample droplets to be handled in a continuous serial format.

This thesis describes a method for *in situ* compartmentalization of biological and chemical samples after separation using Slipchip technology. Isoelectric focusing (IEF) was used to separate biomolecules within the Slipchip. The device was used to compartmentalise the IEF separated samples into micro-droplets. This approach solves the compartmentalization challenge faced by current IEF systems. The digitised sample droplets can be collected serially or in parallel. In serial collection, droplets are collected in tubing that maintains their spatial sequence. For parallel collection, droplets are collected with a multi-pipette. Separated samples were assayed by gel electrophoresis on an Agilent Bioanalyzer. Separated samples were also post-processed on-chip by mixing with pH indicator droplets for calibration of droplet pH. Such continuous-flow/micro-droplet conversion methods have the potential of hyphenating different separation techniques for performing advanced analysis of complex samples.

One disadvantage with droplet microfluidics is the very small dimensions of the sample meaning that classical absorption assays are difficult. Therefore, a high sensitivity absorption-based optical method called Cavity Ring Down Spectroscopy (CRDS) was developed and evaluated. The integration of CRDS with microfluidic devices was explored. Microfabricated cylindrical lenses were used to increase the light coupling efficiency within a chip, but results showed that light losses in the system were too high to enable the effective use of CRDS for analysis.

Contents

List of Figures

List of Tables

DECLARATION OF AUTHORSHIP

I, Yan Zhao declare that the thesis entitled *Droplet microfluidics for biomolecule separation and detection* and the work presented in the thesis are both my own, and have been generated by me as the result of my own original research. I confirm that:

- this work was done wholly or mainly while in candidature for a research degree at this University;
- where any part of this thesis has previously been submitted for a degree or any other qualification at this University or any other institution, this has been clearly stated;
- where I have consulted the published work of others, this is always clearly attributed;
- where I have quoted from the work of others, the source is always given. With the exception of such quotations, this thesis is entirely my own work;
- I have acknowledged all main sources of help;
- where the thesis is based on work done by myself jointly with others, I have made clear exactly what was done by others and what I have contributed myself;
- parts of this work have been published as:

1. **Real-time microfluidic recombinase polymerase amplification for the toxin B gene of *Clostridium difficile* on a SlipChip platform,** M.-N. Tsaloglou, R. J. Watson, C. M. Rushworth, Y. Zhao, X. Niu, J. M. Sutton and H. Morgan, 2015, *Analyst*, 140, 258-264.
2. **Droplet-based *in situ* compartmentalization of chemically separated components after isoelectric focusing in a Slipchip**, Yan Zhao, Fiona Pereira, Andrew J. deMello, Hywel Morgan and Xize Niu, 2014, *Lab Chip*, 14, 555-561.
3. **Sensitive analysis of trace water analytes using colourimetric cavity ringdown spectroscopy**, Cathy M. Rushworth, Yathukulan Yogarajah, Yan Zhao, Hywel Morgan and Claire Vallance, 2013, *Anal. Methods*, 5, 239-247.
4. **Droplet-based compartmentalization after isoelectric focusing in a Slipchip**, Yan Zhao, Fiona Pereira, Andrew J. deMello, Hywel Morgan and Xize Niu, 2013, *in proc. The 17th International Conference on Miniaturized Systems for Chemistry and Life Sciences, Freiburg, Germany.*

Signed: ……..

Date:…….

Acknowledgements

First and foremost, I would like to express my highest appreciation to my supervisors, Prof. Hywel Morgan, Dr. Xize Niu, and Dr. Matt Mowlem for their support and guidance throughout this project. Thanks Prof. Hywel Morgan for providing me this opportunity and studentship to do PhD research, he guided me into microfluidic field. His broad horizon and experiences greatly extended my view in both science and engineering, which I have been and will be further benefitted in my career. Dr. Xize Niu taught me how to how to write a scientific paper and how to plan a research project; his day-to-day supervision greatly accelerated my project and I will never finished this PhD work without his hard work. Dr. Matt Mowlem provided many helpful suggestions on microfluidic work. Prof. Hywel Morgan and Dr. Xize Niu helped to improve the writing of this thesis, on both science and English language, I do highly appreciate for their help, and I learned a lot from this.

In this thesis, part of the Slipchip work were collaborated with Dr. Fiona Pereira and Prof. Andrew deMello in ETH Zuich, and part of cavity ring down analysis work were processed by Cathy Rushworth and Dr. Claire Vallance at University of Oxford, I would like to give thanks to them for collaborating.

I would like to thank all the members in Hywel's group and Xize's group, both past and present. Particularly, I would like to thank Sam Hassan and Yu Zhang in Xize's group for helping with isoelectric focusing work and micro milling fabrication. A special mention also goes to Katie Chamberlain, Maria-Nefeli Tsaloglou, Marie Held, Jonathan West, Sumit Kalsi, Daniel Spencer, Mark Friddin, Chunxiao Hu, Shilong Lu and Xiaojun Han, the knowledge and experiences they shared are very helpful for my PhD project.

I would like to thank Prof. James Wilkinson for discussing and suggesting on the optical work. And finally, I would like to express my love and thanks to my family and friends, they are always being supportive throughout my career.

List of Symbols

α	Light absorption coefficient
ρ	Fluid mass density
η	Dynamic viscosity
σ	Surface tension
P_{e}	Péclet number
p	Pressure
R_e	Reynolds number
S_c	Schmidt number
κ	Interface curvature
u	Flow velocity

List of Abbreviations

AFM	Atomic force microscope
CAs	Carrier ampholytes
CE	Capillary electrophoresis
COC	Cyclic Olefin Copolymer
COP	Cyclic Olefin Polymer
CRDS	Cavity Ring Down Spectroscopy
DAPI	4',6-diamidino-2-phenylindole
DEP	Dielectrophoresis
EHD	Electrohydrodynamic
EOF	Electroosmotic flow
EWOD	Electrowetting on dielectric
IEF	Isoelectric focusing
IPG	Immobilized pH gradient
ITO	Indium tin oxide
ITP	Isotachophoresis
LC	Liquid chromatography
LoC	Lab on a chip
LOD	Limit of detection
MEMS	Microelectromechanical
MS	Mass spectrometry
PDMS	Polydimethylsiloxane
PMMA	Polymethylmethacrylate
PTFE	Polytetrafluoroethylene
RIE	Reactive ion etch
RSD	Relative standard deviation
μTAS	Micro Total Analysis System

Chapter 1

Introduction and motivation

1.1 Introduction

Microfluidics refers to devices for controlling fluid with length scale less than a millimeter (Stone *et al.*, 2004), typically it is capable of manipulating and processing fluid with volume from micro-liters down to pico-liters using channels with dimensions from ten micrometre to hundreds of micrometres (Whitesides, 2006). The integration of microfluidic systems with other components is the basis of the Lab on a Chip (LoC), also called "Micro Total Analysis System (μTAS)". One or more lab functions are performed in a miniaturised platform, including sample preparation, sample injection, fluid and particle handling, mixing and reaction, separation and detection, etc.

Microfluidics has its origin in the microelectromechanical (MEMS) research area, and benefited from the early development of microelectronic technologies. Capillary electrophoresis (CE) was among the first microfluidic devices. In the early 1990s, Harrison and co-workers reported doing CE on glass chips with micro-channels, which integrated sample injection and CE in one device through a cross structure, and demonstrated bio-sample separation and fluorescent analysis (Harrison *et al.*, 1993, Seiler *et al.*, 1993, Harrison *et al.*, 1992); such papers are considered as the earliest demonstration of performing CE separation in a miniaturized device. And in 1999, Hofmann *et al*. demonstrated Capillary Isoelectric Focusing (cIEF) on a glass microfluidic chip (Hofmann *et al.*, 1999), Microfluidics has since rapidly expanded into a fully-fledged research field. Nowadays, the LoC has become a popular and powerful analytically tool in research labs, and is also penetrating the commercial market; the Agilent 2100 Bioanalyzer is an example of such success.

In the early years of microfluidic development, continuous microfluidics, the first generation of microfluidics, was intensively studied. "Micro-plumbing" - how to pump, regulate and mix

microflows in channels spurned the research interests of talented scientists and engineers, leading to the invention of and various micro-pumps, valves, mixers etc (Unger *et al.*, 2000, Stroock *et al.*, 2002). The fundamentals of microfluidics have also been extensively studied, such as mass and thermal dispersion and convection, electroosmotic flow (EOF), dielectrophoresis (DEP) etc. (Squires and Quake, 2005), along with studies on surface chemistry and material properties (McDonald *et al.*, 2000). Various detection techniques have been developed or borrowed from other fields, including optical methods like bright field microscopy, fluorescence microscopy, absorption spectroscopy, confocal microscopy and Raman spectroscopy (Zhu and Fang, 2013); and electrical methods, such as impedance analysis and sorting of single-cell in microfluidic systems developed by Morgan's group (Sun and Morgan, 2010).

1.2 Droplet microfluidics

Continuous flow microfluidics is a single phase system. As shown in Figure 1-1(A), the sample (a) and (b) are moving in the channel, the two samples will mix together, which causes sample cross-contamination (Solvas and deMello, 2011). The sample molecules will also stick to the channel wall, which contaminates rare samples and causes errors in analysis. Droplet microfluidics, which is also called digital microfluidics, is concerned with processing discrete droplets or compartments of liquids (aqueous droplet in oil, or oil droplet in water) independently, By digitizing the sample into droplets separated by an immiscible phase, the information in the continuous flow can be easily secured into compartments (Figure 1-1B), eliminating cross-talk between droplets. In droplet microfluidics, the sample is in discrete format, each droplet is an individual reaction chamber.

Droplet microfluidics can also digitise samples from a continuous stream whilst keep the original spatial or temporal chemical information. For example, the eluents from separation technology such as HPLC or electrophoresis can be compartmentalised into droplets as demonstrated by Niu and co-workers (Niu *et al.*, 2009, Pereira *et al.*, 2013). Another advantage of droplet microfluidics is the volume of the droplets can be extremely small, therefore mixing and thermal dispersion/exchange are extremely fast. Droplets can be produced in a high-throughput manner (thousands per second) with a simple fluidic chip (Guo *et al.*, 2012). Droplet microfluidics has

grown into the 2nd generation microfluidics over the last ten years (Teh *et al.*, 2008, Niu and deMello, 2012).

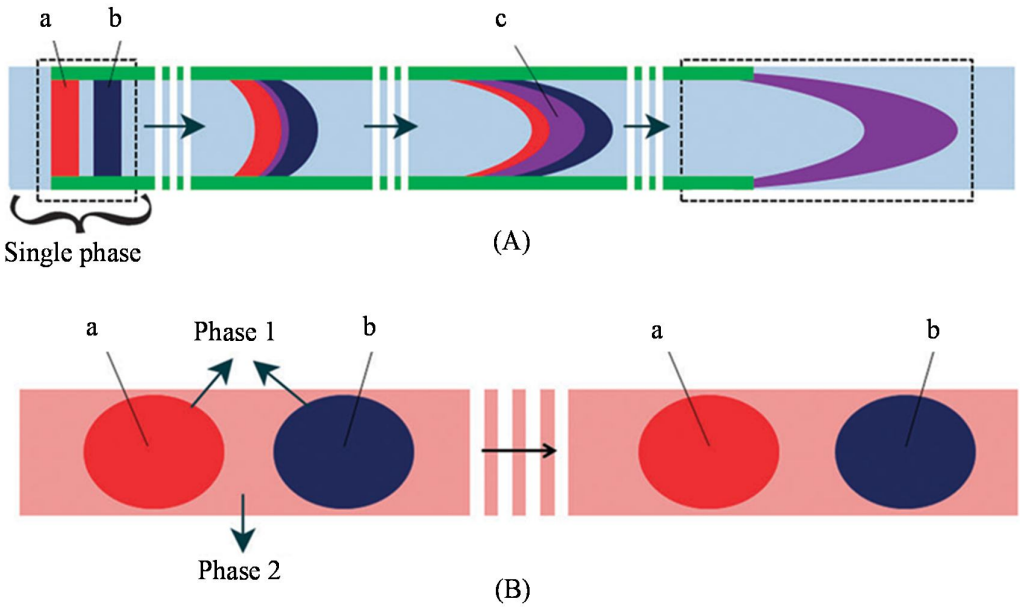

Figure 1-1: (A) In continuous flow, the fluid in the channel is single phase. Part a and b of the fluid is dispersed in the flow and forms c because of Taylor dispersion. (B) In droplet microfluidics, immisible phases compartmentalize samples into droplets, part a and b are in two separate droplets, and dispersion is prevented. From (Solvas and deMello, 2011).

1.3 The aims of the thesis and its structure

While there have been significant developments in both continuous and droplet microfluidics over the past years, and it is undergoing a revolution in which droplet microfluidics has evolved from continuous microfluidics and is now a rapidly developing field in its own right. But there has been very little progress in developing the interface between the two generations of microfluidics, equivalent continuous-flow/micro-droplet converters are less studied. Probably the one exception is the generation of droplets from continuous microflows using T-junctions or flow focusing channels (Garstecki *et al.*, 2006, Hashimoto *et al.*, 2008). Simple microdroplet to continuous

fluidic converters, have been developed by Niu *et.al.* (Niu *et al.*, 2013) and Kennedy's group (Pei *et al.*, 2010), who showed fusion of droplets into continuous flow followed by electrophoretic separation for proteomics or *in vivo* chemical monitoring. However, these approaches are very limited and cannot be multiplexed or up-scaled since they are incompatible with parallel processing and droplet-on-demand functions. Using continuous-flow/micro-droplet converting system we will be able to continuously sample fluids with changing chemistry, e.g. the sample from human body or environment, with discrete droplets at high spatial and temporal resolution. Another example is a converter for sending discrete droplets into a classical continuous flow analytical system such as electrophoresis, chromatography, mass spectrometry, or cell culture environment. In principle, connecting several converters in series will enable multiple steps of continuous-flow/micro-droplet and micro-droplet/continuous-flow conversion operations.

This thesis describes the first attempt at building such missing links and reports progress towards a microfluidic continuous-flow/micro-droplet convertor. In particular it describes the implementation of Isoelectric Focusing (IEF) for separation of biomolecules and the discretisation of a continuous environment into droplets using a Slipchip. A sensitive optical detection method called Cavity Ring Down Spectroscopy (CRDS) is also described and used for the analysis of colorimetric reactions such as the Griess reaction to measure nitrite.

This thesis is structured as follows. Chapter 2 reviews the development of both continuous and droplet microfluidics. A new droplet generation format called the Slipchip is also reviewed. This device forms the basis of one of the key technologies developed in the thesis. Microfluidic separation methods are also introduced, along with reviews on CRDS detection methods. A summary of various fabrication technologies is also given, especially how to manufacture polymers microfluidic devices. Chapter 3 presents a new Slipchip design, a rapid prototyping method and a universal droplet operation platform. Chapter 4 proposes a Slipchip device for IEF separation of proteins, demonstrating the first application of Slipchip for compartmentalization after chemical separation. It solves the problem faced in hyphenation of IEF platforms with other analytical methods, which is a big challenge in developing efficient miniaturized IEF systems. Chapter 5 investigates microfluidic-optical interface to coupling CRDS system with droplet microfluidic devices. Chapter 6 concludes the thesis and provides suggestions for future work.

Chapter 2

Literature Review

2.1 Chapter Overview

This chapter reviews the state-of-the-art in both continuous and droplet microfluidics, and presents the challenges currently faced in the field. In continuous microfluidics, the science and technologies of molecular separation are reviewed. This has always been areas of intensive research interests, with applications from genomics (such as DNA sequencing) to proteomics, diagnostics and drug development. The exciting technologies of droplet microfluidics, developed over the past few years are reviewed, for example, droplet generation, manipulation and analysis.

2.2 Theory and fluid manipulations

2.2.1 Fluid manipulation in continuous microfluidics

In Newtonian fluids (viscosity not related to external stress placed upon it), the motion of a fluid is described by the Navier-Stokes equation:

$$\rho\left(\frac{\partial u}{\partial t} + u \cdot \nabla u\right) = -\nabla p + \eta \nabla^2 u + f \tag{2.1}$$

where u is the flow velocity, ρ is fluid density, p is the pressure, and η is the dynamic viscosity; f is body forces on fluid, such as centrifugal forces, gravity (can be ignored in microfluidics), electrostatic forces etc. According to the continuity equation:

$$\frac{\partial \rho}{\partial t} + \nabla(\rho \cdot u) = 0 \tag{2.2}$$

considering an incompressible fluid with nearly constant density, such as water, ∇u is zero, thus the equation (2.1) can be simplified to:

$$\rho \frac{\partial u}{\partial t} = -\nabla p + \eta \nabla^2 u + f \tag{2.3}$$

Following Navier-Stokes equation, external pressure is generally used to pump fluids in microfluidics, the flow rate relates to the pressure difference between input and output ends, and flow resistance, liquid viscosity etc.. Commercial pumps are available to provide external pressure, like syringe pump, peristaltic pump, pressure pump etc., miniaturized on-chip pumps have also been investigated. Quake and co-workers in California Institute of Technology proposed a miniaturized peristaltic pump formed of three elastomeric micro-valves (Unger *et al.*, 2000) (Figure 2-1). By controlling the open/close status of these valves, fluid can be sucked in and squeezed out of the valves, causing pumping. Thorsen *et al.* presented a large scale integrated microfluidic device using elastomeric micro-valves (Thorsen *et al.*, 2002). Terray *et al.* demonstrated a valve and pump by manipulating 1.5μm diameter colloidal silica spherical particles in channel, controlled by optical trapping (Terray *et al.*, 2002).

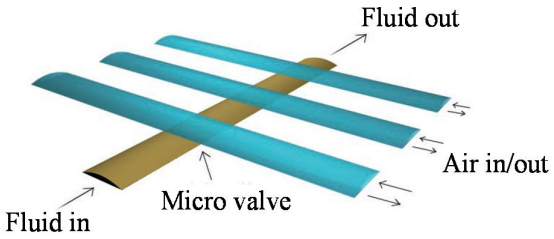

Figure 2-1: A schematic diagram of a peristaltic pump. By controlling the open/close status of the three micro-valves, the fluid in the channel can be pumped. From (Unger *et al.*, 2000).

In the early age of microfluidics, electroosmotic flow (EOF) was intensively studied to pump the fluid (Gaudioso and Craighead, 2002, Kirby and Hasselbrink, 2004, Beattie, 2006). As shown in Figure 2-2A (Tandon *et al.*, 2008), when a microfluidic channel is filled with electrolyte, the channel wall (silica or polymers) will be negatively ionized, the positively charged ions in the electrolyte will move towards the channel wall and an electrical double layer (EDL), which is

also called the Debye layer, is formed at the interface. Figure 2-2A also shows the distribution of electrical potential of EDL (called zeta potential), which is strongest at the interface. The λ_D refers to the Debye length, which is the thickness of the EDL as to the equation (2.4),

$$\lambda_D = \sqrt{\frac{\varepsilon k_B T}{2e^2(\Gamma/2)}} \tag{2.4}$$

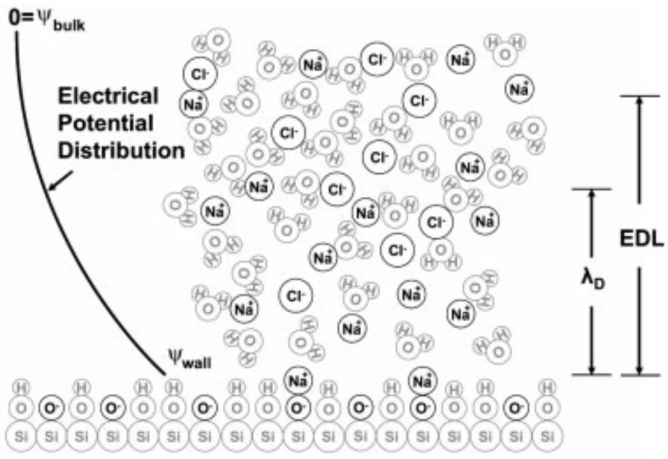

(A)

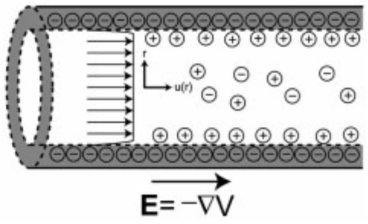

(B)

Figure 2-2: (A) Schematic of electrical double layer and electrical potential distribution. When a microfluidic channel is filled with electrolyte, the channel wall (silica or polymers) will be negatively ionized, it tends to attract positively charged ions in the electrolyte to form an ionic double layer at the solid-liquid interface, which is also called Debye layer. Such electrical potential is strongest at the interface. (B) In a microfluidic channel, when applied electric field, the positively charged mobile ions will move toward cathodic side. From (Tandon *et al.*, 2008).

where ε is electrical permittivity of the medium, k_B is Boltzmann's constant, T is the temperature in K, e is the elementary charge, and $\Gamma/2$ is the bulk ionic strength of the solution; for water at room temperature, $\lambda_D \approx 0.7$nm.

So there will be positively charged ions assembled in the solution very close to the channel wall, the thickness depends on the Debye length. When an electric field is applied to the electrolyte, the positively charged mobile ions in the solution will move toward cathodic side (Figure 2-2B). In EOF, the driven force is applied on the mobile ions close to the channel wall, the movement of fluid in the channel center is due to friction, so in an open micro-channel this movement carries the bulk flow with a flat flow profile (Manz *et al.*, 1994, Stroock *et al.*, 2000, Ghosal, 2004). But EOF pumping needs high voltage to drive the mobile ions and it is material and chemical dependent (Kirby and Hasselbrink, 2004, Tandon *et al.*, 2008).

Besides EOF and pressure pumping, centrifugal microfluidics using a CD motor to drive flows with centrifugal forces. This is a pump-free method, see (Gorkin *et al.*, 2010) for a detailed review. Table 2-1 lists the advantages and disadvantages of these fluidic driving methods.

Table 2-1: Advantages and disadvantages list of fluidic driving methods.

Fluidic driving method	Advantage	Disadvantage
Electro Osmotic Flow	Flat velocity profile avoids Taylor dispersion	High voltage required; fluidic velocity depends on channel surface properties and physicochemical properties of the fluid.
External pumping	Reliable; inexpensive	Difficult to be miniaturized.
On chip pumping	Device is miniaturized.	Supporting system is complex
Centrifugal microfluidics	Inexpensive; system is simple and can be miniaturized.	Limited geometry and available space

From equation (2.3), the flow velocity, *u*, can be analytically or numerically solved by applying appropriate boundary conditions, see (Squires and Quake, 2005). Although the solutions can vary

according to different fluidic systems, some important constants describe common features of a microfluidic system. The Reynolds number (R_e) is one of the most widely used dimensionless numbers in microfluidics, and is the ratio of inertial force f_i (from Newton's second law and representing the kinetic energy of the fluid) to viscous force f_v (energy dissipated by friction).

$$R_e \equiv \frac{f_i}{f_v} = \frac{\rho u L}{\eta} \tag{2.5}$$

where L is the characteristic linear dimension of the fluidic conduit, for example the diameter of a circular channel, or the channel width in rectangular channel.

When *Re* is lower than 1000 the flow is laminar, the viscous force in (2.5) is dominant, When *Re* is higher than 4000, it is turbulent flow, in which case the flow is unpredictable. Generally turbulent flow happens at high flow rates and in channel with large dimensions. When *Re* is between 1000 and 4000, the flow is in transitional, which means a mixture of turbulent and laminar flow.

In microfluidics, the channel dimension is small that the *Re* is generally very low and often less than 1, it is strictly a laminar flow. So when two (or more) streams meet at a junction, they will co-flow in parallel with a clear interface and mixing only occurs by molecular diffusions, in the absence of other perturbations.

The Péclet number (P_e) is a dimensionless number describes the relative importance of convection to diffusion.

$$P_e \equiv \frac{uL}{D} = R_e \cdot \frac{\eta}{D \cdot \rho} \tag{2.6}$$

where D is the mass diffusivity of the content and $\eta/D\rho$ is known as Schmidt number (S_c) (Choban *et al.*, 2004, Squires and Quake, 2005).

To speed up mixing, Stroock *et al.* proposed a staggered herringbone mixer to create chaotic advection in micro-channel (Stroock *et al.*, 2002) (Figure 2-3A); Kim and co-workers split and recombined the fluid (Kim *et al.*, 2005, Lee *et al.*, 2006b) to fold the fluid and accelerate the mixing, such as the "F" shape structures shown in Figure 2-3B. Comprehensive reviews of microfluidic mixer can be seen in (Nguyen and Wu, 2005, Lee *et al.*, 2011).

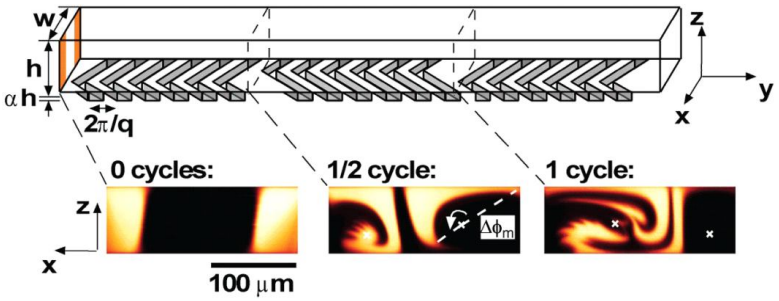

(A)

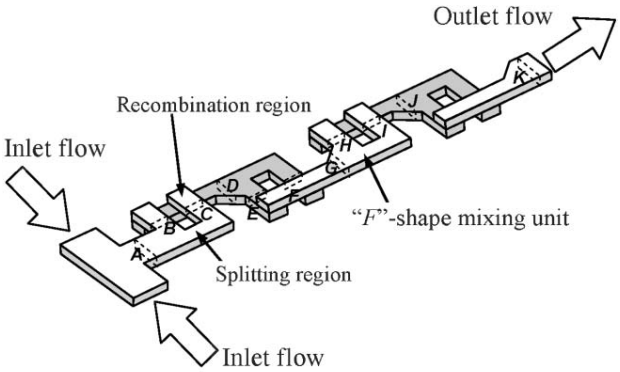

(B)

Figure 2-3: (A) Staggered herringbone mixer proposed by Stroock *et al.*, which creates chaotic advection in micro-channel to accelerate mixing (Stroock *et al.*, 2002). (B) F shape to splitting and recombining fluid (Kim *et al.*, 2005). 2.2.2 Droplet generation and manipulation

In Droplet microfluidics, the generation and manipulation of micro droplet is the basic technology and has been widely studied. Generally, there are two methods to control the droplets, passive method and active method.

In passive method, droplets are generated and controlled by the channel geometry, and by controlling the pumps and valves. T-junction (Xu *et al.*, 2006, Nisisako *et al.*, 2002) and flow-focusing (Anna *et al.*, 2003, Takeuchi *et al.*, 2005)(Yobas *et al.*, 2006) are two main passive droplet generating structures. In T-junction (Figure 2-4A) (Thorsen *et al.*, 2001), the aqueous sample is sheared by the oil to form droplets. The droplet size can be controlled by the geometry

of the micro-channel, and the flow rate of both phases. In flow-focusing structure (Figure 2-4B) (Anna *et al.*, 2003), the oil flow comes around the aqueous sample, focuses and squeezes the aqueous flow to form droplets. The physical fundamental of these two structures has also been systematically studied (Garstecki *et al.*, 2006, Hashimoto *et al.*, 2008, Wehking *et al.*, 2014, Xu *et al.*, 2005,Dupin *et al.*, 2006) .

Double emulsions such as water-in-oil-in-water or oil-in-water-in-oil droplets can also be generated, as presented by Weitz's group (Utada *et al.*, 2005, Abate and Weitz, 2009). The system can be further adapted to produce multiple-emulsions, as shown in Figure 2-5, or to trap and pair small droplets in a large emulsion (Okushima *et al.*, 2004, Nisisako *et al.*, 2005, Abate *et al.*, 2011), which is useful for applications like particle synthesis (Dendukuri and Doyle, 2009).

Other than passive methods, Electrohydrodynamic (EHD) methods such as Dielectrophoresis (DEP) (Ahmed and Jones, 2006, Jones, 2001, Jones *et al.*, 2001)or Electrowetting-on-Dielectric (EWOD) (Lee *et al.*, 2002, Zeng and Korsmeyer, 2004) are used for droplet generation.

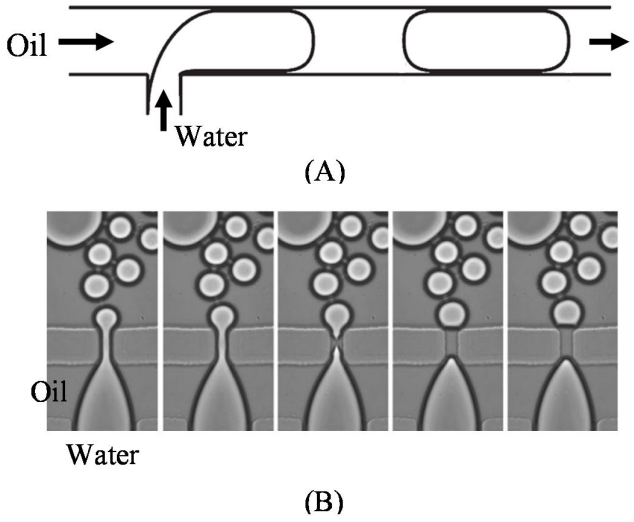

Figure 2-4: Two passive droplet generation structures. (A) T-junction droplet generation strategy (Garstecki *et al.*, 2006), oil phase shears the water flow into droplets. (B) flow-focusing droplet generation strategy (Anna *et al.*, 2003).

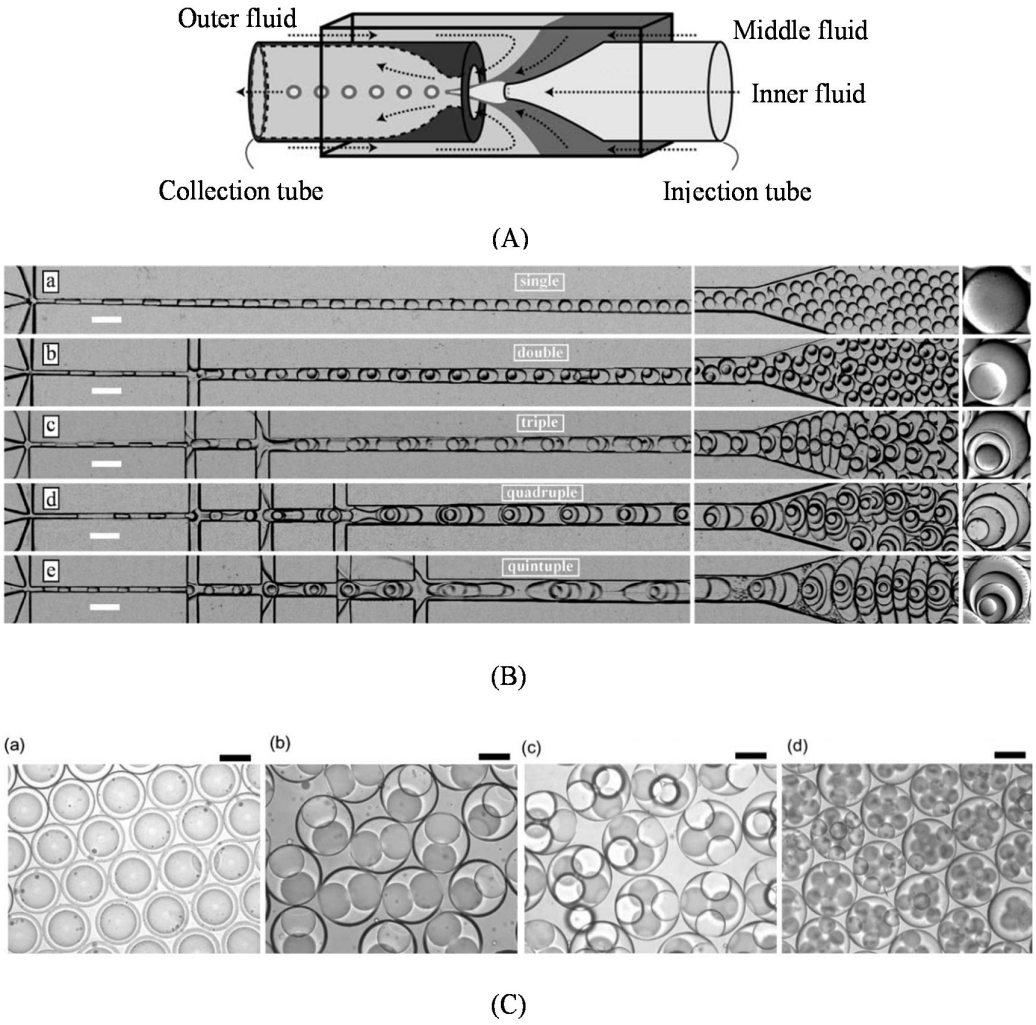

Figure 2-5: Multiple emulsion generation. Multiple emulsion can be generated (A) with capillary (Utada *et al*., 2005) and (B) multi-step cross flowing structure (Abate and Weitz, 2009); (C) Trapping and pairing small droplets containing different species in a large emulsion. (Nisisako *et al.*, 2005).

DEP generates droplets by pulling the liquid from a reservoir. It is based on the fact that a polarizable liquid is attracted to a higher electric field intensity (Jung and Kwak, 2007, Chiu *et al.*, 2007). So in DEP, the dispersed liquid phase should have a higher dielectric permittivity than the carrier phase fluid.

EWOD is based on the phenomenon that the interfacial energy between a fluid and the contacted surface can be changed with an electric field. In the EWOD device shown in Figure 2-6A, at the three-phase interface, the liquid contact angle is given by the Lippmann-Young equation (Lee *et al.*, 2002):

$$cos\theta = cos\theta_0 + \frac{1}{2\gamma_{LG}} cV^2 \tag{2.7}$$

where θ is the contact angle, θ_0 is the contact angle with no electric field; γ_{LG} is liquid-gas interfacial tension, C is the capacitance per unit area, which is related to the dielectric constant and thickness of the dielectric material; V is the electric field applied across the interface. For an EWOD device formed from an electrode made of metal or Indium tin oxide (ITO), a dielectric layer is required (such as SiO_2, Si_3N_4) together with a hydrophobic coating layer (e.g. Teflon AF, CYTOP) to give a high starting contact angle θ_0.

EWOD device is capable of addressing individual droplet and realising droplet-on-demand operations. As shown in Figure 2-6B (Cho *et al.*, 2003), droplets can be pulled from solution reservoirs, moved, split and merged with electrode arrays. Figure 2-6C shows a large scale integrated EWOD device for programmable droplet control (Hadwen *et al.*, 2012), by programming the electric field strength on individual electrodes in the array, fine droplet movement is possible. The droplet size in an EWOD device is typically sub-millimetre, much bigger than for channel based droplet microfluidics, where droplet are in the micrometre to nanometre scale. This is because the liquid-gas interfacial tension becomes large with reduction in droplet size, the contact angle becomes difficult to change, so that the manipulation of a big droplet is easier than a small one (Cho *et al.*, 2003). Another limit is the electrode fabrication, droplets manipulated by EWOD must be bigger than the dimension of a single electrode; the fabrication of a very small electrode is a challenge.

Other active components such as active valves (Guo *et al.*, 2010, Churski *et al.*, 2010), optical tweezers (Lorenz *et al.*, 2006), pulsed laser (Park *et al.*, 2011) can also be used for droplet-generation-on-demand. Recently, Gielen *et al.* (Gielen *et al.*, 2013) presented a robotic compartment-on-demand system, that can compartmentalize samples from 15 sample slots. This system can provide a programmable droplet sequence with controlled size and distance between droplets.

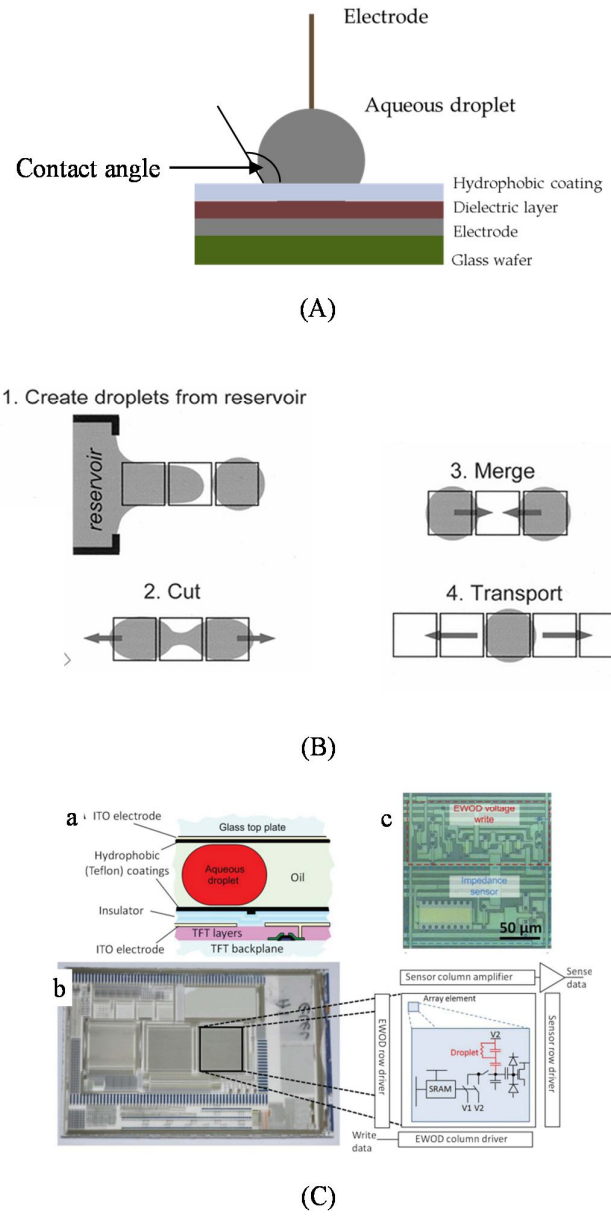

Figure 2-6: Droplet-on-demand with EWOD. (A) A side view of a simple EWOD device; the interfacial tension of the droplet with supporting material is controlled by applying a voltage to the electrodes. The bottom electrode is coated with dielectric material such as SiO_2 or Si_3N_4, and a hydrophobic layer. (B) A schematic of droplet generation, splitting, merging and movement controlled by electrodes (Cho *et al.*, 2003). (C) A programmable large area EWOD electrode-array for droplet manipulations (Hadwen *et al.*, 2012).

Droplets can be manipulated on chip with a variety of functions, such as droplet fission (Adamson *et al.*, 2006), trapping (Huebner *et al.*, 2009), fusion (Mazutis *et al.*, 2009), mixing (Fowler *et al.*, 2002), sorting (Tan *et al.*, 2004, Niu *et al.*, 2007, Xu *et al.*, 2012) and pairing (Frenz *et al.*, 2008). Using these approaches, chemical and biological samples in droplets can be processed and analysed efficiently. Niu *et al.* proposed a droplet dilutor that fuses and mixes buffer droplets within a sample "mother droplet" thus diluting it (Niu *et al.*, 2011) (Figure 2-7A), When the buffer droplet is merged with the mother droplet the output droplet is split from the mother droplet. A series of droplets containing sample with a concentration gradient can be generated, which makes nano-litre titration possible for the first time. Shi *et al.* trapped *C. elegans* worms in droplets (Shi *et al.*, 2008) (Figure 2-7B). By trapping droplets in an array, these worms were detected and analysed in parallel. Theberge *et al.* (Theberge *et al.*, 2010), Guo *et al*. (Guo *et al.*, 2012), Niu *et al*. (Niu and deMello, 2012) provide comprehensive reviews of recent development of droplet microfluidics and their application in chemistry and biology.

2.2.3 Slipchip

The Slipchip is a novel droplet microfluidic platform that can perform parallel droplet operations by slipping (moving) two halves of a chip into different positions. A schematic diagram of the device is shown in Figure 2-8. The device has two un-bonded plates (a top plate and a bottom plate). Ducts and wells are patterned on each plate (Figure 2-8A). By sliding the plates relative to each other, the wells in the top plate can be aligned with the ducts in the bottom plate (Figure 2-8B), and samples can be loaded into the wells (Figure 2-8C and D), or droplets generated in the wells. Such slipping process can be performed many times so that the sample droplets and reagent droplets can be mixed (Figure 2-8E and F).

Unlike bonded microfluidic devices, the channels in each half of the Slipchip are open and the fluidic pathway is controlled by positioning the plates. This makes micro-valves unnecessary. Droplet pairing and reaction also become easier than in conventional droplet microfluidics. The Slipchip device shown in Figure 2-9 is capable for screening a sample against 16 different reagents at 11 mixing ratios (Li *et al.*, 2010b).

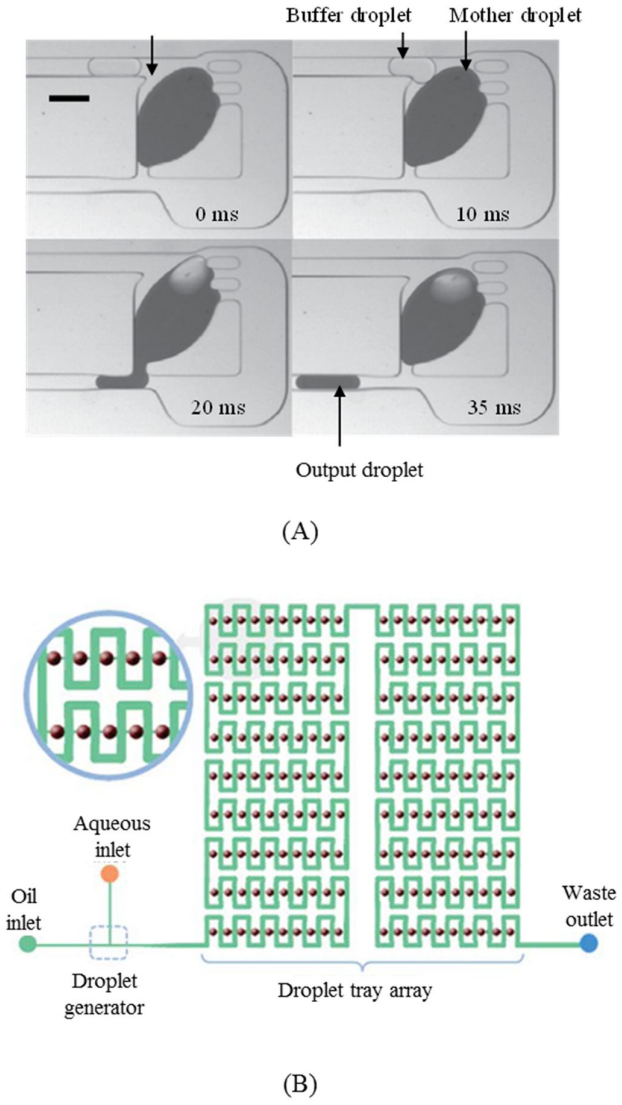

Figure 2-7: Processing of chemical and biological samples in droplet microfluidics. (A) A droplet diluter generates a sequence of droplets with a concentration gradient. The diluting chamber traps a sample droplet that behaves as a "mother droplet". When a buffer droplet approaches (0 ms), contacts (10 ms), and mixes within the mother droplet and dilutes it, an output droplet is generated (35 ms). A series of output droplets with sample concentration decreasing exponentially can be generated and used for screening (Niu *et al.*, 2011). (B) Schematic of a droplet trapping array. Droplets containing *C elegans* worms are generated at the T-junction structure, and trapped in a array for high throughput analysis on chip (Shi *et al.*, 2008).

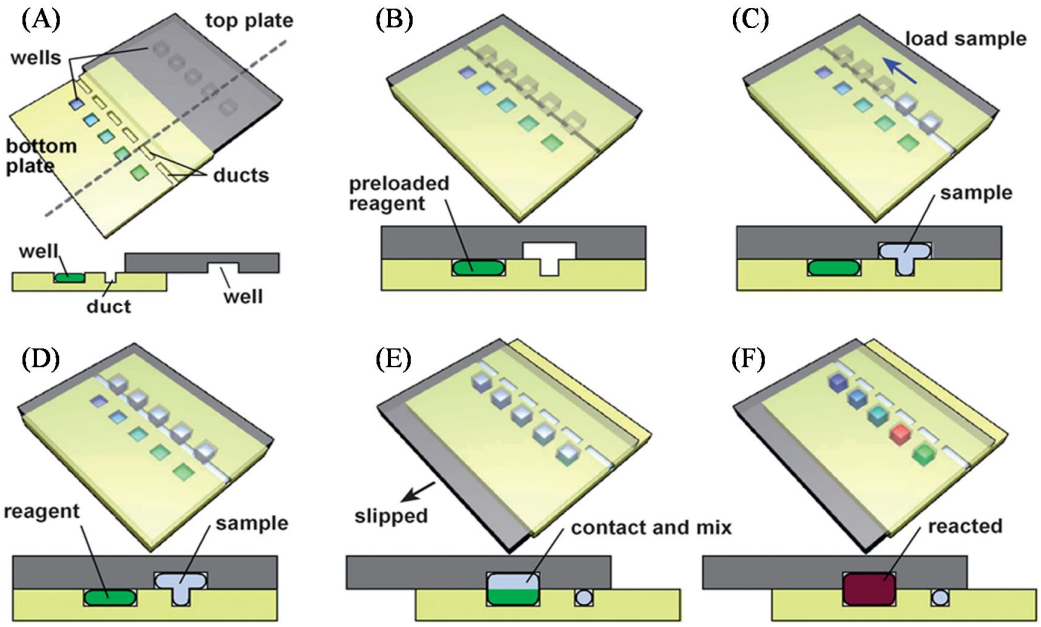

Figure 2-8: Schematic diagram showing the operation of a Slipchip. (A) A Slipchip device has two plates, with ducts and wells patterned in each half. (B) The plates can be slipped so that the ducts and wells are aligned (C) and (D); when the ducts and wells are aligned they form a continuous channel and a sample can be loaded into the wells. (E) After loading, sample droplets can be generated in wells by slipping the device to disconnect the wells and ducts. (F) The sample droplets can be merged and reacted with reagent droplets in another half plate. From (Du *et al.*, 2009).

Another significant advantage of the Slipchip is its ability to perform multi-step processes. Liu *et al.* demonstrated a bead-based heterogeneous immunoassays (Liu *et al.*, 2010). This multi-step process can be easily performed by slipping the chip (Figure 2-10), with 48 sample droplets assayed in parallel. Such a device is simpler than an EWOD immunoassay device (Hadwen *et al.*, 2012). Shen *et al.* demonstrated digital PCR processing 1280 droplets on one chip (Shen *et al.*, 2010). However, the disadvantage of the Slipchip is the half opened channels where oil and/or sample leak out if the seal pressure is not high enough and uniform, or if the surfaces are contaminated (Schneider *et al.*, 2013). One big disadvantage of Slipchip is the sample processing throughput is relatively low compares to conventional microfluidics; and the pressure and flow velocity have to be controlled at relatively low level to prevent leakage. Table 2-2 compares the Slip with conventional microfluidics and EWOD device.

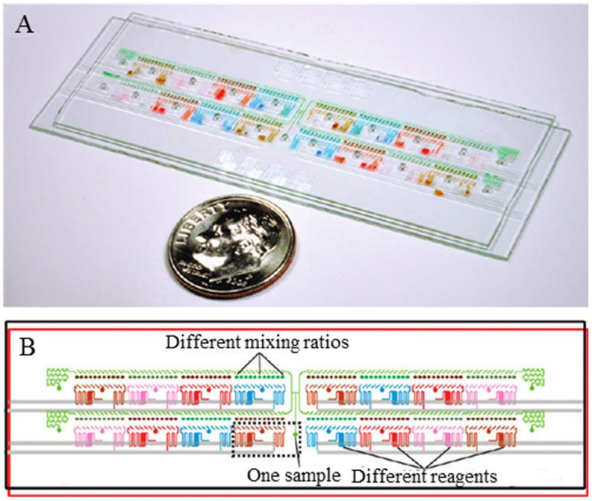

Figure 2-9: A Slipchip device for screening as proposed by Li *et al.* (Li *et al.*, 2010b). One chip is able to screen a sample against 16 different reagents at 11 mixing ratios. There are a total of 176 droplets of ~12nL volume each, and the total sample volume is 3.5μL.

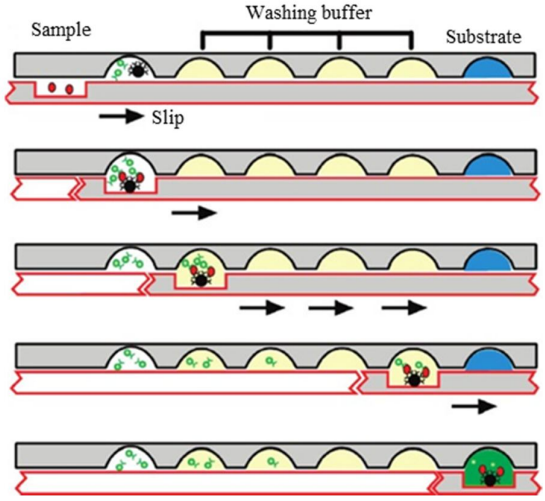

Figure 2-10: Schematics of Slipchip for bead-based heterogeneous immunoassays multi-step process. By slipping the chip, the sample and reagents are mixed and combined with magnetic beads (A). Then the complex is pulled down in the bottom wells by magnets (B). Four-step washing is controlled by magnets and slipping mechanism (C-D), and the washed complex is finally combined with substrate (E).From (Liu *et al.*, 2010).

Table 2-2 Comparison of conventional droplet microfluidics, EWOD and Slipchip.

	Conventional droplet microfluidics	EWOD	Slipchip
Valves or/and pumps to control the droplets	Need	No need	No need
Electronics to control the droplets	Maybe	Need	No need
Flow rate	High	Low	Low
Throughput	High	Very low	Low
Individually address each droplet	Hard	Easy	Easy
Prototype device cost	Medium	high	Low
High volume device cost	Low	High	Low
Multi-step processing	Hard	Easy	Easy

In Table 2-2, some features are compared between conventional droplet microfluidics, EWOD and Slipchip. Slipchip does not need any external valves, pumps or electronics to control the movement of droplets; compares to conventional droplet microfluidics, the flow rate in Slipchip is low; the throughput in Slipchip is lower than conventional microfluidics but higher than EWOD. Slipchip can easily address each single droplet and do multi-step processing, but it is not multi-functional like EWOD, one Slipchip device can only do the functions it is designed for.

2.3 Fabrication techniques

In the early stages, microfluidic devices were made of silicon or glass using semiconductor fabrication technologies. To make these channels, the design is first transferred to a photo-mask, usually a fused silica plate coated with a patterned Chrome layer, and then transferred to photoresist coated onto a silicon or glass substrate by UV exposure, followed by development and

etching. Using this technique, patterns as small as submicron scale can be fabricated (Revell and Goldspink, 1984, Bu *et al.*, 2004). Silicon and glass (SiO_2) are chemically stable and having excellent optical properties, therefore they are still being used in many commercial microfluidic products, such as DNA and Protein chips for the Agilent 2100 Bioanalyzer. However, fabrication of these hard materials is usually expensive, requiring cleanroom facilities, such as spinner for coating photoresist, mask aligner for UV exposure and plasma etcher or wet bench for etching. Furthermore, the prototype cycle is usually long, taking weeks or even months, making microfluidics research an expensive and time consuming adventure.

Whitesides and co-workers proposed the use of "soft lithography" to fabricate microfluidics chips from Polydimethylsiloxane (PDMS) (Qin *et al.*, 1996). PDMS is an inexpensive silicon-based organic polymer and is optically clear and bio-compatible. Micro-structures (such as SU-8) are made on a silicon substrate as moulds for making PDMS devices. Un-cured PDMS is then poured onto the mould and after curing the pattern on the master is transferred into the PDMS. The PDMS chips can be bonded to glass, silicon or other PDMS devices via Oxygen plasma bonding (Bhattacharya *et al.*, 2005, Eddings *et al.*, 2008). The masters can be re-used to make multiple batches of devices (Figure 2-11) in a short time (one day or less). Soft-lithography technique requires less costly facilities and is faster for prototyping. The method has dramatically accelerated microfluidic research over the last 15 years.

Other polymers used for fabricating microfluidic devices includes polymethylmethacrylate (PMMA) (Hong *et al.*, 2010), Cyclic Olefin Copolymer (COC), Cyclic Olefin Polymer (COP) (Jena *et al.*, 2012, Lee *et al.*, 2005, Sun and Kwok, 2006). These hard polymer materials are inexpensive, bio-compatible and transparent. Fabrication techniques like thermal embossing (Lee *et al.*, 2001, Leech, 2009), laser machining (Klank *et al.*, 2002, Hong *et al.*, 2010) and mechanical micro milling (Ogilvie *et al.*, 2010) have been used to make chips. Bonding is performed with solvent exposure (Brown *et al.*, 2006, Lin *et al.*, 2007), thermal heating (Zhu *et al.*, 2007), or UV exposure (Tsao *et al.*, 2007, Tsao and DeVoe, 2009). Fabrication methods such as laser machining and micro-milling do not need expensive cleanroom facilities, so that the prototype cost and design cycle can be dramatically reduced.

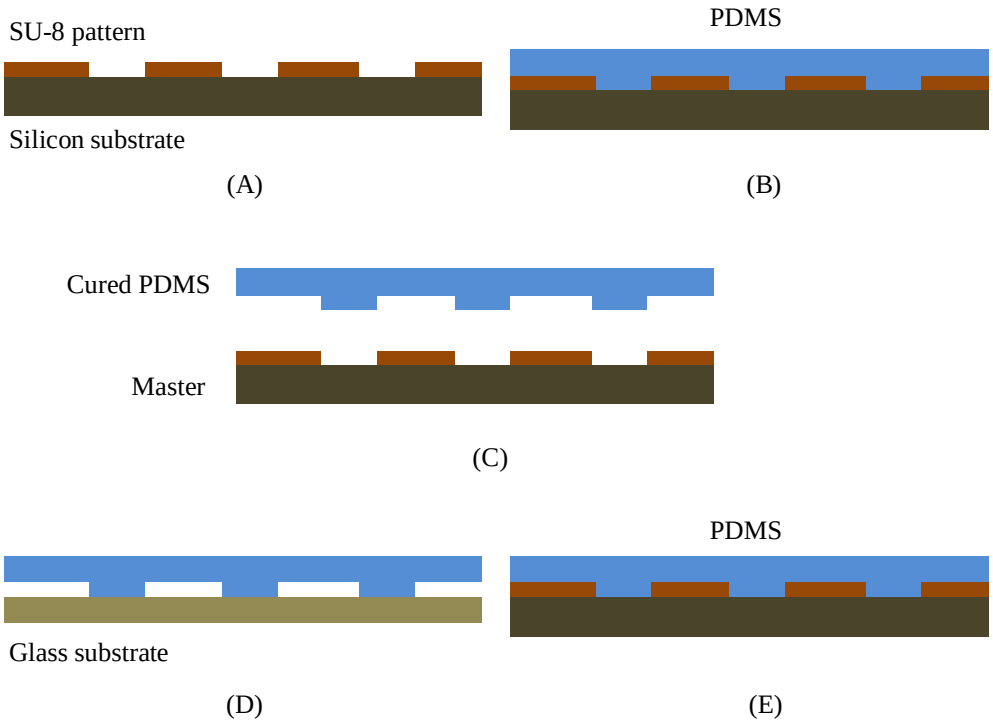

Figure 2-11: PDMS device fabrication procedure. (A) A micro-structure is patterned from an SU-8 layer onto a Silicon substrate with photo-lithography. This is the master for casting the PDMS devices; (B) PDMS is poured onto the master and cured at 65˚C for 4 hours. (C) The cured PDMS is peeled from the master, and (D) bonded to a glass substrate with Oxygen plasma treatment; (E) the master can be re-used to make another PDMS device.

2.4 Separation in microfluidics

Separation was one of the earliest applications of microfluidics and from the 1980s, biomolecules were separated by electrophoresis. In recent years, microfluidic separation continues to play an important role in analysing complex mixtures such as DNA, proteins and the other biomolecules. There are many embodiment of “micro” separations, such as microfluidics capillary electrophoresis (CE) (Duffy *et al.*, 1998, Guijt *et al.*, 2011, Rossier *et al.*, 2002), isoelectric focusing (IEF) (Tan *et al.*, 2002, Cui *et al.*, 2005a, Kohlheyer *et al.*, 2007, Jezierski *et al.*, 2013)

and liquid chromatography (LC) (Xie *et al.*, 2005, Mellors *et al.*, 2013). Many commercial devices are now available such as the Agilent 2100 Bioanalyzer which is based on microfluidic CE. More than one separation techniques can be hyphenated to form two dimensional (2D) or multi-dimensional separation (Wang and Hanash, 2003, Das *et al.*, 2007), and this has dramatically improved the separation capabilities, especially for resolving protein mixtures with hundreds or even thousands of species for proteomics.

2D separation normally includes IEF as the first dimension, which separates protein samples according to isoelectric point, and CE as the second dimension, which separate samples according to mass. The device shown in Figure 2-12A is a cyclic olefin copolymer (COC) microfluidic chip for 2D protein separation presented by Das *et al.* (Das *et al.*, 2007). The channel a-b is used for IEF separation, which is the first dimension of separation. When the sample proteins are focused to their isoelectric points, i.e. separated by IEF, the focused proteins are coupled with channel array c-d, which are the CE channels and perform the second dimension of separation. Fluorescently labelled proteins are observed with a high sensitivity CCD camera. Mathies' group in University of California Berkeley (Emrich *et al.*, 2007) described a glass microfluidic device containing an arch-shaped channel for IEF with twenty CE channels (Figure 2-12B). In their device, an interface channel of smaller size than the separation channel was used to connect the two separation channels. The small channel reduces the channel cross section and prevents fluid flow and diffusion-driven transport.

2.4.1 Compartmentalization after chemical separation

In recent years, droplet microfluidics has been used for compartmentalizing samples after chemical separation such as liquid chromatography (LC) or capillary electrophoresis (CE).

For example, Niu and co-workers demonstrated compartmentalisation of samples separated by liquid chromatography (Niu *et al.*, 2009, Pereira *et al.*, 2013) and capillary gel electrophoresis (Draper *et al.*, 2012); Chiu (Chiu, 2010) presented the segmentation of CE separated sample into nL-volume droplets, with compartments further analysed by CE (Niu *et al.*, 2009) or MS (Edgar *et al.*, 2009, Pereira *et al.*, 2013) (Figure 2-13). However, it should be noted that compartmentalisation, i.e. continuous-flow/micro-droplet conversion, is typically performed at a

fixed point (normally the outlet) for both LC and CE. Such an approach is not applicable to IEF, where focused analytes are distributed along the pH gradient.

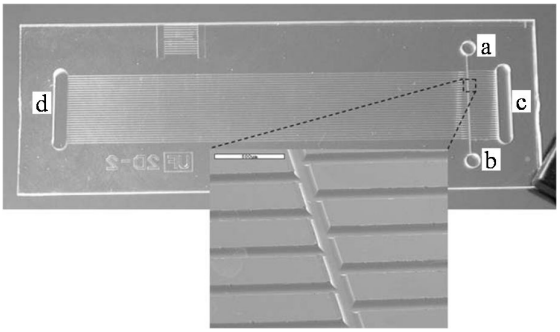

(A)

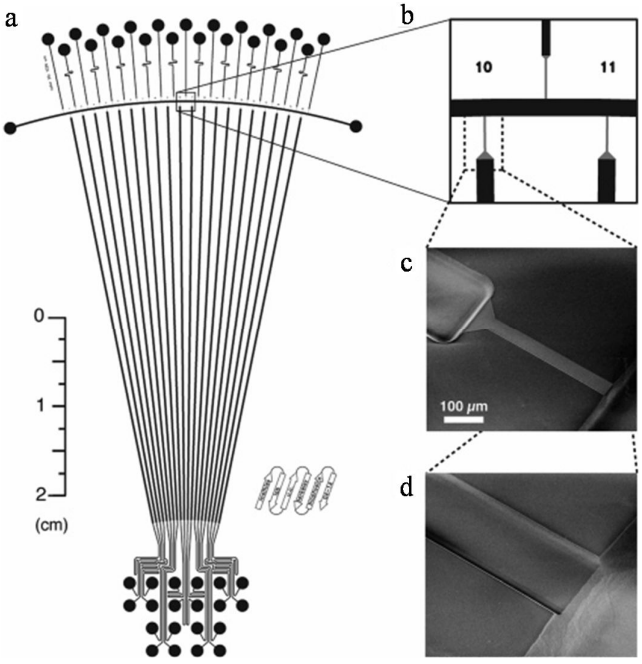

(B)

Figure 2-12: Microfluidic devices for two-dimensional separation. (A) The vertical channel a-b is the IEF channel for the first dimension of separation; the horizontal channel array c-d is connected to the IEF channel for the second dimension CGE separation (Das *et al.*, 2007). (B) The IEF channel (arch-shaped channel) is coupled with the CGE channel (vertical channel) via a small channel, which can prevent fluidic flow and diffusion-driven transport by reducing the channel cross section (Emrich *et al.*, 2007).

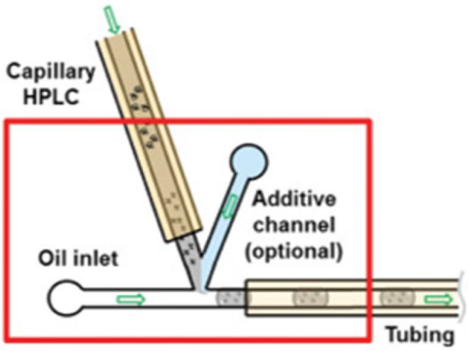

(A)

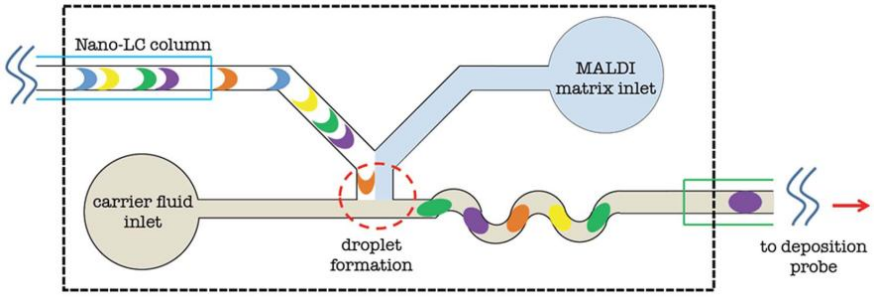

(B)

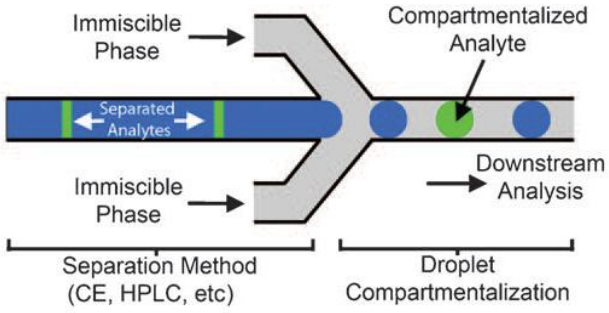

(C)

Figure 2-13: Schematic of compartmentalization of (A) capillary liquid chromatography (LC) separated sample for capillary electrophoresis (CE) analysis (Niu *et al.*, 2009); (B) Nano-LC separated sample for mass spectrometry analysis (Pereira *et al.*, 2013); and (C) cross-flow geometry for segmenting chemically separated samples (Edgar *et al.*, 2009). All these segmentations are performed at a fixed point.

To compartmentalise a sample separated by IEF, Geiser *et al.* presented an approach of cutting the immobilized pH gradient gel with a scalpel (Geiser *et al.*, 2011). In capillary IEF or microfluidic IEF, the focused analytes are normally removed from the capillary or micro-channel by pressure-driven flow, electroosmotic flow or chemical mobilization (Huang *et al.*, 1994, Hua *et al.*, 2010, Yu *et al.*, 2006, Ramsay *et al.*, 2009, Zhong *et al.*, 2011b). Such methods introduce dispersion and remixing of the focused analytes. To address this limitation, Righetti *et al.* cut the separated sample into 8 fractions (Righetti *et al.*, 2007a), and Wang *et al.* used a rotary valve to create fractions after IEF in a capillary loop (Wang *et al.*, 2013).

2.5 Detection techniques

Microfluidics can analyse smaller amount of samples with all of the aforementioned advantages, however this also brings in challenges for detection.

Fluorescence analytical method such as laser induced fluorescence (LIF) is a sensitive analytical tool for biological or chemical detection. It is the light emitted by certain molecules when light of higher energy is adsorbed; the wavelength of emission light is longer than the excitation light; by filtering the emission light with a band-pass (or long-pass) filter with specific wavelength, fluorescence detection shows a bright object against a dark background with a high signal to noise ratio. Fluorescence is also widely used in microfluidics such as for single cell sorting and analysis (Brouzes *et al.*, 2009, Mazutis *et al.*, 2013), digital PCR (Zhong *et al.*, 2011a) and screening of protein evolution (Agresti *et al.*, 2010).

Fluorescence method is sensitive, but fluorescent label needs to be introduced to the target sample, and it has photo-bleaching problem. Absorption spectroscopy is a label-free technique that measures the absorption of radiation as a function of wavelength. Commercial UV/Vis spectrometers are routinely used in chemistry and biological analysis. The Beer-Lambert law in equation (2.8) describes the light absorption of a sample. As shown in Figure 2-14, when a light beam traverses a liquid sample, the ratio between the transmitted light intensity I_1 and the incident light intensity I_0 is given by:

$$T = \frac{I_1}{I_0} = 10^{-\alpha l} = 10^{-\varepsilon l C} \tag{2.8}$$

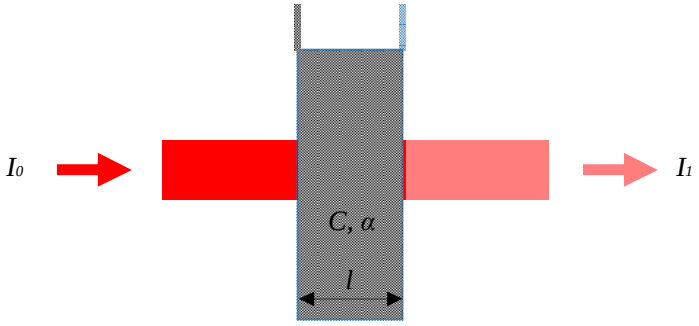

Figure 2-14: Schematic of an optical absorption experiment. When light traverses a liquid sample, the relationship between transmitted light intensity I_1 and the incident light intensity I_0 is proportional to the sample concentration C, the absorption coefficient α, and the light path length l.

where l is the distance the light traverses through the sample, i.e. the light path length; α is the absorption coefficient of the sample, written as the product of molar absorptivity ε and the molar concentration of the sample C.

It can be seen from equation (2.8), that the measurement sensitivity of a sample concentration, i.e. the smallest measurable difference of sample concentration (ΔC) is related to the detection sensitivity of the incident light intensity (ΔI_1):

$$\frac{\Delta I_1}{I_0} = 10^{-\varepsilon l \Delta C} \tag{2.9}$$

For the same light source and detector, ΔI_1 and I_0 are constant. Equation (2.7) shows that ΔC can be reduced by increasing light path length (l). To enhance the light path length, Sieben *et al.* (Sieben *et al.*, 2010) described a microfluidic system with 25mm long absorption cell, and used this device for nitrite detection, as shown in Figure 2-15, with a detection limit of 14nM.

Beside the long absorption cell, the effective optical path length can also be extended using multi-pass absorption strategies (Figure 2-16). Wang *et al.* extended the light path length in capillary electrophoresis by coating a mirrored capillary to reflect light (Wang *et al.*, 1991) (Figure 2-16A); Verpoorte *et al.* reflected light in a silicon flow cell to increase the light pass length (Verpoorte *et al.*, 1992) (Figure 2-16B); and Duggan *et al.* loaded sample into a capillary to form a liquid core waveguide using total internal reflection (Duggan *et al.*, 2003) (Figure 2-16C).

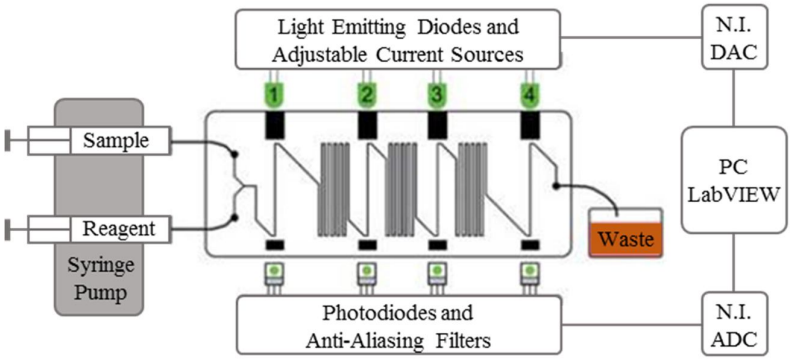

Figure 2-15: Schematic of a long light path microfluidic chip. The light sources are LED and the detectors are photodiodes. The absorption measurement cell is a 25mm long micro-channel. From (Sieben *et al.*, 2010).

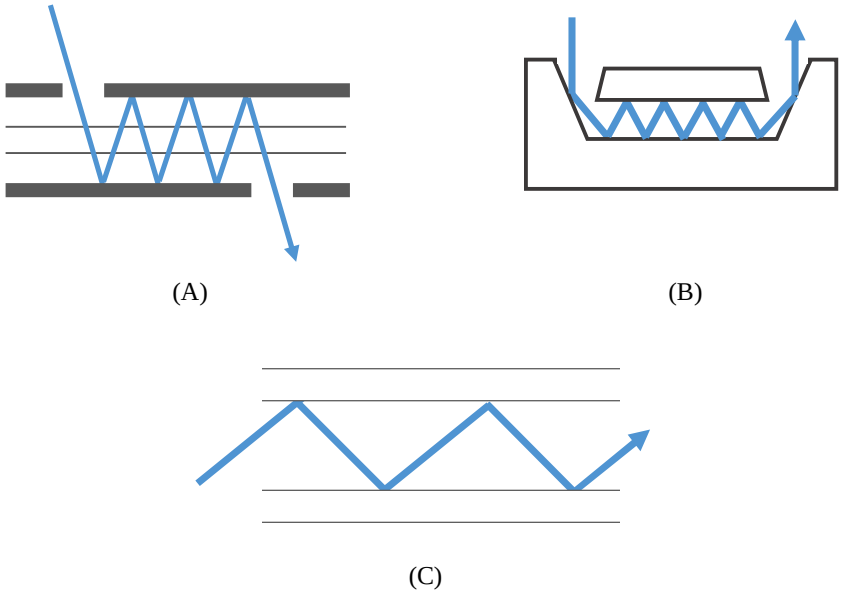

Figure 2-16: Multi-pass absorption methods that have been used to increase light path length. (A) Mirror coated capillary reflects light for absorption measurement in capillary electrophoresis (Wang *et al.*, 1991). (B) Silicon flow cell for multi-pass reflection (Verpoorte *et al.*, 1992). (C) Total internal reflection in high refractive index sample liquid core waveguide (Duggan *et al.*, 2003).

Cavity Ring Down Spectroscopy (CRDS) is an advanced multi-pass absorption measurement method first introduced in 1980s (Okeefe and Deacon, 1988). It uses an optical cavity, which is a

pair of mirrors (Figure 2-17) or a fibre loop (Figure 2-18) to trap light that passes through a sample many times, it greatly increases the light path length without increasing the sample volume.

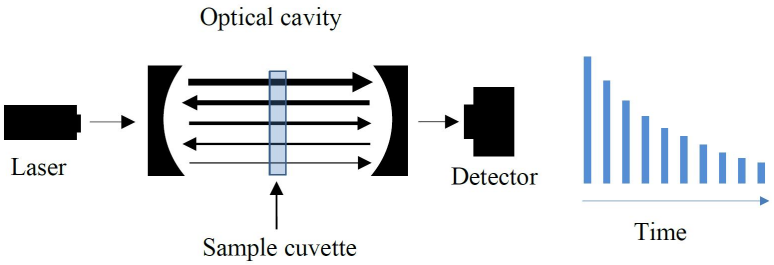

Figure 2-17: Schematic diagram of Cavity Ring Down Spectroscopy. A beam from a light source (laser) is trapped in an optical cavity. The light beam passes through the sample in the cavity many times, thus increasing the light path length without increasing the sample volume. The light intensity is monitored by a detector. The light absorption is related to the ring down time, which is the time taken for the light to decay to 1/e of its initial intensity.

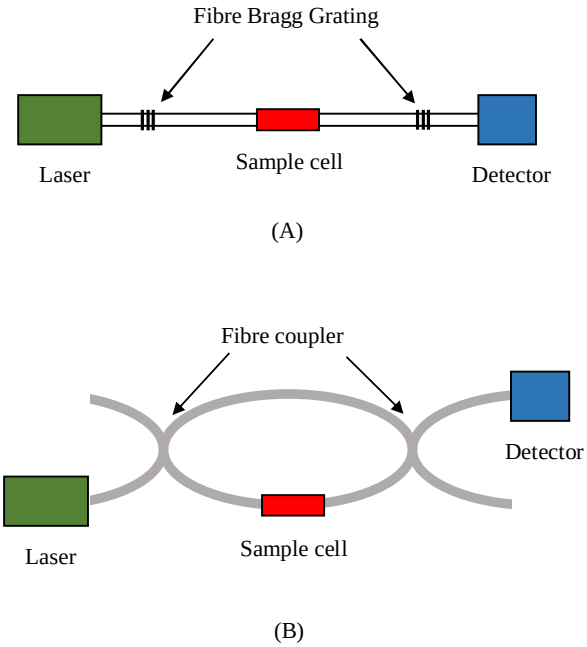

Figure 2-18: Schematic of a waveguide based optical cavity. (A) A Fibre Bragg grating can be used as the reflecting component to form a ring down cavity; (B) an optical fibre can also form a fibre loop to trap light.

CRDS is conventionally used for gas phase sample analysis (Wheeler *et al.*, 1998), but it remains a challenge to analyse liquid sample, a big problem is how to effectively couple the light into the flow cell like microfluidic device. To couple liquid samples with a mirror cavity, two geometries have been developed for the liquid-cavity interface. First, the cavity can be filled directly with the sample liquid (Figure 2-19A), such as the device presented by Hallock *et al*. (Hallock *et al.*, 2003) (Figure 2-20A); Li *et al.* filled a capillary with sample coupled with fibre ends of a fibre loop (Li *et al.*, 2006) (Figure 2-20B), which also belongs to direct coupling. The other one, liquid sample can be filled in a cell and placed in a cavity (Figure 2-20B and C). Snyder *et al*. presented a device that placed a flow cell in a mirror cavity with Brewster's angle (Snyder and Zare, 2003) (Figure 2-20C), with a P-polarized light the reflection on the interface of two mediums can be eliminated, light coupling efficiency can be increased.

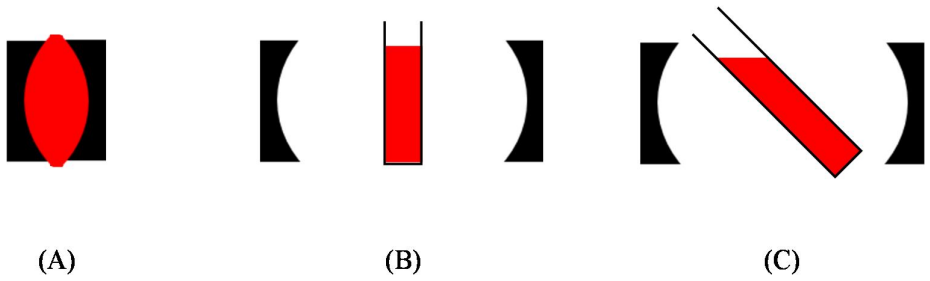

Figure 2-19: Three geometries for a liquid-cavity interface. (A) Liquid sample fills an optical cavity directly; (B) it can be contained in a liquid cuvette placed within the cavity, or (C) at the Brewster angle.

Coupling of CRDS with droplet microfluidics has also been investigated. Neil *et al.* placed a droplet microfluidic chip in a cavity to perform droplet analysis with CRDS (Neil *et al.*, 2011) (Figure 2-21A); James *et al.* placed a droplet microfluidic chip in a mirror cavity at Brewster's angle (James *et al.*, 2012) (Figure 2-21B).

Other analytical methods such as Surface-Enhanced Raman Spectroscopy (SERS) (Cristobal *et al.*, 2006), Fourier Transform Infrared (FT-IR) imaging (Chan *et al.*, 2011), electrochemical detection and Mass spectrometry (Vertessy *et al.*, 2013) are also used for droplet analysis. Zhu *et al.* published a review on droplet analytical methods (Zhu and Fang, 2013).

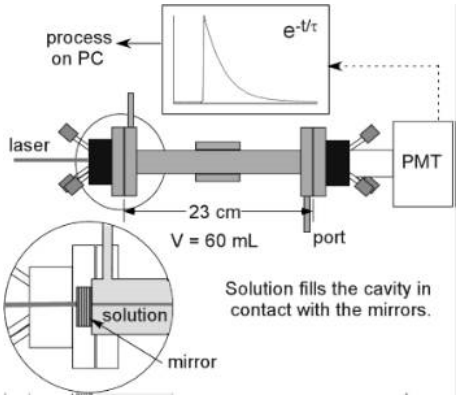

(A)

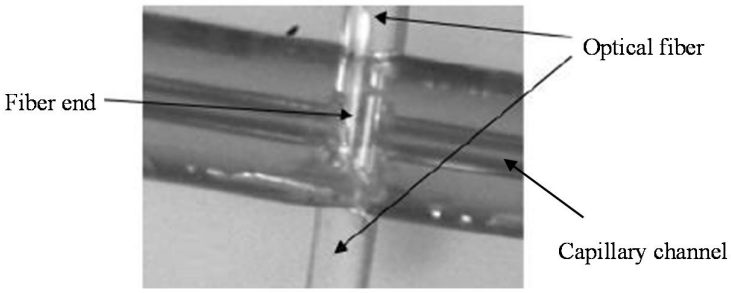

(B)

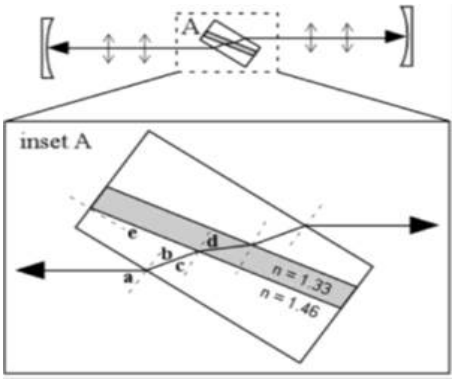

(C)

Figure 2-20: (A) Sample solution fills a cavity formed by two mirrors (Hallock *et al.*, 2003). (B) An optical fibre loop couples to a capillary channel that is used for capillary electrophoresis. The fibre ends are in contact with the sample in the capillary (Li *et al.*, 2006). (C) A flow cell is placed at Brewster's angle in mirror cavity (Snyder and Zare, 2003).

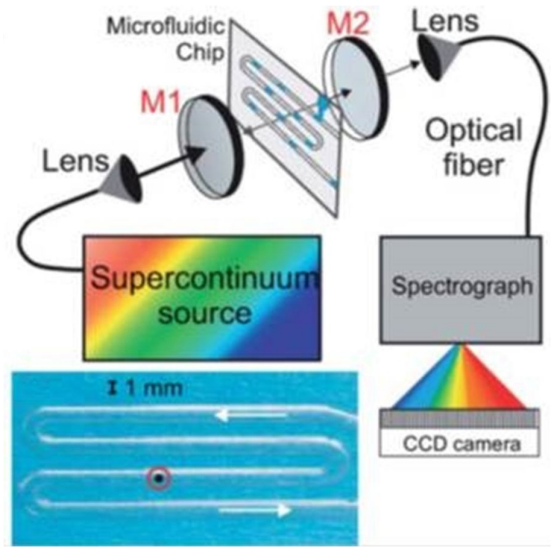

(A)

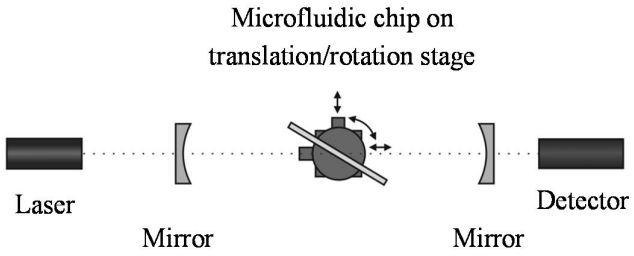

(B)

Figure 2-21: CRDS for analysis of droplet microfluidic. (A) a laser beam is aligned with microfluidic channel (Neil *et al.*, 2011). (B) A microfluidic chip is placed in mirror cavity, the angle is adjusted with a rotational stage (James *et al.*, 2012).

2.6 Summary and challenges

From the review above, both continuous and droplet microfluidics are greatly developed in recent years, both theory and application. Although continuous microfluidics has been commercialized for CE separation like Agilent Bioanalyzer, separation is still of important for microfluidic research. Droplet microfluidics, a 2nd generation microfluidic technology, digitalises samples into droplets with no cross-talk between them, each droplet is an individual capsule that can be

analysed independently. But such digitisation occurs at a particular point, such as a T-junction in a passive droplet device, or a droplet generation electrode in an active device, parallel *in situ* compartmentalization is still a challenge, which is very important for separation technologies. The Slipchip is a novel droplet microfluidic device which performs functions by slipping chips. It has been used for screening, immunoassay and digital PCR and has capabilities for parallel operation and multi-step processes. The Slipchip is therefore a promising method for *in situ* continuous-flow/micro-droplet conversion.

Analytical methods such as absorption spectroscopy, and fluorescence detection are used to analyse tiny droplets in microfluidics. CRDS enhances the effective light path length without increasing sample volume; it is therefore a promising method for on-line detection of micro-droplet. The development of an efficient interface between an optical cavity and a microfluidic system remains a challenge. Such challenge can be investigated from microfluidic side to optimise the CRDS-microfluidic optical interface, which is promising to increase sensitivity of the current absorption method for droplet on-line analysis.

Chapter 3

Slipchip Design and Fabrication

3.1 Introduction

Chapter 2 reviewed the state-of-the-art of microfluidics, including fluid manipulation, device fabrication, and analytical techniques. The Slipchip is a new generation of droplet microfluidics device, mostly fabricated on glass substrates using cleanroom facilities as described by Du *et al.* (Du *et al.*, 2009) and Li *et al.* (Li *et al.*, 2010b). This is an expensive and time-consuming process. In this chapter, the original Slipchip concept is re-engineered, and manufactured with CO_2 laser machining system or mechanical micro milling on inexpensive plastic material; These rapid fabrication methods have been used to make microfluidic devices (Hong *et al.*, 2010)(Ogilvie *et al.*, 2010), which reduced the prototyping cycle time from several days to less than two hours. In the Slipchip devices described in the literatures, the two half chips are clamped with binder clips (Du *et al.*, 2009) or paper clips (Li *et al.*, 2010c), and slipping is performed by hand (Shen *et al.*, 2010). In this chapter, a generic operation mechanism is described for mounting and aligning the chips. This allows the Slipchip to be easily operated by rotating a micro-meter drive with graduation of 10μm. An *in situ* droplet generator is demonstrated as an example. A generic Slipchip platform, including a chip pair and a control mechanism is proposed for fast Slipchip design.

3.2 Slipchip and operation mechanism design

Following on from the two layers design of the original Slipchip device (Du *et al.*, 2009), a design of a Slipchip droplet generator is shown in Figure 3-1.

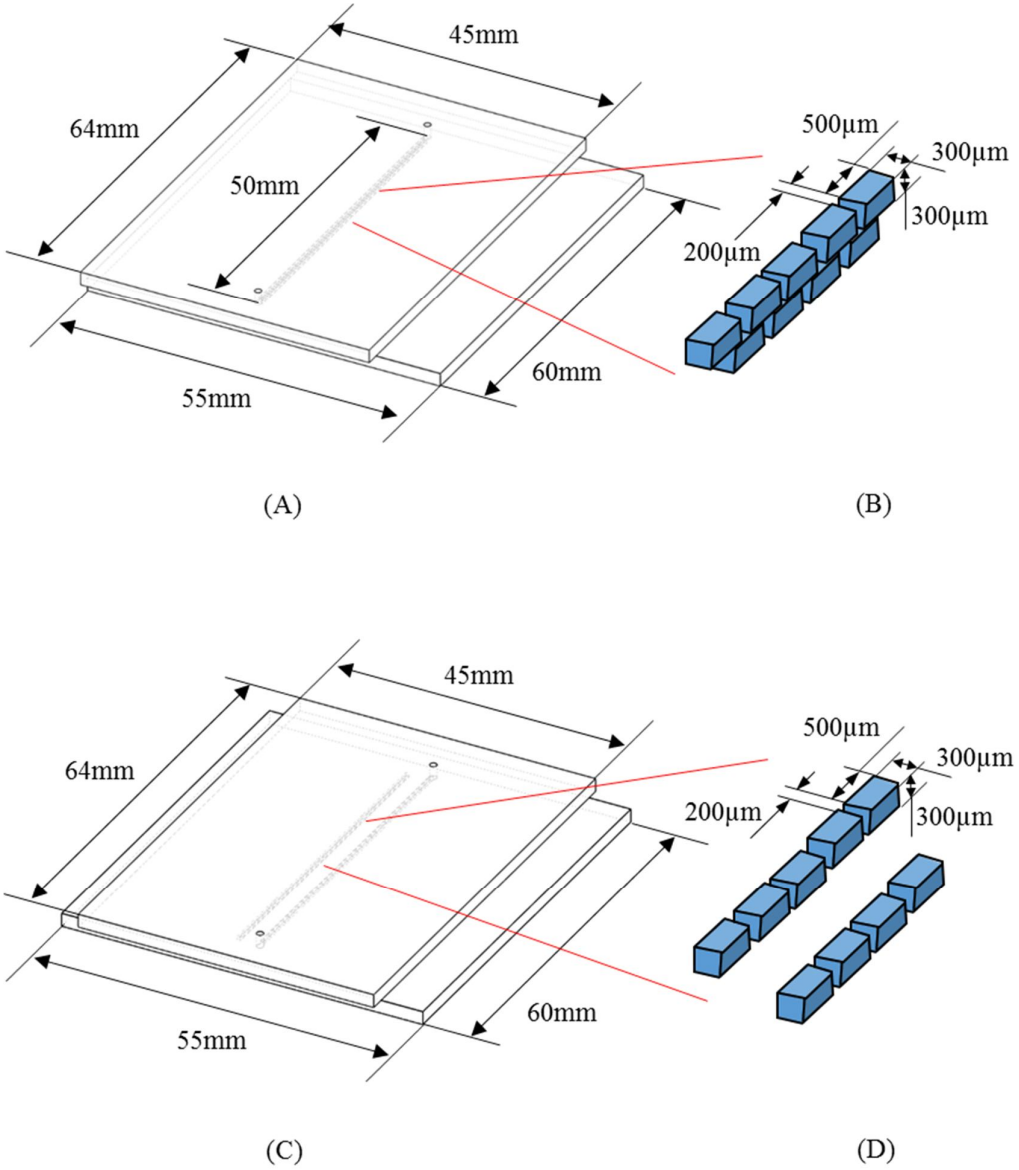

Figure 3-1: Slipchip droplet generator design. The device is formed of two half plates (A). The top plate is 64mm × 45mm × 2mm with 71 wells, and the bottom plate is 60mm × 55mm × 2mm with 70 wells. Two inlet/outlet holes are drilled on the top plate for sample loading. (B) The dimension of each well is 300µm × 500µm × 300µm. To generate droplets, the wells are first aligned forming a zig-zag channel (A and B) and the sample loaded into the wells. Then the wells are disconnected by slipping the chip (C and D), generating droplets with a volume of 45nL in the wells.

The Slipchip is formed of two halves chips with thickness of 2mm. The dimension of the top chip is 64mm × 45mm, whilst that of the bottom chip is 60mm × 55mm. There are 71 wells patterned on the top chip, and 70 wells on the bottom chip. The dimension of the well is 300μm × 500μm × 300μm. Inlet/outlet holes are drilled in the top plate for sample loading. To generate droplets, the wells are first of all aligned to form a zig-zag channel (Figure 3-1A and B). Then by slipping the chip thus disconnecting the wells (Figure 3-1C and D), sample droplets with a volume of about 45nL are generated in wells.

To control the moving of the chips, a Slipchip operation mechanism shown in Figure 3-2 is proposed. In this design, the top plate of the Slipchip is the fixed plate, and the bottom one can be slipped during operation. Two pairs of magnets are used to clamp the two plates, allowing the chips to be easily mounted and de-mounted. Slipping is performed by rotating a 150-801ST micro-meter drive (Thorlabs Inc., NJ, US).

As shown in Figure 3-2, the operation platform is formed of three layers: the bottom layer supports the whole device, and provides grooves for the bottom magnets. The middle layer has two parts: the frame part and the slipping part. The frame part is bonded with the top layer and bottom layer and provides grooves for slipping part. The slipping part mounts the slipping chip, and is connected with a micro-meter drive. The top plate is mounted in a fixed position on the top layer. By rotating the micro-meter drive, the slipping part in the middle layer will be moved, and the chip mounted in it will be moved. The maximum slipping distance is 10mm. The total dimension of the platform is 100mm × 75mm × 9mm (the micro-meter drive is not included).

3.3 Fabrication

3.3.1 Materials and reagents

Poly(methyl methacrylate) (PMMA) sheets were obtained from RS Components Ltd.; Cyclic olefin copolymer (COC) and Cyclic Olefin Polymer (COP) wafers were obtained from TOPAS Advanced polymers GmbH (Frankfurt, Germany) and Zeon Europe GmbH (Düsseldorf, Germany) separately; UV transparent PMMA sheets were from Nitto Jushi Kogyo Ltd. (Tokyo, Japan);

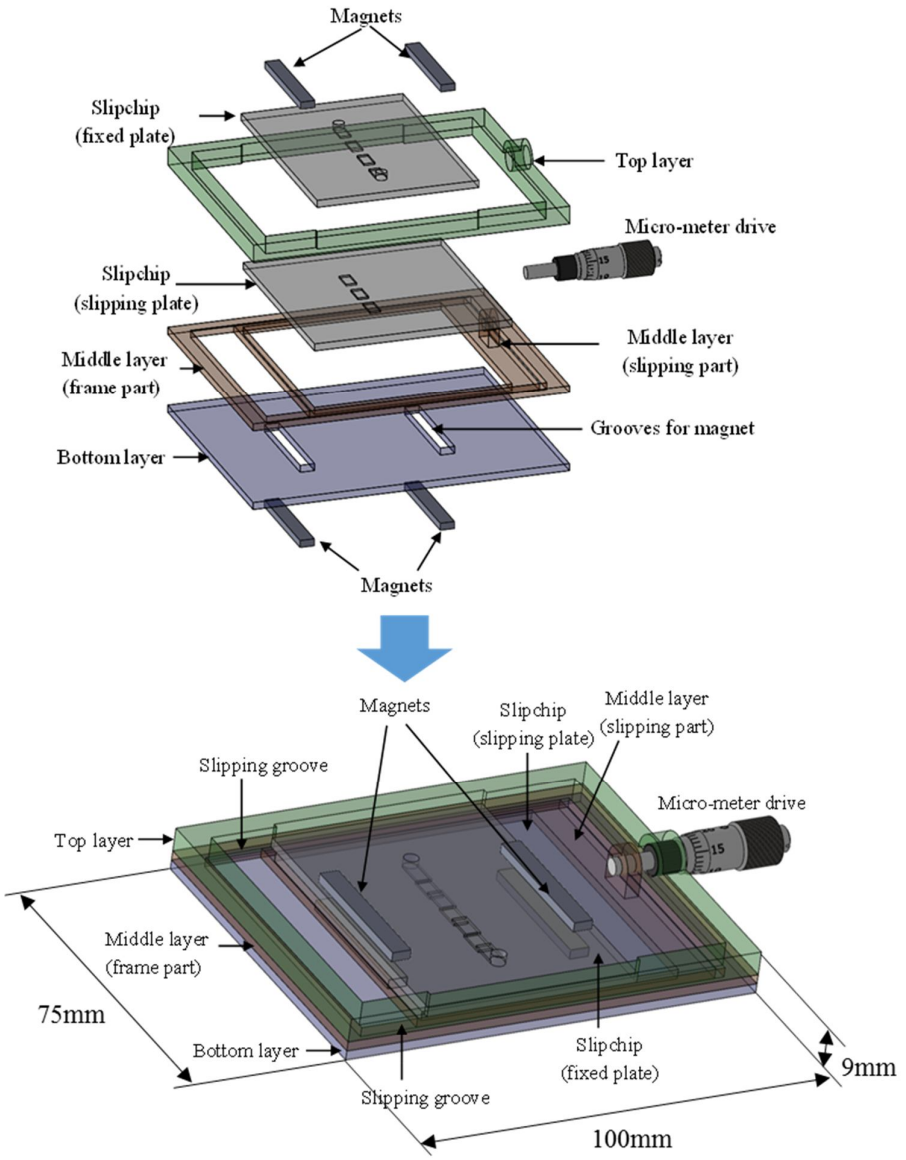

Figure 3-2: Slipchip operation mechanism. It is formed of three layers. The bottom layer supports the two chip. The middle layer and top layer provide the slipping mechanism. The middle layer has two parts, the frame part and the slipping part. The frame part is bonded with the bottom layer and the top layer, and provides grooves for slipping. The slipping part is used to mount the slipping chip and connected to a micro-meter drive to control the slipping. The total dimension of the platform is 100mm × 75mm × 9mm (micro-meter drive not included) and the maximum slipping distance is 10mm.

3.3.2 Fabrication with laser machining

The chip design was made with Clewin design software (WieWeb software, Hengelo, Netherlands), and exported to a dxf file, a universal file format accepted by most Computer Assisted Design (CAD) software.

An Epilog Mini 18 laser system (Epilog Laser, CO, US) was used to fabricate the devices by cutting material and ablating patterns on substrates. It is a CO_2 laser system with a power of 30 Watts, the dxf file was loaded into CorelDraw software which controls the laser machine. The diameter of laser beam is 75μm (according to the manufacturer's datasheet), the cutting or ablating depth is controlled by the laser power and movement speed, in which deep patterns can be made by using high power and low movement speed. Before fabricating the device, the machine is calibrated first: with the laser machine set to 100% power and 100% speed, one circle of laser printing ablates 60μm of PMMA. The whole laser processing time for the Slipchip droplet generator chip was about 5 minutes.

The profile of the laser ablated channel is parabolic as shown in Figure 3-3, which was studied by Klank *et al.* (Klank *et al.*, 2002) and Hong *et al.* (Hong *et al.*, 2010). This parabolic profile could reduce the light transmitted through the channel and limit the using of optical analysis methods such as microscopy and spectroscopy, negating the advantages of laser machining.

Therefore an alternative fabrication method was developed to fabricate channel with good optical property based on a PMMA-tape-PMMA sandwich structure as schematically shown in Figure 3-4. First, a 50μm thick 3M 467MP double sided tape (3M, Berkshire, UK) was laminated onto a 200μm thick PMMA film (Figure 3-4A). This laminated substrate was then patterned with the CO_2 laser machine (Figure 3-4B). The patterned PMMA-tape sheet was then laminated onto a 2mm thick PMMA plate (Figure 3-4C). In this case the channel will have a square profile, and the depth of the channel will be 250 μm, as per the thickness of the PMMA film (200μm) and the tape (50μm). The bottom surface of the channel, which is the surface of the 2mm PMMA sheet, is not ablated (Figure 3-4D), so it has optical properties same with original PMMA sheet. Furthermore, other materials such as glass, silica, patterned electrodes etc. can also be used as substrates with this method.

The operation platform is fabricated by laser cutting PMMA sheets, and assembled with screws, the picture in Figure 3-5 shows the fabricated platform.

Figure 3-3: Schematic profile of a laser ablated channel which is parabolic.

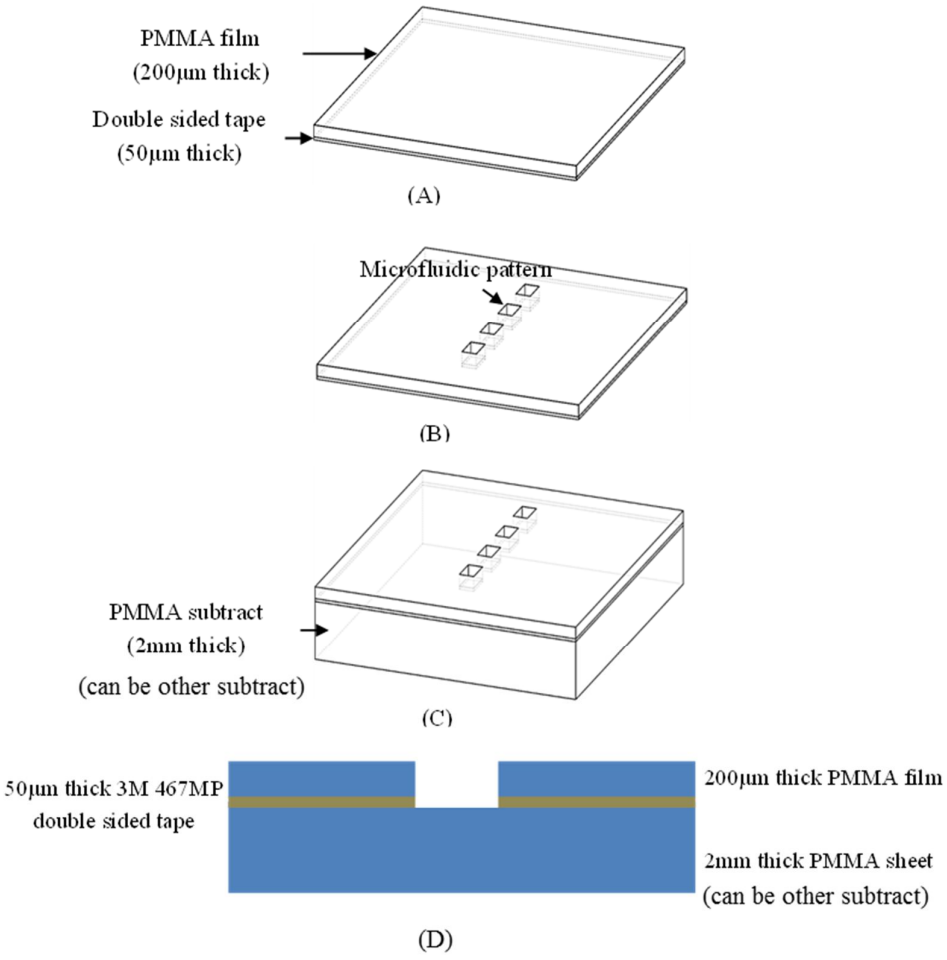

Figure 3-4: Fabrication of a PMMA-tape-PMMA sandwich structure. (A) First a 50µm thick double sided tape is laminated onto a 200µm thick PMMA film, (B) then the laminated PMMA-tape film is patterned by laser cutting. (C) The patterned film is laminated onto a 2mm thick PMMA sheet. (D) Schematic cross section of the chip showing the channel which has a square profile.

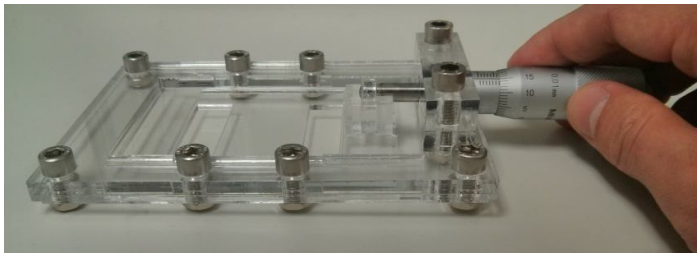

Figure 3-5: Photograph of the Slipchip platform, fabricated from laser cut PMMA sheets, and assembled with M4 screws.

3.3.3 Fabrication with micro milling

The laser machining with Epilog Laser is a fast prototyping method, but the fabrication precision and resolution are low, and the ablated surface has bad optical properties due to high surface roughness. Computer numerical controlled (CNC) mechanical micro machining is a precision fabrication method, a LPKF Protomat S100 micro milling machine (LPKF Laser & Electronics Ltd, Berkshire, UK) was used to make patterns, the accuracy of which is 0.5μm according to manufacturer's datasheet. The dxf file was loaded into CircuitCAM software (LPKF laser and electronics, Garbsen, Germany) to assign tools and convert the pattern to the milling paths. The wells were milled with a 300μm diameter HAM 423R end milling bit (HAM GmbH, Germany), and holes were drilled with a 700μm diameter drilling bit. The whole milling process took about 1 hour.

3.4 Results and optimization

3.4.1 Surface properties

The profiles of channels (300μm × 300μm) patterned by laser machining and micro milling were measured with a surface profiler, and are shown in Figure 3-6. The laser ablated channel had a parabolic profile (Figure 3-6A); with width of 405μm, 105μm wider than the design dimensions. The laser fabricated channel made from the PMMA-tape-PMMA sandwich structure had a square

profile (Figure 3-6B), 405µm wide – the same as the laser ablated channel. The micro milled channel had dimension of 300µm × 300µm (Figure 3-6C), which has the lowest fabrication error. Therefore, when fabricating channels by laser machining, the fabrication error in dimensions should be taken into account. For example, to make a 300µm wide channel the dimension of the design should be 195µm.

Optical properties of the material and fabricated device is important as optical analytical method will be used. PMMA, COC and COP are thermoplastic polymer materials with good biocompatibility and are frequently used to make microfluidics devices by micro milling or bot embossing (Steigert *et al.*, 2007, Ogilvie *et al.*, 2010). The light transmission properties of these materials were measured to ensure that they were appropriate for DNA and protein imaging. Tests were performed with 1mm, 2mm and 5mm thick PMMA, 2mm thick COP, and 1mm thick COC plates. The light transmission ratio of a 1.1mm thick microscope glass slide was measured as a reference. Measurements were performed with a LAMBDA 650 UV/VIS Spectrophotometer (PerkinElmer Inc., MA, US) over the range 260nm to 500nm. As shown in Figure 3-7, a 1mm thick PMMA sheet from RS Components has a -3dB point at 375nm, compared with a 1.1mm thick microscope glass slide at 305nm. 1mm thick UV transmission PMMA obtained from Nitto Jushi Kogyo Ltd. has a cut off at 270nm, while COC and COP are 290nm and 310nm respectively. Across the entire spectrum (260nm to 500nm), the UV transmission PMMA has higher light transmission ratio than that of glass slide, COC and COP.

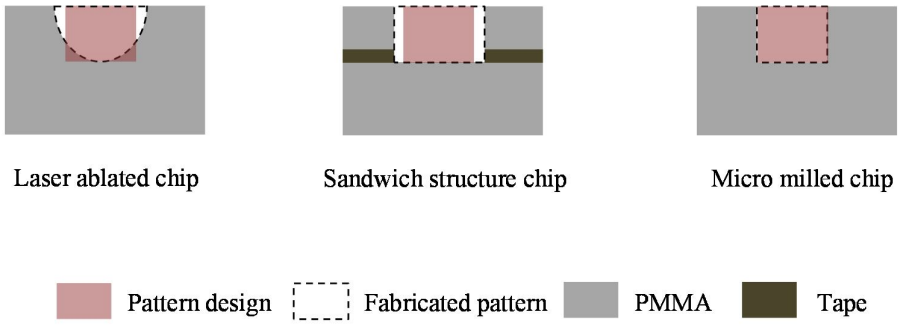

Figure 3-6: Schematics of profiles of wells. The laser ablated well is a parabolic shape; the width is 105µm larger than the design. The PMMA-tape-PMMA sandwich structure chip has a square profile, 105µm larger than the design. The micro milled well is the same dimension as the design.

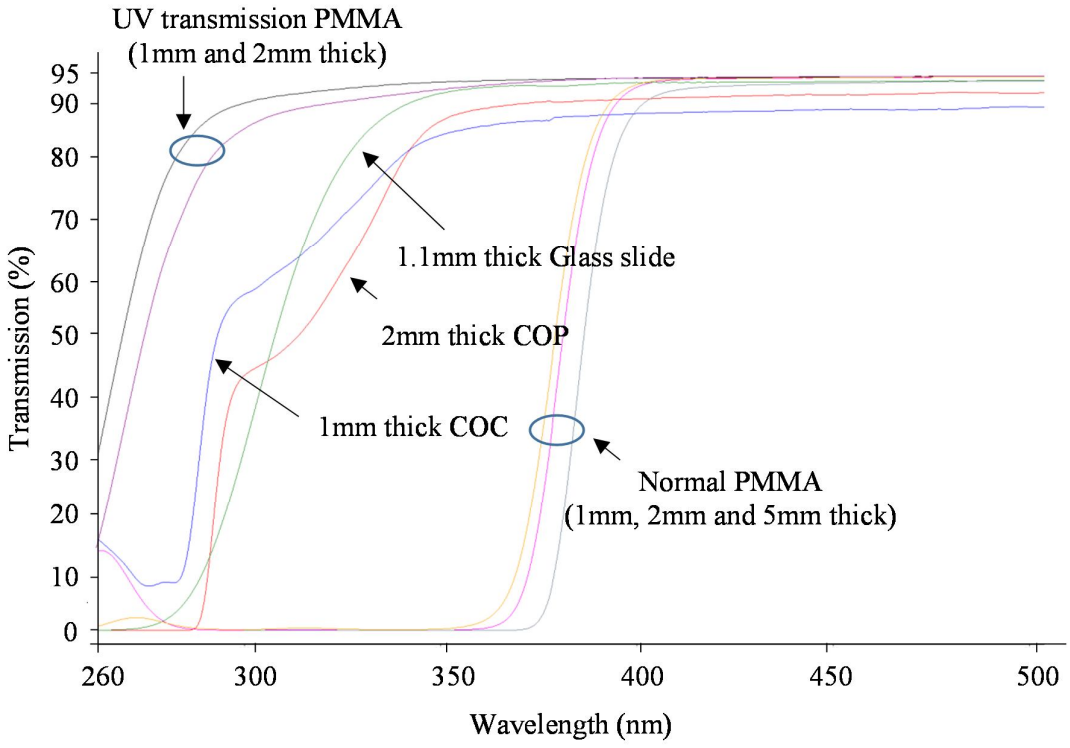

Figure 3-7: Light transmission ratio for normal PMMA, COC, COP, glass slide and UV transmission PMMA. Scanning was performed from 260nm to 500nm with a UV/Vis spectrometer.

The light transmission properties of the channels were measured with bright field microscopy. The channel area of the device was imaged with a microscope using transmission light, the picture was analysed with ImageJ, and the brightness on the image indicates the intensity of the light transmitted. The 2mm thick UV transparent PMMA plate transmitted 91.3% of the light, but only 18.8% of the light passes through the laser ablated channel. The channel in the PMMA-tape-PMMA sandwich structure had the same light transmission ratio as the original PMMA substrate, which was 91.3%. For micro milled channels, the light transmission ratio was 76.6%.

3.4.2 Surface reflow

The optical properties of the device can be optimised by modifying the surface roughness; for PMMA, Chloroform vapour can be used to reflow the surface to reduce the surface roughness (Ogilvie *et al.*, 2010).

After laser machining and micro milling, the chips were rinsed with water and ultrasonicated in isopropanol for 10 minutes, then rinsed with fresh isopropanol and dried in a nitrogen flow. The chips were then dehydrated at 60°C for 30 minutes. To perform Chloroform reflow, Chloroform liquid was contained in a 100mm diameter glass petri dish, with the liquid about 1mm below the top (Figure 3-8). A Polytetrafluoroethylene (PTFE) plate was used to cover the petri dish and hold the chip. Reflow was performed at room temperature in a fume hood for 3 minutes, followed by dehydration at 60°C for 10 minutes. The surface roughness was measured with an atomic force microscope (AFM), for laser ablated device, the surface roughness was reduced from 930nm to 160nm after treating with chloroform vapour; for milled chip, the surface roughness was 170nm before surface reflow, and 21nm after exposing to chloroform vapour. The surface roughness of fresh PMMA sheet is 11nm (Figure 3-9).

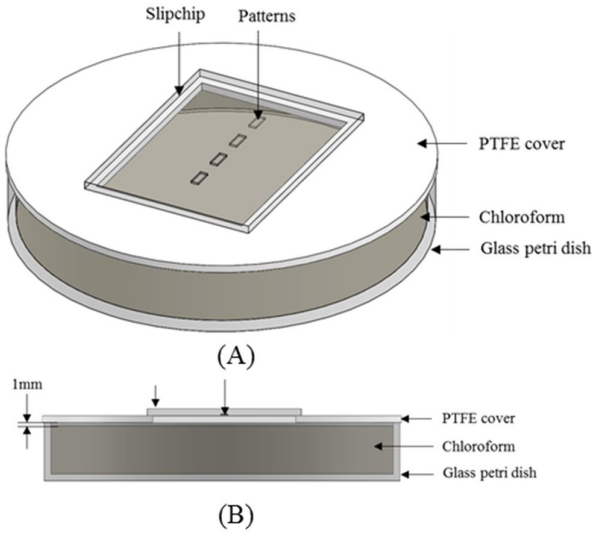

Figure 3-8: Schematic of surface reflow setup, (A) is the 3D view, and (B) is the side view. Chloroform is contained in a 100mm diameter glass petri dish; a Polytetrafluoroethylene (PTFE) plate covered the petri dish and supported the chip. The Chloroform liquid level was about 1mm from the top of the petri dish.

It was noticed the exposure time is critical in surface reflow process, chips with short chloroform exposure of 2 minutes will have the similar surface roughness and optical transmission ratio as an unexposed chip; but a long exposure time of >4 minutes can cause cracking of the chip surface. An important issue in the surface reflow process is to ensure that the petri dish containing the chloroform is covered well as this traps the chloroform vapour.

The light transimission ratio of surface reflowed channel was measured with bright field microscopy as discribed above. As shown in Figure 3-10, after surface reflow, the light transmission ratio of laser ablated chip was increased from 18.8% to 35.1%, for micro-milled chip it was increased from 76.6% to 88.3%.

It can be clear seen from Figure 3-9 and Figure 3-10 that the surface reflow significantly reduced the surface roughness and increased the optical transmission ratio of the device.

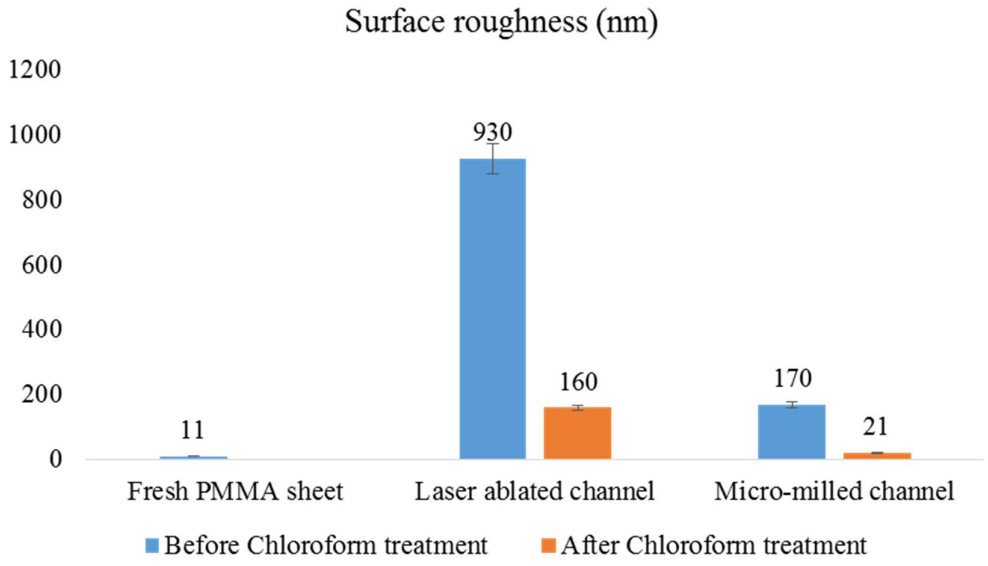

Figure 3-9: Surface roughness measured by AFM. For fresh PMMA sheet it is 11 nm; for laser ablated channel, it is 930nm and 160nm after surface reflow; for micro-milled channel, it is 170nm and 21nm after chloroform exposure. The error bar is standard error (n=7).

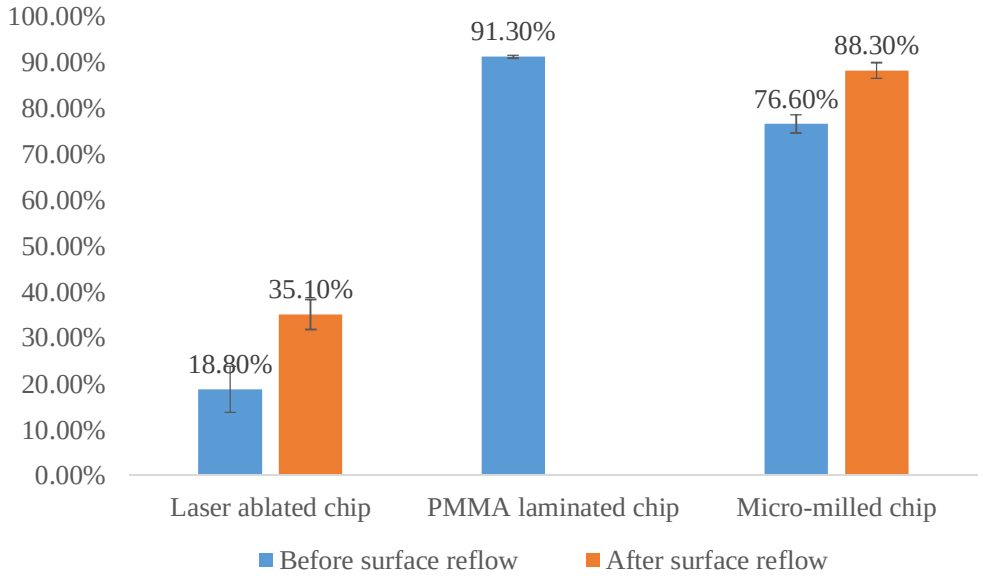

Figure 3-10: Optical transmission of laser ablated chips, laminated chips, and micro milled chips. The laser ablated well transmits 18.8% of the light. The wells in the PMMA-tape-PMMA sandwich structure chip have the same light transmission ratio as the original PMMA substrate, which is 91.3%. For micro milled wells, the light transmission ratio is 76.6%. After chloroform surface reflow, the light transmission ratio of the laser ablated well increases to 35.1%, and the micro milled well to 88.4%. The error bar is standard error (n=7).

3.4.3 Surface treatment

The surface with high hydrophobicity helps to prevent the leakage in Slipchip (Du *et al.*, 2009). The contact angle of the surface was measured by a Drop Shape Analyzer DSA25 system (KRÜSS GmbH, Hamburg, Germany) with a 1μL DI water droplet. It was 62.3˚ for a PMMA sheet.

Parylene C is a hydrophobic material widely used for surface treatment in microfluidics, such as working as hydrophobic layer in EWOD device (Pollack *et al.*, 2000). Duxcoat Nano is a commercial surface treatment solution supplied by Duxback Ltd. UK. It makes surfaces like glass

and plastic hydrophobic and is safe and rapid. In this section, these two materials are used to increase the hydrophobicity of the chip surface.

Parylene C coating is performed with a Parylene coater in Southampton Nanofabrication Centre. After 0.5□m thick Parylene C coating, the surface contact angle was measured at 91.6 ˚.

Duxcoat Nano is a two-part kit and prior to use the two parts were mixed 1:1, then the mixture was applied to the chip surface with a lens tissue. The treated chips were baked at 60ºC for 5 minutes, and the whole process took 10 minutes. After surface treatment, the surface contact angle was measured at 101.4˚. Duxcoat Nano is also treated on a surface with 0.5µm thick Parylene C coating, the surface contact angle was measured at 114.2˚. The Parylene C and Duxcoat Nano combined surface treatment gives the highest contact angle (Figure 3-11).

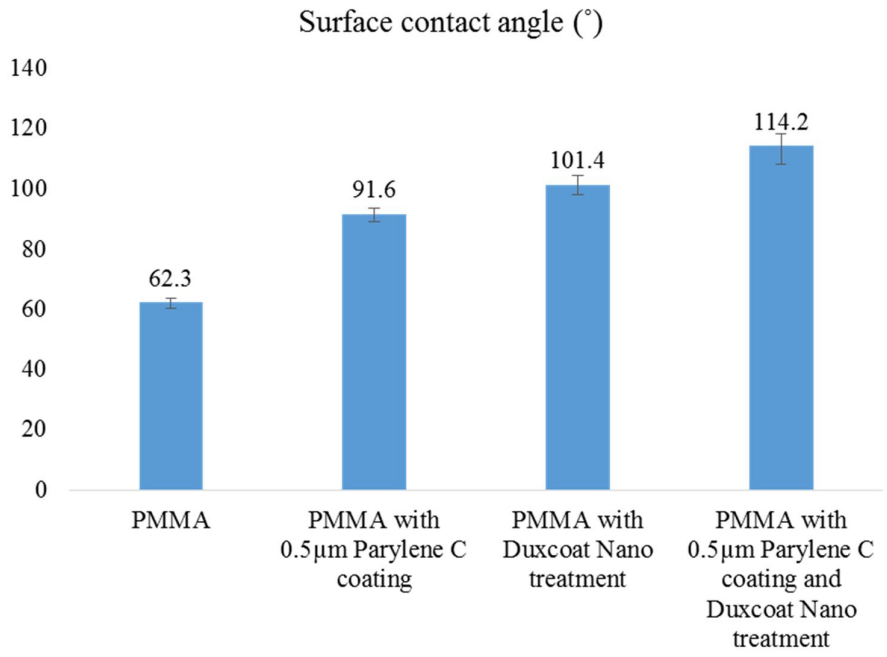

Figure 3-11: The contact angle of PMMA after various treatments. Uncoated PMMA is 62.3˚. After coating with 500nm of Parylene C, the surface contact angle increased to 91.6˚, and increased further 114.2˚ after Duxcoat Nano treatment. A PMMA sheet with only Duxcoat Nano treatment (no Parylene C coating) had a surface contact angle of 101.4˚. Error bar is standard error (n=7).

Duxcoat Nano (Duxback Ltd., Somerset, UK), and FC-40 oil was obtained from 3M (Berkshire, UK). After surface reflow, the chip was first coated with a 0.5□m thick Parylene C layer, followed by treatment with Duxcoat Nano solution.

After surface treatment, the light transmission ratio of the UV transparent PMMA plate was compared with the original as shown in Figure 3-12. The surface coating reduces the light transmission ratio to about 80% for wavelengths above 300nm, 10% lower than the original material, but acceptable for the devices.

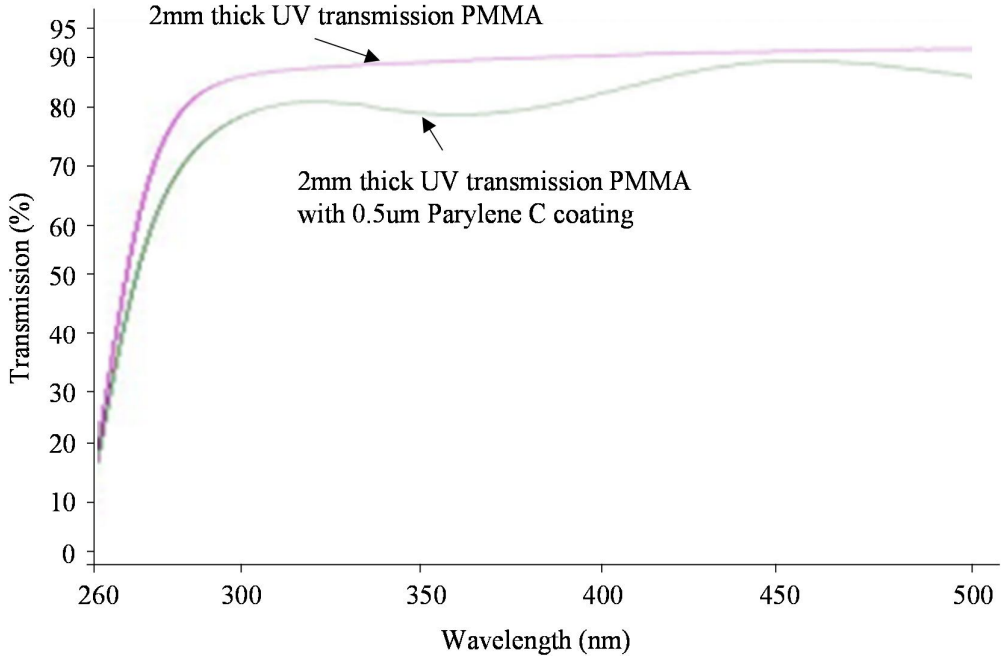

Figure 3-12: Light transmission ratio for 2mm thick UV transmission PMMA sheet, and for the same PMMA sheet with a 500nm thick Parylene C coating.

After coating with 0.5µm of Parylene C and treating with Duxcoat solution, the optical transmission ratio of the channels for the laser ablated chip, PMMA-tape-PMMA laminated chip, and micro milled chip were 32.4%, 78.6% and 88.4% respectively as shown in Figure 3-13.

In conclusion, compared with microscope glass slide, COC, COP and normal PMMA, UV transmission PMMA material supplied by Nitto Jushi Kogyo Ltd. gives the best optical properties, which is best suitable for making optical analytical devices. The micro-milling makes chips with higher accuracy and better surface properties, which is suitable for fabricating chips; laser

machining is a fast process and is suitable for fabricating operation platform. The Parylene C coating plus Duxcoat Nano treatment greatly increased the surface contact angle of the device, which is selected as a standard process in fabricating chips in this chapter.

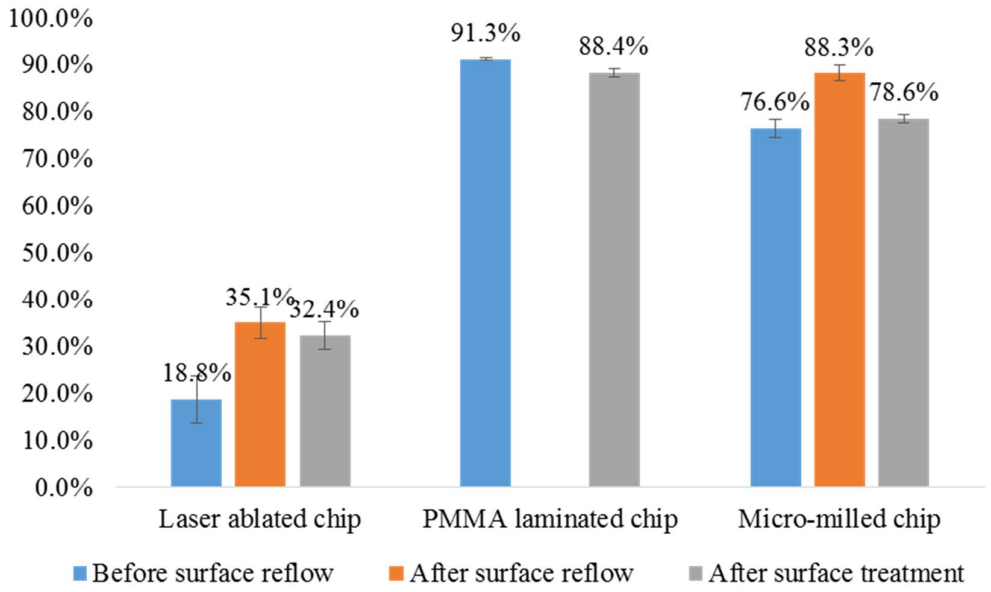

Figure 3-13: Optical transmission of laser ablated chips, laminated chips, and micro milled chips. After surface treatment, the optical transmission ratio of the channels for the laser ablated chip, PMMA laminated chip, and micro milled chip were 32.4%, 78.6% and 88.4% respectively. The error bar is standard error (n=7).

3.4.4 Slipchip assembly and operation

Before mounting chips on the operation platform, 200μL FC-40 oil was used to wet the chip surfaces, then the device was assembled, and two pairs of magnets with force about 50N each were used to clamp the chips. After the chips were clamped, the FC-40 oil between the chips was squeezed out and a thin oil film left on the surface, preventing leakage of the aqueous phase in the wells and lubricating the slipping (Du *et al.*, 2009).

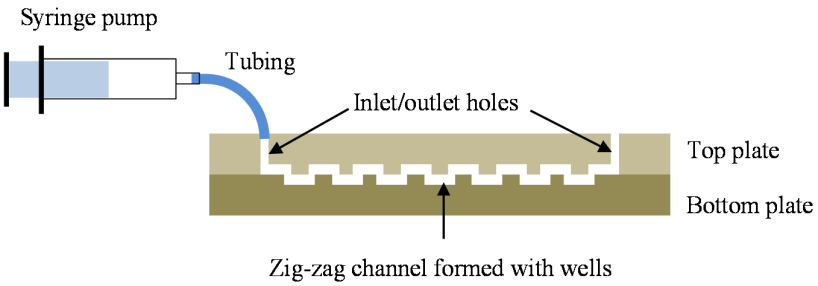

Figure 3-14: Schematic diagram showing sample loading. After the wells are aligned to form a zig-zag channel, the sample is loaded with a syringe connected to the inlet hole via tubing. The flow rate is controlled with a syringe pump.

After device assembling, the wells on both half of Slipchip were first aligned to form a continuous zig-zag channel. A 10% (v/v) diluted red food dye sample was loaded into the zig-zag channel with a syringe pumps (Harvard Apparatus Ltd, Kent, UK) at a flow rate of 60µL/min (Figure 3-14). Figure 3-15A shows a bright field microscopy image of the Slipchip zig-zag channel with the dye. The chip was then slipped by rotating the micro-meter drive; the wells were disconnected and droplets were generated in the wells (Figure 3-15B).

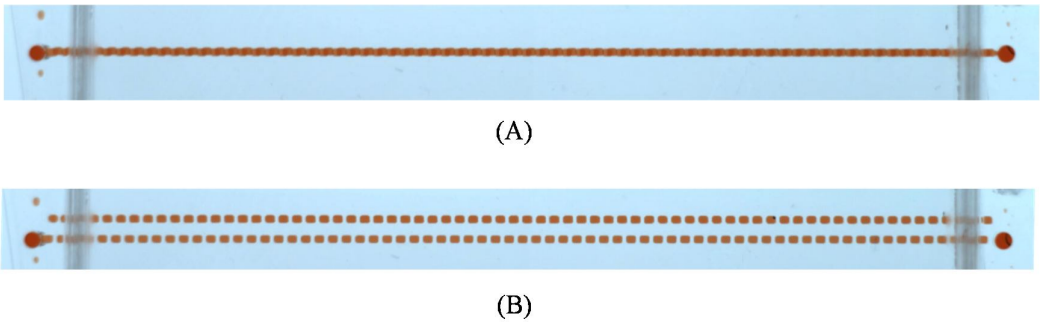

Figure 3-15: Bright field microscope image of Slipchip droplet generation. The wells were first aligned to form a continuous zig-zag channel, and then the channel filled with red colour food dye (A). After sample loading, the chip was slipped by rotating the micro-meter drive, the wells disconnected and the droplets left in the wells (B). The total length of the channel is 5cm.

The device was also tested with 100mM Rhodamine fluorescence dye, the sample loading flow rate was changed from 20μL/min to 150μL/min. Observation was performed with a Zeiss LSM 5 confocal fluorescence microscope with Rhodamine filter set (excitation wavelength: 535-580nm, emission wavelength: 600-655nm), the microscope was working in Epi-fluorescence mode. When flow rates were lower than 100μL/min, no fluorescence was observed outside the wells, i.e. no leakage occurred.

When the clamping force of the magnets was reduced to 30N, leakage was observed at flow rates of 40μL/min. Increasing the clamping force to 70N did not improve the sealing, however such a high clamping force leads to high friction and makes operation difficult. In practice, slipping was difficult with a clamping force above 50N.

This droplet generator is scalable; by changing the wells dimensions the droplet size can be changed. For example, the device in Figure 3-1 can create 141 droplets with 45nL volume; when the well dimensions changed to 500μm × 1000μm × 300μm, the device with the same channel length will be able to generate 71 droplets, each droplet has volume about 150nL; when the well dimensions changed to 100μm × 300μm × 100μm, the device will be able to generate more than 500 droplets as the same slipping operation, each droplet will have 3nL volume. But the fabrication and operation should be considered during the scaling.

3.5 Generic Slipchip platform

This droplet generator Slipchip device can modified to make a generic Slipchip platform for fast Slipchip prototype. Such platform includes a chip design standard and an operation platform. The chip design standard is shown in Figure 3-16. In which the dimension of the top chip and bottom chip are 64mm × 45mm and 60mm × 55mm separately. A minimum 5mm space is left between patterns (wells, ducts and holes) and chip edges to prevent leakage. The pattern area on the chip, which is also the functional area, has dimension of 50mm × 25mm. The maximum slipping distance is 10mm, Figure 3-16C and D show the two slipping limit. The overlapping area in Figure 3-16D is the critical functional area, because this area is always touching with the functional area in the opposite chip, so this area is suitable for patterning sample channels, reaction wells etc.. The two assistant functional areas are suitable for patterning loading channels etc., because the

patterns in this area will be out of touching of functional patterns in the opposite chip during slipping.

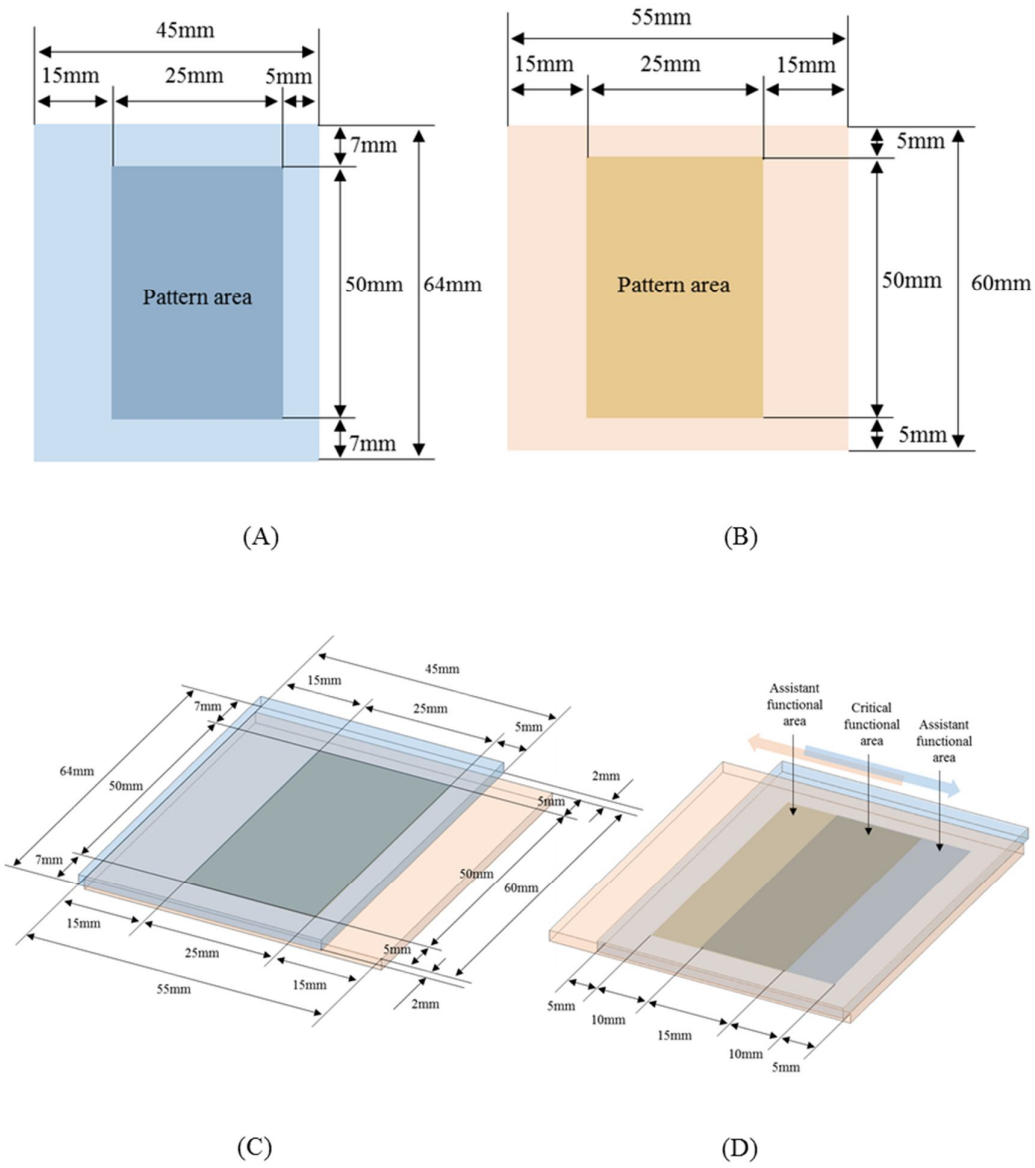

Figure 3-16: Generic Slipchip platform - chips. The device is formed of two chips with thickness of 2mm, the top chip is the fixed chip with dimensions of 64mm × 45mm (A); the bottom chip is the slipping chip with dimensions of 60mm × 55mm (B), the pattern areas in both plates are 50mm × 25mm. To avoid leakage, a 5mm space is left between pattern area and the chip boundaries (C). The maximum slipping distance is 10mm (D).

Tsaloglou *et al.*(Tsaloglou *et al.*, 2015) presented a Slipchip device for real-time isothermal recombinase polymerase amplification as shown in Figure 3-17, which is an example of using this generic Slipchip platform for fast prototyping Slipchip device.

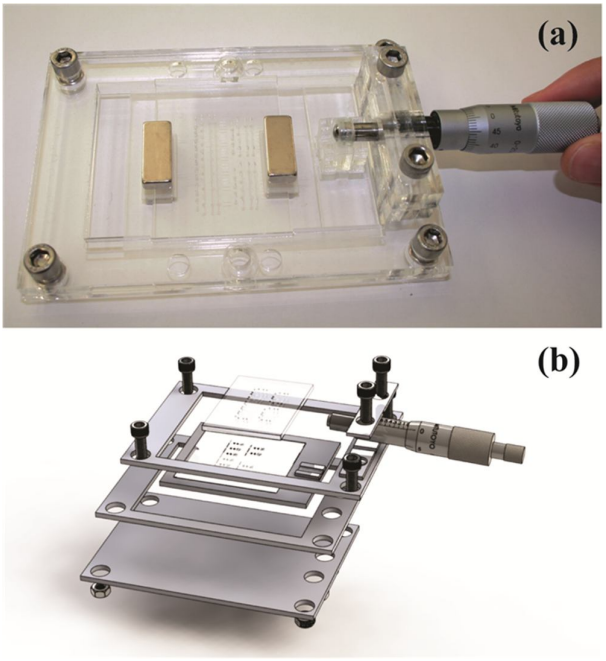

Figure 3-17: Slipchip real-time isothermal recombinase polymerase amplification device (Tsaloglou *et al.*, 2015), (a) picture (b) schematic drawing. It is based on the Slipchip platform described in this chapter.

3.6 Conclusions

This chapter describes a re-engineered Slipchip device for droplet generation. In conventional droplet generation strategies such as T-junctions (Garstecki *et al.*, 2006), cross-flow (Hashimoto *et al.*, 2008) or electrodynamic methods like ElectroWetting-On-Dielectric (EWOD) (Nelson and Kim, 2012), samples are compartmentalized into droplets at a particular droplet generation point such as the junction of channels. In the Slipchip droplet generation method described in this chapter, the sample can be compartmentalized *in situ* using a zig-zag channel by slipping the chip.

A generic Slipchip operation platform was proposed which uses magnets to clamp the two halves of a Slipchip plate and a micro-meter drive to control the slipping. The maximum slipping distance is 10mm, and the alignment resolution is 10μm. Compared to previously reported methods (Li *et al.*, 2010c), this platform makes operation of the Slipchip easy and precise without special training or practice.

A Slipchip rapid prototyping method with plastic material has been described. Chips were fabricated from PMMA, three fabrication methods were investigated. First, direct ablation with a CO_2 laser, which is very fast, but the final pattern has a parabolic profile with poor optical properties - only 18.8% of the light is transmitted through the pattern. The PMMA-tape-PMMA sandwich structure has a square profile and good optical transmission ratio; about 91.3% of light is transmitted. The depth of the pattern is controlled by the thickness of the PMMA film and tape. The tolerance of the pattern fabricated with laser machining is about 30μm; the smallest feature is about 104μm, which is limited by the size of laser beam. Micro milling achieves a tolerance smaller than 1μm and the milled pattern has an optical transmission ratio higher than 76%. With this method, the Slipchip fabrication time is about 2 hours. Solvent reflow improves the optical properties of the surface. After reflowing, the light transmission ratios of the device fabricated with these three methods were 35.1%, 90.1% and 88.4%.

Among the three methods, laser ablation is suitable for very fast prototyping and first concept verification. The PMMA-tape-PMMA sandwich structure chip has the best optical properties, because the channel bottom surface is the original PMMA plate, and this method does not need surface reflow process. But it uses tape as a bonding material, and these devices cannot be used for long term experiments. The channel depth depends on the thickness of the PMMA film and tape, which may reduce design flexibility, i.e. the channel depth cannot be changed. Micro milling has the highest resolution (down to 1μm), but the fabrication time is the longest. It can be used to make high quality devices and cleanroom facilities are not needed.

A UV transmission PMMA material is used to make microfluidics chips. This material has a -3dB cut-off wavelength of 265nm, lower than COC (285nm), COP (320nm), normal PMMA (370nm), and microscope glass slides (310nm). It is a good option to make microfluidics device for UV detection using wavelength higher than 265nm.

A surface treatment method using Duxcoat Nano solution is presented. It is a fast and easy process taking less than 10 minutes. It increases the surface contact angle of PMMA from 62.3° to 101.4°;

on a Parylene surface it can increase the contact angle from 91.6˚ to 114.2˚. This method is fast and low cost, but the hydrophobicity is lower than a surface with nano patterns (Li *et al.*, 2010a), which have contact angles of 137.9°. Tests with Rhodamine dye showed that coating with Parylene and Duxcoat prevents leakage. A clamping force of 50N was found to be the best for this Slipchip device, enabling sample loading at flow rates up to 100μL/min with no leakage.

In conclusion, a generic Slipchip design standard and operational platform has been presented. Fast prototyping methods are discussed and an *in situ* droplet generator is demonstrated. The Slipchip *in situ* droplet generation strategy will be used for protein isoelectric focusing separation in the next chapter.

Chapter 4

Isoelectric Focusing with a Slipchip

4.1 Introduction

A design of Slipchip together with a fast prototyping method was presented in chapter 3. This chapter describes the development of a Slipchip device that is able to efficiently compartmentalize IEF focused analyte bands *in situ* into micro-droplets. The device contains a microfluidic zig-zag separation channel that is composed of a sequence of wells formed in the two halves of the Slipchip. The analytes are focused in the channel and then compartmentalised into droplets by slipping the chip. Importantly, sample droplets can be analysed on-chip or collected for subsequent analysis, for example by electrophoresis or mass spectrometry. As proof of principle of this approach, IEF separation using standard pI markers and protein samples was performed, together with on-chip pH calibration. Compared to alternative approaches for sample collection, the method is free of re-mixing, scalable and easily hyphenated with the other analytical methods.

4.1.1 Theory of IEF

Isoelectric focusing (IEF) is a technique that separates and focuses complex mixtures of amphoteric molecules like proteins according to their isoelectric points (pIs). Amphoteric molecules like amino acids and proteins contain both acidic and basic groups such as carboxylic acid group (R-COOH) and amine group ($R\text{-}NH_3$). They can be ionized to make the molecule negatively or positively charged (Figure 4-1A), the net charge of the molecule depends on the pH of the surrounding environment. In an acidic environment, the molecule will gain a proton and become positively charged, and in a basic environment it will lose a proton becoming negatively charged. There is a pH at which the magnitude of the positive charge on the molecule equals the

negative charge and the net charge is zero. This is called the isoelectric point (pI). Therefore, an amphoteric molecule is positively charged in a pH value below its pI, and negatively charged in a pH value above its pI. When amphoteric molecules like proteins are placed in a pH gradient and subjected to an electric field, the molecules will move toward the electrode with opposite charge. During migration through the pH gradient, proteins will pick up or lose protons, and ultimately focus to a point where the pH is equal to their pIs (Figure 4-1B), allowing proteins to be separated. IEF is already routinely used in labs, and recognised as one of the most powerful techniques for protein purification and separation.

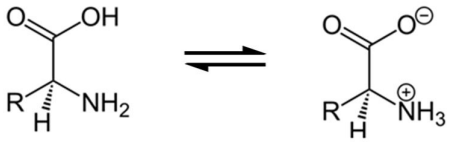

(A)

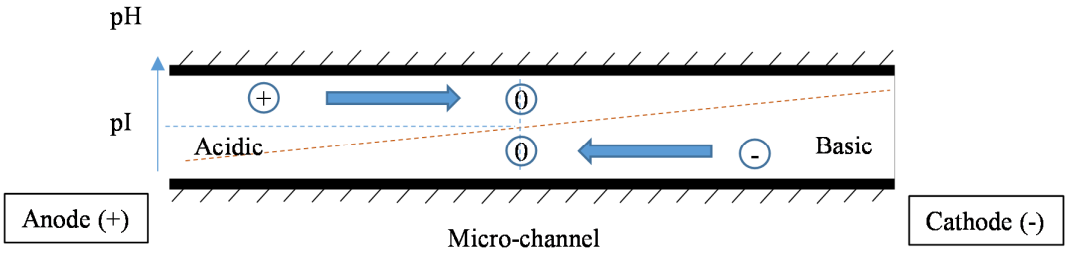

(B)

Figure 4-1: (A) Ionization of an amino acid molecule. (B) Movement of amphoteric molecules in a pH gradient in a channel during the application of an electric field.

4.1.2 Literature review

IEF separation of protein mixtures was first described almost 60 years ago (Kolin, 1955). Since then, there have been many embodiments of the IEF separation process. A good example is a gel-based IEF using an immobilized pH gradient (IPG) gel (Bjellqvist *et al.*, 1982, Gorg *et al.*, 1998,

Gianazza and Righetti, 2009). The IPG gel is based on a polyacrylamide matrix co-polymerized with a pH gradient. The pH gradient is obtained by a continuous change in the ratio of immobiline (a weak acid or base defined by its *pK* value), which gives a completely stable gradient (Gorg *et al.*, 2009). IPG is the first dimension in 2-dimensional gel electrophoresis for protein separation and analysis (Figure 4-2), followed by Sodium Dodecyl Sulphate – Poly-Acrylamide Gel Electrophoresis (SDS-PAGE), which is the second dimension that separates molecules according to mass. A good recent review of 2D gel separation is given by (Rabilloud *et al.*, 2010).

After separation in a polyacrylamide gel, the proteins can be electrophoretically transferred to a nitrocellulose membrane, and then analysed by staining with antibodies specific to the target protein (Renart *et al.*, 1979, Towbin *et al.*, 1979), a method called Western Blot or Immunoblot. The gel containing the IEF separated proteins or peptides can also be cut manually (using a scalpel) (Geiser *et al.*, 2011), to enable the proteins or peptides to be extracted and purified for downstream analysis using techniques such as Liquid Chromatography (LC) or Mass Spectrometry (MS). However, this method is labour intensive and low efficiency.

Another method of forming a pH gradient is with carrier ampholytes (CAs). CAs are mixtures of small molecules (about 300-1000Da) with closely spaced pIs and high conductivity. Normally, the CAs are included in an IEF gel within a container like a capillary or a small channel, the ends of which are connected to two reservoirs filled with anolyte (acidic solution) and catholyte (basic solution). When an electric field is applied, the CA molecules move to their pIs, buffering the medium at this point and producing a smooth pH gradient. The pH range of the gradient is determined by the range covered by CAs. The pH values of the anolyte and catholyte should be outside the pH gradient range to provide sufficient capability to provide or accept protons.

Capillary IEF (cIEF) is a method that uses CAs to generate the required pH gradient (Righetti *et al.*, 2007b, Silvertand *et al.*, 2009, Sobrova *et al.*, 2012, Salplachta *et al.*, 2012, Righetti *et al.*, 2013). In cIEF, protein samples are mixed with CAs and inserted into a long and thin capillary (fused silica or Teflon (Liu and Pawliszyn, 2003)). The capillary connects the anolyte and catholyte reservoirs and an electric field is applied via electrodes immersed in the anolyte and catholyte reservoirs. IEF separation occurs within the capillary.

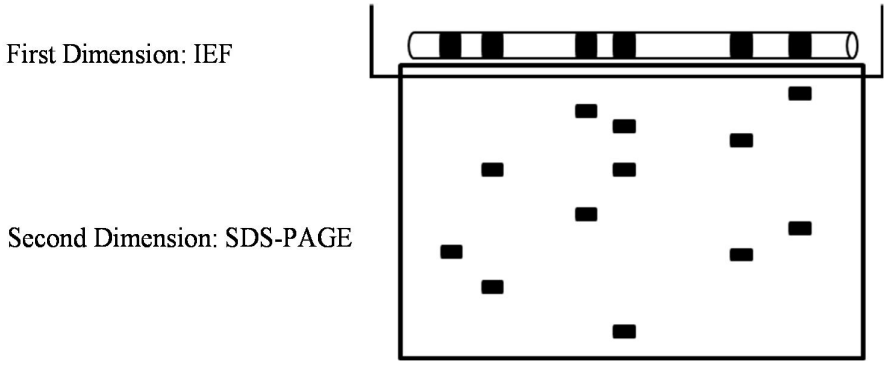

Figure 4-2: IEF in IPG gel for the first dimensional separation in 2-D gel electrophoresis to separate proteins by the pIs, the second dimension is Sodium Dodecyl Sulphate – Poly-Acrylamide Gel Electrophoresis (SDS-PAGE), which separates proteins according to the mass.

Microfluidic chip-based IEF (μIEF) (Cui *et al.*, 2005a, Cui *et al.*, 2005b, Dolnik and Liu, 2005, Chen and Fan, 2009) also uses carrier ampholytes to provide the required pH gradient. It reduces the size of the capillary by using a small microfluidic chip, such as a PDMS channel as shown in Figure 4-3(Cui *et al.*, 2005a). μIEF has the advantage of very low sample consumption, like cIEF, and also has the potential for high throughput and automatic hyphenation to analytical methods such as mass spectrometry (Silvertand *et al.*, 2009).

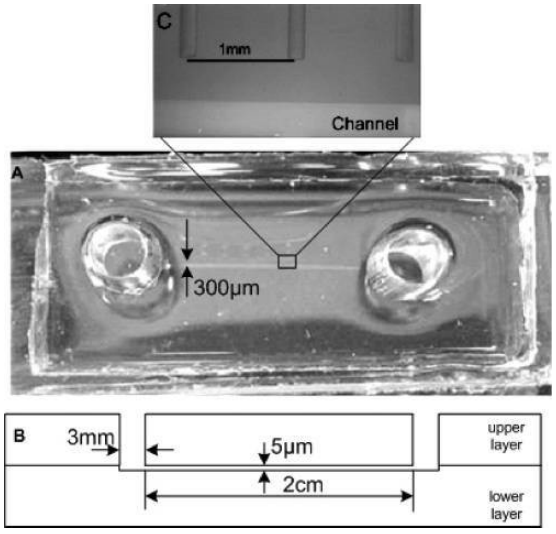

Figure 4-3: A PDMS IEF microchip. The chip has a 2cm-long separation PDMS channel with dimension of 300μm × 5μm. From (Cui *et al.*, 2005a).

Samples separated by cIEF or µIEF are normally analysed using UV absorption (Shimura *et al.*, 2000) or Laser Induced Fluorescence (LIF) as presented in (Liu and Pawliszyn, 2003) and (Ramsay *et al.*, 2009). The commercial iCE280 cIEF system (ProteinSimple Ltd. California, US) shown in Figure 4-4 uses whole column UV absorption to detect samples in the capillary.

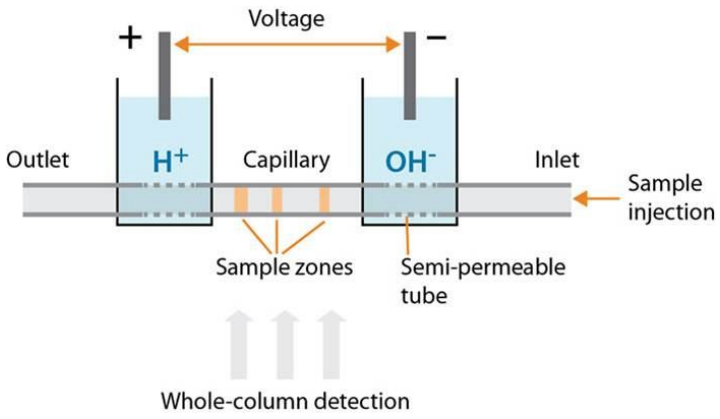

Figure 4-4: Commercialised iCE 280 cIEF system from ProteinSimple Ltd. (California, US). The whole-column UV absorption detection method is used.

cIEF and µIEF consume extremely small amounts of sample compared to other methods and have the potential for high throughput operation and automatic hyphenation to downstream analytical methods such as electrophoresis or mass spectrometry (Yu *et al.*, 2006, Silvertand *et al.*, 2009, Weiss *et al.*, 2010). Miniaturized two-dimensional electrophoresis systems have been presented (Emrich *et al.*, 2007). However, hyphenation of miniaturised IEF platforms with other analytical methods is not without challenges. Indeed, a significant hurdle remains in how to collect the discrete separated bands for subsequent transfer to a downstream analytical system. The focused analyte can be removed from the capillary or microchannel by pressure-driven flow (Huang *et al.*, 1994, Yu *et al.*, 2006, Hua *et al.*, 2010), electroosmotic flow or chemical mobilization (Ramsay *et al.*, 2009, Zhong *et al.*, 2011b). In the system shown in Figure 4-5, separation was processed in a capillary. The separated sample was pumped through the capillary and compartmentalized at the end by spotting onto a matrix-assisted laser desorption/ionization (MALDI) plate for MS analysis (Weiss *et al.*, 2010). However these methods introduce dispersion and remixing of the focused bands during sample migration, negating many of the advantages of the technique. To address this limitation, a method to cut the separated sample into 8 fractions was presented (Righetti *et al.*, 2007a). Similar systems for IEF separation in a single droplet have been presented (Egatz-Gomez and Thormann, 2011, Weiss *et al.*, 2011) where the large droplet

was cut into two after separation (Figure 4-6). This method demonstrated *in situ* compartmentalization, but the resolution was very poor (just two compartments), with very low throughput. Very recently, *Wang et al.* presented a rotary valve which can create fractions after IEF in a capillary loop (Wang *et al.*, 2013). The analyte collection is diffusion free, but the system is very complicated.

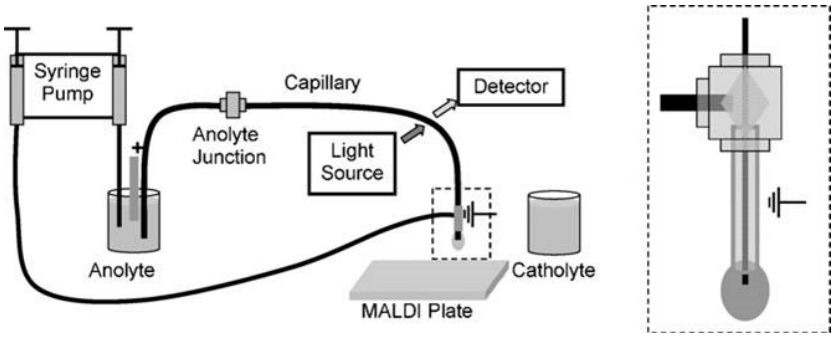

Figure 4-5: Schematic illustration of experimental system performing IEF in a capillary, then mobilizing focused sample out with pressure driven controlled by a syringe pump. The sample is compartmentalized at the end of capillary and spotted on a matrix-assisted laser desorption/ionization (MALDI) plate for Mass Spectrometry (MS) analysis. From (Weiss *et al.*, 2010).

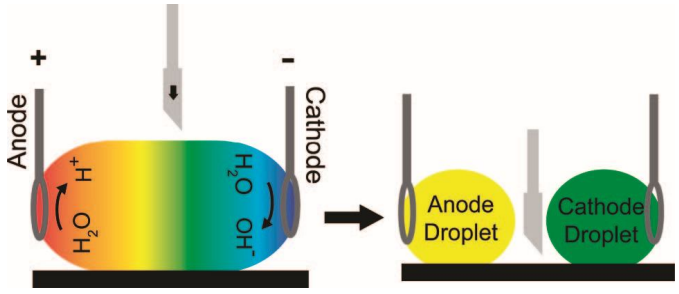

Figure 4-6: Schematic drawn of IEF in a single droplet. After sample separation, the droplet was split with a scalpel. From (Weiss *et al.*, 2011).

Free flow IEF (FF-IEF) is an embodiment of microfluidic based separation, where IEF is performed in a laminar flow. The separated species are collected by dividing the flow stream into several different outlets (Wen *et al.*, 2010b). A FF-IEF system that can compartmentalize the separated sample into 96 fractions has been commercialized (FFE Service GmbH, Munich, Germany). However, FF-IEF consumes samples in mg quantities, much more than cIEF or µIEF,

and the miniaturized system like the microfluidic FF-IEF device shown in Figure 4-7(Wen *et al.*, 2010a) has not yet been shown to provide high separation resolution and throughput.

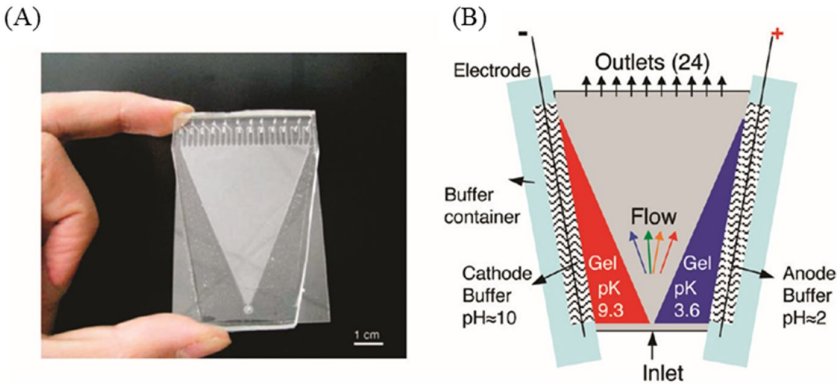

Figure 4-7: (A) Image of a microfluidic free flow IEF device. (B) Schematic of Microfluidic FF-IEF system. Functionalized pH gradient polyacrylamide gels are polymerized into the gel regions connected to the separation channel. Posts are included in the gel regions for support. The device is 50mm by 75mm with the centre triangular separation channel 46mm wide at the top and 56mm long. All channels and gel sections have a depth of 160µm. From (Wen *et al.*, 2010a).

4.1.3 Motivation

From the introduction, it can be seen that over the past 60 years, a large number of IEF systems have been developed, and some have been commercialized. The development of efficient and miniature IEF platforms remains a challenge, principally because of the difficulty in hyphenating miniaturised IEF platforms with the other analytical methods. Indeed, a significant hurdle remains in how to collect the discrete separated bands for subsequent transfer to a downstream analytical system.

In recent years, micro-droplets formed within microfluidic channels have been shown to be useful for compartmentalizing chemically separated components. For example, Niu *et al.* demonstrated compartmentalisation of samples separated by both liquid chromatography (Niu *et al.*, 2009, Pereira *et al.*, 2013) and capillary gel electrophoresis (Draper *et al.*, 2012), while Edgar *et al.* presented a method for segmentation of Capillary Electrophoresis (CE) separated samples into

nL-volume droplets (Chiu, 2010). In each case, the droplets could be further analysed by CE (Niu *et al.*, 2009) or MS (Edgar *et al.*, 2009, Pereira *et al.*, 2013). However, it should be noted that compartmentalisation is typically performed at a fixed point (normally at the outlet) for both LC and CE. Such an approach is not applicable to IEF, where focused analytes are distributed along the pH gradient. To this end, the scalpel cutting method is capable for *in situ* compartmentalization (Geiser *et al.*, 2011, Weiss *et al.*, 2011); although it is labour intensive with low resolution and efficiency, it demonstrates a method for eliminating the diffusion and re-mixing by *in situ* compartmentalizing separated samples.

The Slipchip droplet generator described in the last chapter is capable of *in situ* sample compartmentalization. This chapter presents a Slipchip device for sample *in situ* compartmentalization after isoelectric focusing separation, the first application of a Slipchip for separation.

4.2 Experimental section

4.2.1 Device and experimental setup

A Slipchip device that incorporates microfluidic IEF separation followed by *in situ* compartmentalisation is shown schematically in Figure 4-8(A-C). The working principle is as follows: a sequence of wells is patterned in two halves of a Slipchip plate. These wells are first aligned to form a zig-zag channel. IEF sample is loaded into this channel and electrolyte loaded into the reservoir inlet/outlet holes. Electrodes connected to a power supply are immersed into the electrolyte (Figure 4-8A). When an electric field is applied, a pH gradient is established and analytes are focused along the channel due to the electric field (Figure 4-8B). After IEF separation, the wells are disconnected by slipping the chip, leaving the separated analyte in isolated compartments (i.e. single droplets) in each of the wells (Figure 4-8C). This compartmentalization strategy is an *in situ* method and occurs via a single slipping operation; sample mobilization is not necessary so that re-mixing during sample migration is almost eliminated. The compartments containing samples with different pIs can then be collected by removal from the wells for post-processing on chip.

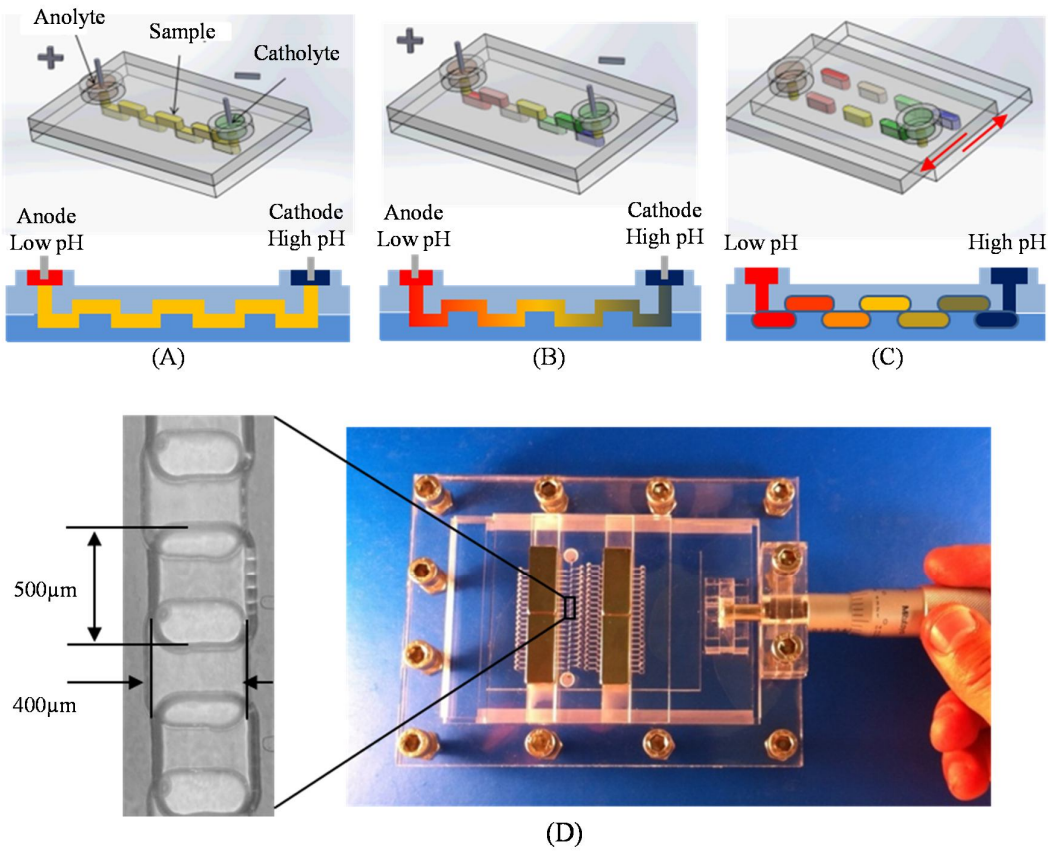

Figure 4-8: Principle of the Slipchip as used for IEF separation and *in situ* compartmentalization. Wells are formed into a continuous "zig-zag" channel by slipping the chip; sample is loaded in the channel, anolyte and catholyte is added in the reservoirs separately and platinum wire electrodes are placed in the reservoirs in contact with electrolyte (A). An electric field is applied and a pH gradient is formed in the zig-zag channel by CA. The protein molecules move along the pH gradient and focus to their pI so that different wells contain samples with different pIs (B). After focusing, wells are isolated by slipping the chip. Proteins with different pIs are compartmentalized into droplets in different wells (C). To prevent focused bands remixing, the electric field is stopped after droplet formation. (D) Picture of whole device. Magnets are used for clamping, and a micro-meter drive is used for precise control.

The device design and fabrication was based on the generic Slipchip platform described in Chapter 3. Two reservoirs for the anolyte and catholyte were placed on the top plate and connected

to the separation channel via inlet/outlet holes. The dimensions of each droplet well were 400µm × 500µm and 250µm deep, giving a well volume of 50nL (Figure 4-8D). The separation channel consisted of 141 wells in series (71 on the top plate and 70 on the bottom plate), with associated inlet and outlet holes. The total length is 5cm giving a total sample volume of 7µL. The acrylic plates were micro-milled using a LPKF Protomat S100 milling machine (LPKF Laser & Electronics Ltd, Berkshire, UK) as described in section 3.3.3, and post-processed for surface treatment as described in section 3.4. The operation mechanism presented in section 3.2 was used to control the slipping. Figure 4-8D shows an image of the entire device.

300µm diameter platinum wires (Goodfellow Cambridge Ltd.) were used as electrodes and connected to an LKB 2197 high voltage DC power supply (LKB, Bromma, Sweden), a multi-meter was used to monitor the current continuously. Fluorescent IEF markers were used to indicate the focusing, the fluorescence was imaged with a Zeiss LSM 5 confocal fluorescence microscope using a DAPI (4',6-diamidino-2-phenylindole) filter set, whose excitation wavelength is 352-402nm, and emission wavelength is 417-477nm. The schematic of the experimental setup is shown in Figure 4-9.

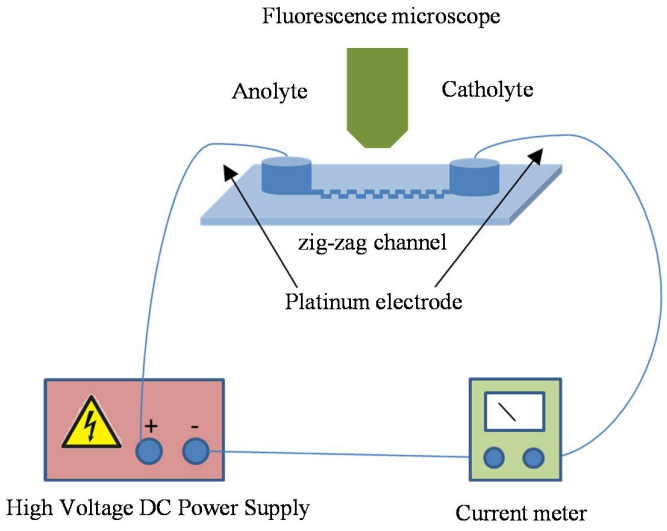

Figure 4-9: Schematic diagram of a Slipchip IEF experimental setup. The PMMA zig-zag microchannel Slipchip is made by micro milling with platinum wires for electrodes. A high voltage DC power supply provides the electric field and a current-meter records the current in the channel. A fluorescence microscope (DAPI filter) is used to observe focusing in the channel.

In Figure 4-9, the microscope was working in Epi-fluorescence mode, by programming the movement of microscope stage, the entire channel was imaged by moving the chip with respect to the microscope objective at a speed of 4.5mm/second, and a video was recorded at the frame rate of 45fps, so each frame was a fluorescence microscopy image of the 100µm long channel. The video was analysed with ImageJ software, by calculating the average fluorescence intensity in the 100µm long channel in each frame, the focusing of fluorescent markers can be observed.

When the zig-zag channel was filled with sample and applied electric field, the current density distribution in the 3D channel was simulated with COMSOL Multiphysics software (COMSOL, Inc., MA, US) as shown in Figure 4-10. A segment of zig-zag channel with 3 wells was used in the simulation, the electric filed strength was 100V/cm. The current was not uniformly distributed in the channel. The current density was high along the central of the channel, the highest current density was 4.51×10^4 A/m^2; while the lowest current density was 4.51×10^{-3} A/m^2, which was on the corner of the wells.

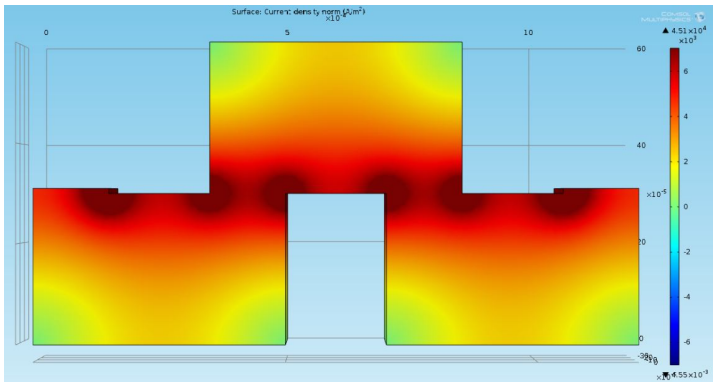

Figure 4-10: Comsol simulation of the current density distribution in zig-zag channel.

4.2.2 Sample preparation

IEF buffer was prepared from 3M Urea cIEF gel (Beckman Coulter, Buckinghamshire, UK), 3% Pharmalyte pH 3-10 broadband carrier ampholyte (GE Healthcare Life Sciences, Buckinghamshire, UK), 0.5mM Iminodiacetic acid (Sigma-Aldrich, Dorset, UK), 6mM L-Arginine (Sigma-Aldrich, Dorset, UK), and 3% (w/v) Hydroxypropyl methylcellulose (HPMC) (Sigma-Aldrich, Dorset, UK). Additionally, 26mM H_3PO_4 (Sigma-Aldrich, Dorset, UK) and

4mM NaOH (Sigma-Aldrich, Dorset, UK) in cIEF gel with 3% (w/v) HPMC were prepared as the anolyte and catholyte respectively.

Five IEF protein markers (Trypsin Inhibitor, β-Lactoglobulin A, Carbonic Anhydrase Isozyme II, Myoglobin, and Lectin) from Sigma-Aldrich (Dorset, UK) were obtained as lyophilized powder and reconstituted according to the manufacturer's instructions, i.e. 4mg/ml of protein in 200mM glycine. Lectin and Carbonic Anhydrase Isozyme II were further diluted to 2mg/mL, and Trypsin Inhibitor β-Lactoglobulin A and Myoglobin were further diluted to 0.5mg/mL as the stock for IEF experiment. Three fluorescence pI markers (pI 4.0, 6.2, and 8.1) (Sigma-Aldrich, Dorset, UK) were used to indicate the focusing. Finally, 3μL of each protein stock solution and 3μL of each fluorescence pI marker were mixed in 400μL IEF buffer.

4.3 Results

4.3.1 IEF separation

As described in section 3.4.4, prior to use 3M™ Fluorinert™ Electronic Liquid FC-40 oil was injected between the two plates to wet both surfaces. The oil creates a seal preventing leakage and also acts as a lubricant (Du *et al.*, 2009). After device assembly, the wells on both plates were aligned by rotating the micro-meter drive and connected to form a continuous "zig-zag" channel. 7μL IEF sample was loaded into the separation channel with a syringe pump at the flow rate of 1μL/s. Subsequently anolyte and catholyte were loaded into the reservoirs simultaneously with two pipettes. The Platinum wire electrodes were immersed in the electrolytes and connected to the high voltage power supply.

The formation of a uniform pH gradient is a critical step in IEF; pH gradient squeezing and drift affect the stability and reproducibility in CA based IEF systems like cIEF and μIEF. In the CA based IEF system shown in Figure 4-11, the liquid phase sample and CA mixture contacts the liquid phase electrolyte. At the anolyte-sample boundary, as the pH value of anolyte is lower than that of CA, the H^+ concentration of the anolyte is higher than that of the CA, and therefore the H^+ in anolyte may diffuse into the sample mixture. The same thing happens on the cathodic side; the OH^- in the high pH catholyte also diffuse into the sample mixture, so the electrolyte-sample

boundaries will move to the middle of the channel (Mosher *et al.*, 1988), i.e. the pH gradient is squeezed.

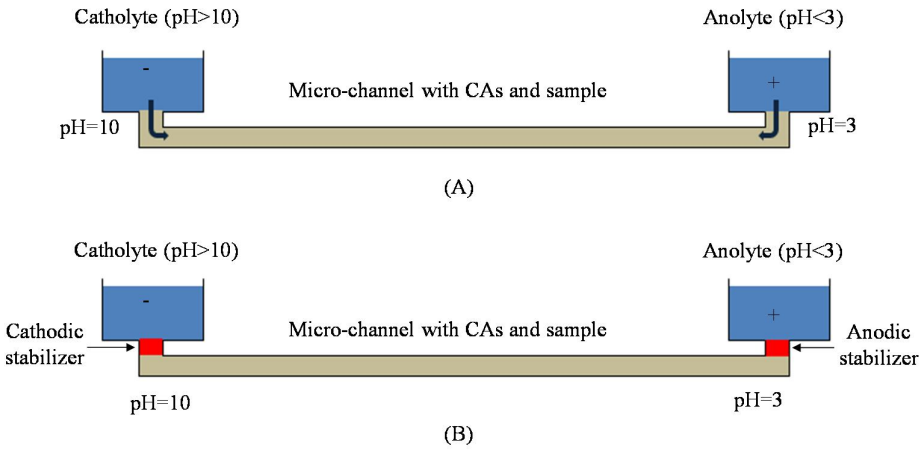

Figure 4-11: Schematic showing the function of the stabilizer in cIEF. The liquid phase sample contacts the liquid phase electrolyte. (A) The ions in the sample and electrolytes are exchanged so that the boundary of electrolyte and sample mixture is moved to the middle of the channel squeezing the pH gradient. (B) Stabilizers form barriers between the sample mixture and electrolytes to prevent chemical boundary movement.

To prevent chemical boundary movement, stabilizers were used to create a barrier between sample mixture and electrolytes (Mosher and Thormann, 1990). Stabilizers are high- conductivity molecules; the pI of the anodic stabilizer should be lower than that of the CA and higher than the pH of the analyte; similarly the pI of the cathodic stabilizer should be higher than that of the CA and lower than the pH of the catholyte. Mack *et al.* used L-Arginine and Iminodiacetic acid as barriers between IEF buffer and electrolyte, and used H_3PO_4 and NaOH as anolyte and catholyte solution (Mack *et al.*, 2009), which is now a standard protocol for the commercial cIEF system supplied by Beckman Coulter, Inc. and used in this research.

The standard cIEF protocol (for 50 μm I.D., 30.2 cm long capillary) commercialised by Beckman Coulter, Inc. was firstly used in this Slipchip IEF device, in which the Anolyte was 200mM Phosphoric Acid in DI water, Catholyte was 300mM Sodium Hydroxide in DI water; the sample buffer was made 5% (v/v) Pharmalyte 3-10 CA, 41.7mM L-Arginine as cathodic stabilizer, 1.7mM Iminodiacetic acid as Anodic stabilizer and 1% (v/v) of three fluorescence pI markers (pI 4.0, 6.2, and 8.1) in 3 M urea-cIEF Gel. The electric field strength applied was 100V/cm. Before

applying the electric field, a uniform fluorescence was observed in the channel. When the electric field was applied, the fluorescence was quickly squeezed to the centre and disappeared in less than one minute.

According to Mosher's boundary movement theory (Mosher *et al.*, 1988), this can be explained as the electrolyte was mixed with the sample and moved the boundary to the middle. If this is correct, increasing the stabilizers' concentration will provide a longer space area and prevent the squeezing. The concentration of cathodic stabilizer (L-Arginine) was then increased to 61.5mM, and the concentration of Anodic stabilizer (Iminodiacetic acid) was increased to 15.4mM. After applying electric field, 3 highlight points can be clearly observed in the channel after about 3 minutes, but squeezing was still severe and the entire fluorescence band was disappeared in about 7 minutes.

Increasing the viscosity of the sample and electrolyte can also prevent this squeezing (Cui *et al.*, 2005a), because according to the Stokes-Einstein equation, the diffusion rate D is inversely proportional to the viscosity η; and reducing the pH difference of sample and electrolytes can also reduce the speed of this squeezing (Mosher *et al.*, 1988). To do this, the consentration of electrolyte was reduced to 26mM H_3PO_4 and 4mM NaOH, and was prepared in IEF gel instead of DI water. After applying the electric field, fluorescence peaks started to be observed after about 3 minutes, and be stabled after 30 minutes. A fluorescence intensity profile shown in Figure 4-12 was measured.

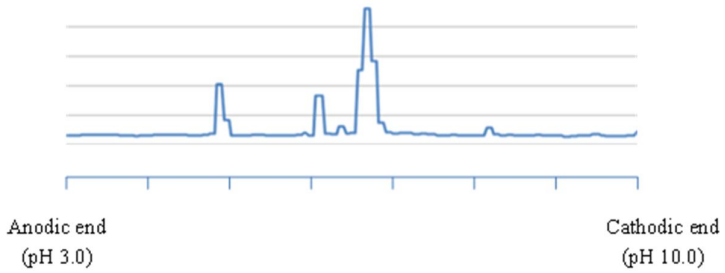

Figure 4-12: The fluorescence intensity profile measured after 30 minutes of focusing under the electric field of 100V/cm. The protocol was, Anolyte: 26mM Phosphoric Acid in 3 M urea-cIEF Gel; Catholyte: 4mM Sodium Hydroxide in 3 M urea-cIEF Gel; the sample buffer: 5% (v/v) Pharmalyte 3-10 CA, 61.5mM L-Arginine, 15.4mM Iminodiacetic acid and 1% (v/v) of three fluorescence pI markers (pI 4.0, 6.2, and 8.1) in 3 M urea-cIEF Gel.

From Figure 4-12, three clear peaks can be measured, which were the focused fluorescence markers, but the sample was still squeezed. For a uniform pH gradient in a 5cm long channel, the theoretical distance of the pI 4.0 peak and pI 8.1 peak can be simply calculated. The pH range formed by CAs is 3-10, so the distance of pI 4.0 and pI 8.1 in a uniform pH gradient should be 5×(8.1-4.0)/(10-3), which is 2.9cm. From Figure 4-11, the distance from pI 4.0 peak and pI 8.1 peak was about 1.3mm.

HPMC was reported being used in IEF (Cui *et al.*, 2005a, Kohlheyer *et al.*, 2006), which can increase the fluid viscosity. To investigate optimizing sample compression by adding HPMC, a study shown in Figure 4-13 was performed. In Figure 4-13, sample (a) contained no HPMC in either sample or electrolyte; sample (b) contained 1% (w/v) HPMC and sample (c) contained 3% (w/v) HPMC in sample and electrolytes. After 30 minutes focusing with an electric field of 100V/cm with the sample without HPMC (experiment (a)), the distance between these two peaks was 1.3cm, 44.8% of the theoretical value; for sample (b), the distance of the pI 4.0 and pI 8.1 peaks was 1.8cm, 62.1% of the theoretical value; the distance of the pI 4.0 and pI 8.1 peaks for sample (c) was 2.8cm, 96.6% of the theoretical value. No obvious improvement was observed with further increase of HPMC concentration. Too much HPMC made the liquid very viscose, and made sample and electrolyte difficult to load, so therefore the 3% (w/v) HPMC was used in the sample and electrolytes.

In this case, reducing concentration of stabilizers did not observe clear difference of peak profile. But when the concentration of Iminodiacetic acid is lower than 0.3mM, sample squeezing from anodic side was observed, so the Iminodiacetic acid concentration of 0.5mM was selected. The same reason, the L-Arginine concentration was selected at 6mM.

For a theoretical prediction, at the beginning of the focusing, the fluorescence markers are uniformly distributed in the channel, so the fluorescence intensity should be uniform along the channel. After applying electric field, the markers will be focused gradually to the pI points. For the current, the charged molecules in the sample, which are the current carriers, will be moved by the electric field to their pI points, so there will be the most amount of current carriers at the beginning; during the focusing, more and more molecules will be staying at their pI points, the current will drop and be stable at the end. The plots shown in Figure 4-14 is the fluorescence profile recording during the 30 minutes focusing. One scan was performed every minute for the first 5 minutes, and then once every 5 minutes thereafter.

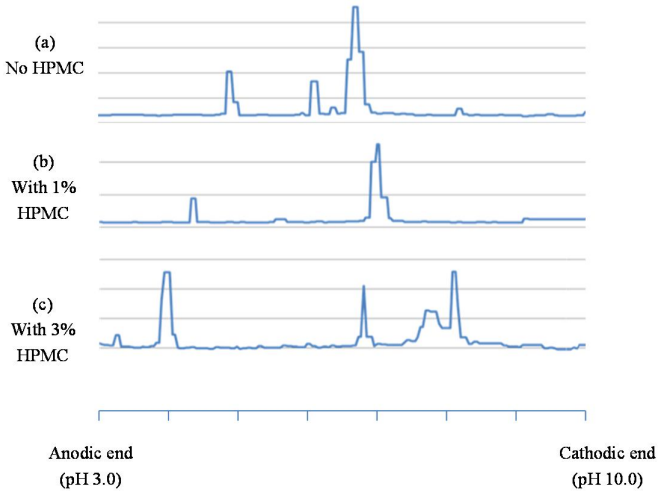

(A)

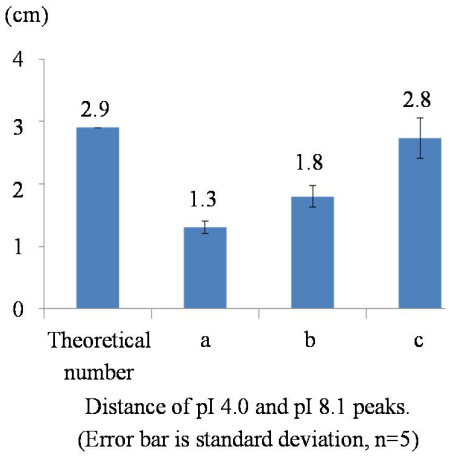

(B)

Figure 4-13: Position of focused fluoresence bands in the channel for different HPMC concentrations in the sample mixture and electrolyte after 30 minutes of focusing with an electric field of 100V/cm (A). The distance of pI 4.0 and pI 8.1 peaks for diffent HPMC concentration (B). HPMC increases the viscosity of the sample and electrolyte thereby reducing diffusion. Sample (a) does not contain HPMC, the distance of pI 4.0 peak and pI 8.1 peak is 1.3cm, that is 44.8% of the theoretically calculation. Sample (b) contains 1% (w/v) HPMC in both electrolytes, and the distance of the pI 4.0 and pI 8.1 peaks is 1.8cm, 62.1% of the theoretically number. Sample (c) contains 3% (w/v) HPMC; the distance of pI 4.0 and pI 8.1 peaks is 2.8cm, 96.6% of the theoretically number.

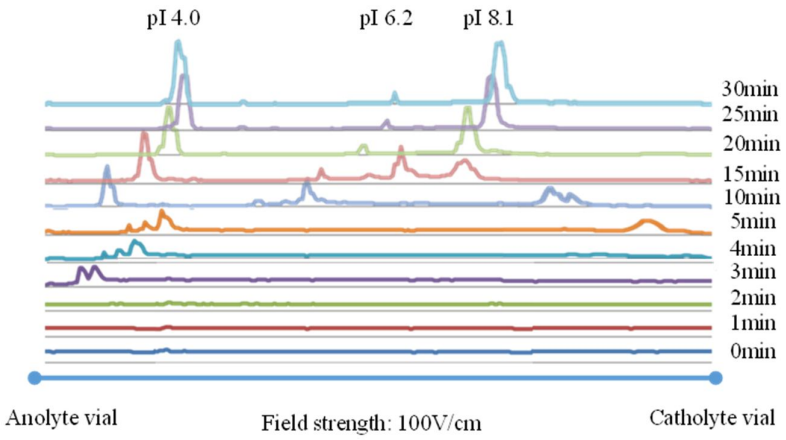

Figure 4-14: Time traces of fluorescence intensity along the separation channel. Three fluorescence pI markers (pI 4.0, 6.2 and 8.1) were used. The channel dimension was 400µm wide, 250µm deep and 5cm long; the field strength was 100V/cm. At the beginning the fluorescent pI markers are uniformly distributed in the channel, producing a uniform fluorescence intensity. After 30 minutes of focusing, the three fluorescence markers are at their pIs, and three fluorescence peaks are clearly visible.

In Figure 4-14, at the beginning of an experiment, the fluorescence intensity was uniformly distributed along the channel, indicated fluorescent pI markers were uniformly distributed in the channel. After 30 minutes of focusing, the three fluorescence markers were focused at stable positions with three fluorescence peaks. The left peak was about 7.2mm to the anolyte vial, which was the position of pI 4.9 marker. The half peak width was 0.7mm, which was counted from the point where fluorescence intensity is higher than three times of background noise. The middle peak was about 22.9mm to the anolyte vial with half peak width of 0.1mm, it was the pI 6.2 position; and the right peak was about 36.5mm to the anolyte vial with the half peak width of 0.9mm, it was the position of pI 8.1 marker. The electric current in the channel was 180µA at the beginning of the focusing, which is the peak current point (Figure 4-15), and it was dropping during the IEF focusing, at the end the current dropped to a stable value of about 12µA, which fits to the theoretical analysis mentioned above. The fluorescence marker was photo-bleached after exposing to excitation light, the fluorescence intensity in this case cannot be quantitatively analysed.

Figure 4-16 shows the average distance of the focused pI markers from the anodic end of the device, obtained from 25 repeats on 5 devices. It can be seen that the position of pI 4.0 marker

(the distance of the focused peak to the anodic end) is highly reproducible with a relative standard deviation (RSD) of less than 3%. However, the error bar is larger for pI 6.2 marker, with RSD about 4%, and even worse for pI marker 8.1, with RSD about 7%. This trend was also observed by Mack *et al*. (Mack *et al.*, 2009), and is considered to be attributed to isotachophoresis (ITP), which can migrate the focused molecular bands in order of their mobility and may cause anodic drift (Mosher and Thormann, 1990). The time trace fluorescence intensity curve previous shown in Figure 4-12 also suggests that after about 25 to 30 minutes, ITP tends to dominate over IEF in the channel. This problem has been studied for decades (Righetti *et al.*, 2007b, Mack *et al*., 2009, Xu *et al.*, 2010, Pager *et al*., 2012), but further effort is still needed to optimise the protocol.

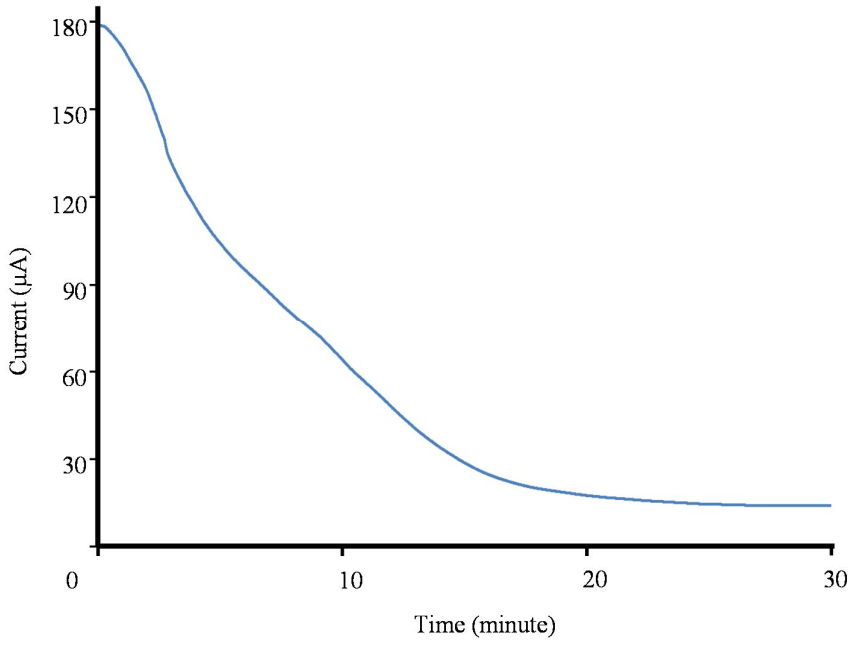

Figure 4-15: Current-time curve for an IEF separation with an electric field of 100V/cm. The channel dimension was 250μm wide, 250μm deep and 5cm long. At the beginning of an experiment, the current is at its peak value of 180μA, and then the current falls as IEF focusing occurs. After 30 minutes of focusing, the current drops to a stable value of about 12μA.

Another issue needs be considered in IEF is pH drift, it is thought to be mainly caused by Electro-Osmotic Flow (EOF), which occurs due to the formation of an electrical double layer on the surface-sample interface. In cIEF, EOF is employed to mobilise the separated sample, and in Beckman Coulter's protocol, 350mM Acetic Acid was used as chemical mobilizer. In the Slipchip

IEF system, compartmentalization is processed *in situ*; the separated sample does not need to be migrated, and a stable pH gradient is expected. HPMC has been added in the sample, which is used as a dynamic coating on the channel wall to reduce the surface charge density to suppress EOF (Cui *et al.*, 2005a, Kohlheyer *et al.*, 2006). In practice, by adding 3% HPMC in the sample mixture, EOF was not observed during the 30 minutes of IEF separation with an electric field of 100V/cm. The average RSD of the focused peak position of 4.9% (Figure 4-16) confirms that IEF separation can be performed reproducibly in the Slipchip. The positions of the three known pI markers fits with a linear distribution of pH gradient in the channel and no obvious drift was observed.

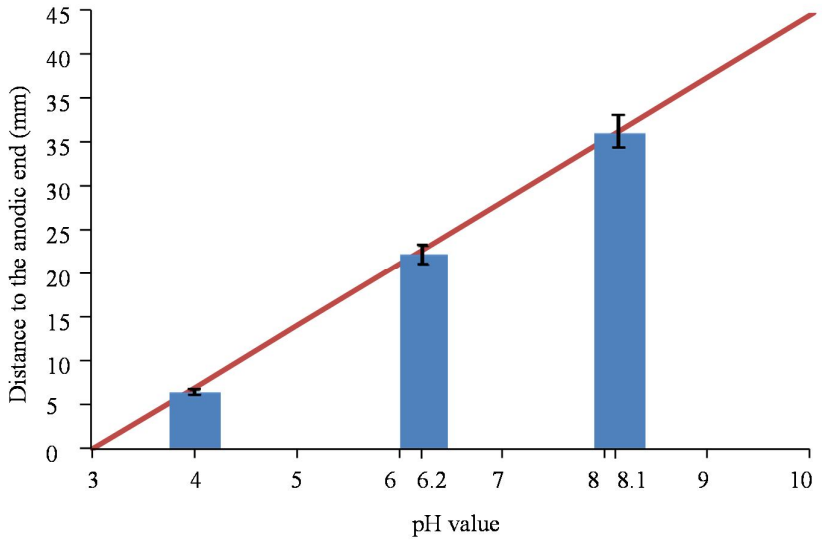

Figure 4-16: Average distance of the focused pI markers (pI 4.0, 6.2 and 8.1) from the anodic end of the device. Data were collected after 30 minutes of focusing at an electric field of 100V/cm. Results were obtained from 5 similar devices giving 25 repeats. The error bar is the standard deviation.

A comparison of focusing time with the literature is shown in Table 4-1. It can be seen that the focusing time varies for different IEF systems, depending on different capillary/channel dimensions, electric field strength, etc. Focusing is quick with high electric field strength and short separation channel length. The 30 minutes focusing time measured for this system is reasonable compared with the reported IEF devices.

Table 4-1: Comparison of focusing times with the literatures.

Reference	Channel/Capillary length	Electric field strength	Focusing time
This thesis	5cm	100V/cm	30 minutes
(Wang *et al.*, 2013)	120cm	83.3V/cm	2-3 hours
(Pager *et al.*, 2012)	81.3cm	200V/cm	14-24 minutes
(Weiss *et al.*, 2010)	50cm	300V/cm	20 minutes
(Shimura *et al.*, 2008)	2.4cm	500V/cm	2 minutes
(Das *et al.*, 2007)	1.7cm	118V/cm	5 minutes

4.3.2 *In situ* compartmentalization

In situ compartmentalisation was achieved by slipping the chip to disconnect the zig-zag channel, as described in section 3.4.4. In this experiment, IEF separation was performed with six pI markers (pI 4.0, 5.5, 7.2, 7.6, 8.1 and 9.0). After 30 minutes of IEF with an electric field of 100V/cm, the 6 pI markers were focused to their pIs (Figure 4-17A). The peak capacity of IEF separation can be calculated as $n = L/w \approx 140$, where L is the total channel length and w is a measure of the average analyte half peak width (Herr *et al.*, 2003). The half peak width was measured by analysing the florescence intensity with ImageJ software, and the theoretical minimum resolvable difference in isoelectric point $\Delta(pI) = (10-3)/140 = 0.05$.

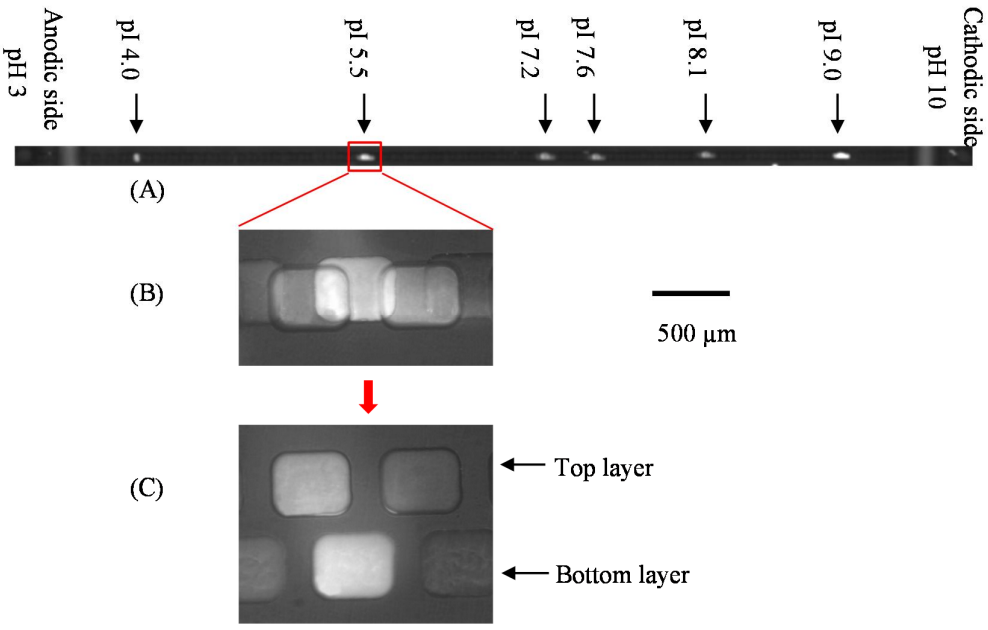

Figure 4-17: Fluorescence image of six focused pI markers (pI 4.0, 5.5, 7.2, 7.6, 8.1 and 9.0) in a zig-zag channel. (A) The whole channel before compartmentalization. (B) The focused pI 5.5 marker before compartmentalization; (C) By slipping the chip, the focused pI 5.5 marker was compartmentalized into a droplet in a well.

After IEF separation, the device was slipped perpendicular to the direction of the separation channel and the focused pI markers were encapsulated into droplets (Figure 4-17B and C). To avoid de-focusing, the electric field was maintained during slipping until the wells were completely separated and discrete droplets created. It should be noted that after compartmentalisation, analytes located in the same well (droplet) mix by molecular diffusion; therefore it is crucial that the number of wells in each chip should be at least equal to the peak capacity of the separation to prevent remixing of two or more focused peaks. The Slipchip device used in this chapter can make 141 droplets, which matches the peak capacity.

During slipping, no fluorescence was observed outside the wells, meaning that the oil prevents sample leakage and loss of sample. However, the Duxcoat hydrophobic coating can degrade with time causing some leakage between the plates. Therefore, the substrates have to be re-coated with Duxcoat after three runs. The Parylene C coating lasts much longer, but after approximately 50 runs, the PMMA chip was disposed of.

4.3.3 Droplet collection

Two methods were developed for collecting the compartmentalized droplets for further analysis, namely parallel collection and serial collection.

Serial collection is shown schematically in Figure 4-18A and B. A separation channel was made in the centre of the device, and two zig-zag collection channels were placed on both sides of the separation channel, pre-filled with FC-40 oil. The outlets of the collection channels were connected to tubing to collect the droplets. After compartmentalization, discrete droplets were moved to align with the collection channels forming a continuous conduit. The separated droplets were removed from the chip with a pressure-driven flow and collected into a tubing. Since the sequence of the droplets can be maintained in the tubing, the pI value of each droplet can be easily tracked from its relative position in the entire sequence of droplets.

Parallel collection is shown schematically in Figure 4-18C. As for serial collection, a separation channel was placed in the centre of the device. One well in the separation channel was connected with two collection ducts and two holes for collecting the sample in the well with a pipette. The distance of the collection holes was designed to fit with a multi-channel pipette (Figure 4-18D). This parallel collection method is especially suitable for on-demand collection of droplets, for example when collecting only those droplets containing analytes at particular pI values of interest, which will be demonstrated in section 4.3.4. For this method, extra collection ducts and holes need to be introduced, but due to fabrication limitations, the well density in this case cannot be as high as for the serial collection device. A parallel collection device with 29 wells was made, and the dimension of each well was 250μm × 1.7mm × 250μm, with a volume of 103nL. The total channel length was 5cm, so for a uniform pH gradient formed by Pharmalyte pH 3-10 broadband CAs, each droplet can cover a pH range of 0.24. Experiments were performed with 6 fluorescence pI markers (pI 4.0, 5.5, 7.2, 7.6, 8.1 and 9.0). A microscope image of focused pI markers is shown in Figure 4-19. It should be noted that the segment number for this device is 29, much less than the separation peak capacity (i.e. 140). It could be combined with downstream separation method to increase separation resolution.

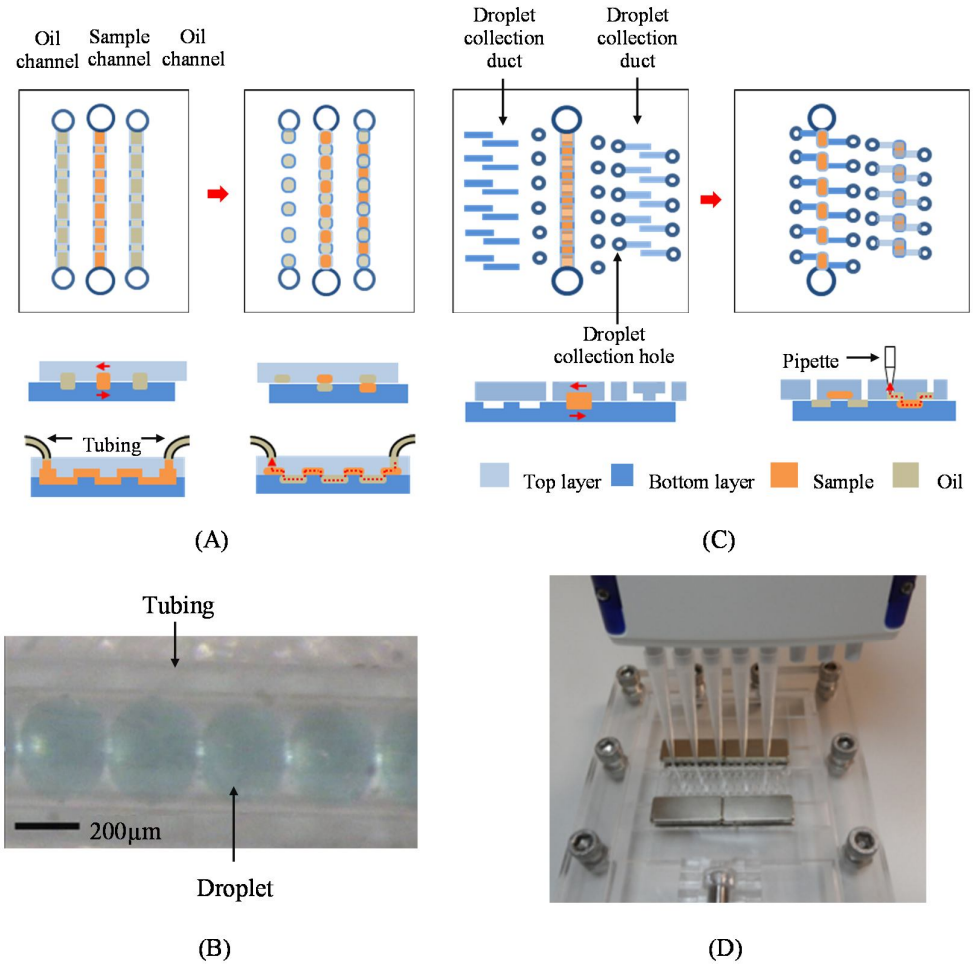

Figure 4-18: Serial and parallel droplet collection. (A) Schematic of serial droplet collection. Two zig-zag collection channels are placed on each side of the main separation channel and pre-filled with oil. The outlets of the collection channels are connected to tubing to collect droplets. (B) Microscope image of serially collected droplets in a length of tube. (C) Schematic of parallel droplet collection. Collection ducts and holes are fabricated on each side of the separation channel. After compartmentalization, the droplets are moved to the interface with the collection ducts and holes, facilitating droplet collection in parallel using a multichannel pipette. (D) Photograph of parallel droplet collection with a pipette.

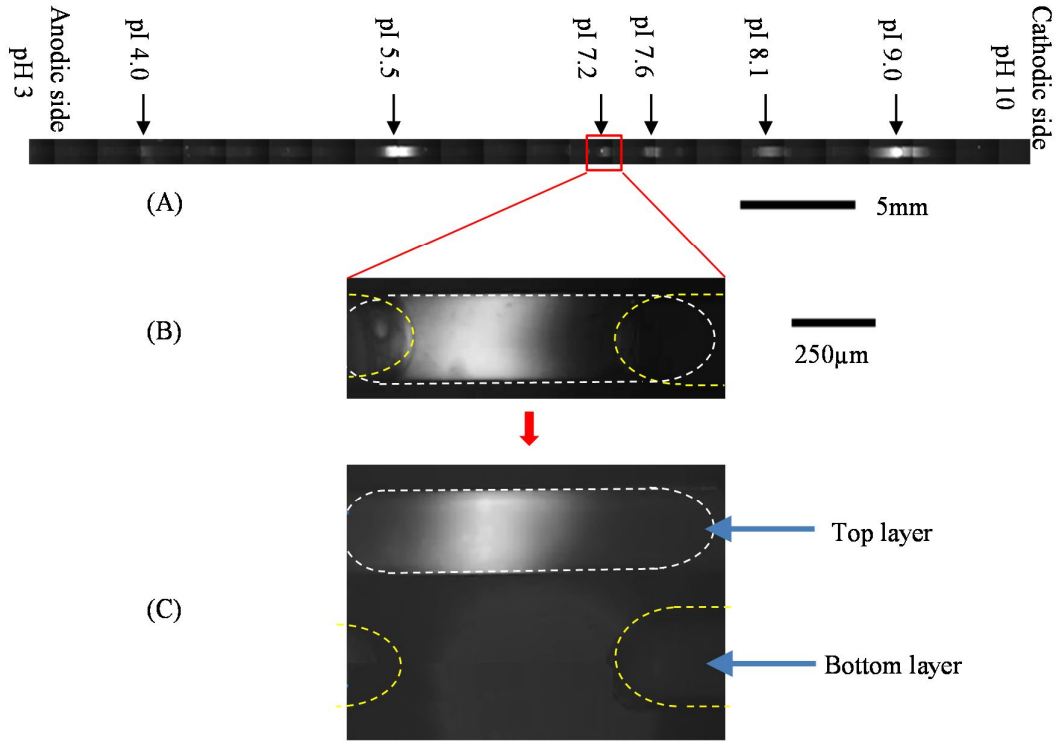

Figure 4-19: Focused fluorescence markers in the parallel collection channel. Fluorescence image of six focused pI markers (pI 4.0, 5.5, 7.2, 7.6, 8.1 and 9.0) in a zig-zag channel. (A) The whole channel before compartmentalization. (B) The focused pI 7.2 marker before compartmentalization; (C) By slipping the chip, the focused pI 7.2 marker was compartmentalized into a droplet in a well. The focusing was performed under electric field strength of 100V/cm for 30 minutes.

The measurement of droplet collection efficiency was performed by loading 100mM Rhodamine fluorescence dye in the zig-zag channel, generating droplets, collecting single droplet and then mixing with 206µL DI water. The concentration of the diluted Rhodamine solution is:

$$C = \frac{V}{206\mu L + V} \times 100mM \tag{4.1}$$

where V is the droplet volume collected, and the collection efficiency is:

$$E_{collection} = \frac{V}{103nL} \times 100\% \tag{4.2}$$

as $V \leq 103nL << 206nL$, equation (4.1) can be written as:

$$C = \frac{V}{206\mu L} \times 100mM \tag{4.3}$$

so

$$V = \frac{C}{100mM} \times 206\mu L \tag{4.4}$$

Combining (4.2) and (4.4):

$$E_{collection} = \frac{C}{50\mu M} \times 100\% \tag{4.5}$$

A microfluidic device with a 200µm × 200µm channel was made to load the diluted Rhodamine solution, and fluorescence intensity measurement were performed with a fluorescence microscope with a 10× objective lens and an exposure time of 10ms. First the fluorescence intensities of standard Rhodamine solution with concentrations of 30µM, 35µM, 40µM, 45µM and 50µM were measured. A plot of fluorescence intensity is shown in Figure 4-20. It can be seen that over this range, the fluorescence intensity is nearly linear with Rhodamine concentration.

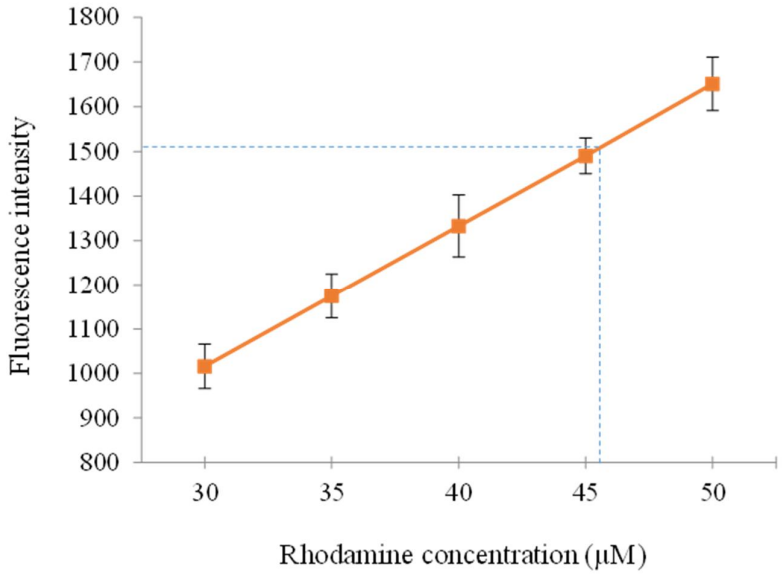

Figure 4-20: Fluorescence intensity of standard Rhodamine solutions. The standard solutions were loaded into a microfluidic channel with dimensions of 200µm × 200µm. The fluorescence was measured with a Zeiss LSM 5 confocal fluorescence microscope with a 10× objective lens with an exposure time was 10ms. The error bar is standard deviation, n = 5.

Seven individual compartmentalization operations were performed, and 5 droplets were collected from each operation, i.e. a total of 35 droplets were collected and analysed. The average fluorescence intensity of these 35 samples was 1508 with standard deviation of 61.8. These fluorescence intensity results correspond to the concentration of 45.5 (SD=1.92) μM. According to equation (4.5), the average collection efficiency was 91% (SD=3.8%).

4.3.4 Protein separation

As a proof of principle for the entire system, an IEF separation of a mixture containing 5 standard proteins was performed on the parallel collection chip described above. After 30 minutes separation with an electric field of 100V/cm, the sample was compartmentalised into droplets and collected for analysis using an Agilent 2100 Bioanalyzer.

Trypsin Inhibitor (pI 4.6, MW 20.1kDa), β-Lactoglobulin A (pI 5.1, MW 18.4kDa), Carbonic Anhydrase Isozyme II (pI 5.9, MW 29kDa), Myoglobin (pI 7.2, MW 17.7kDa), and Lectin (pI 8.2, MW 46kDa) were used. All these proteins are standard IEF markers and were obtained from Sigma-Aldrich (Dorset, UK). The pI range of the 5 protein markers is from 4.6 to 8.2, so a total of 21 single droplets was collected using the parallel collection device, covering the pH range from 3.7 to 8.6. To simplify verification, each single droplet was mixed with 3 consecutive droplets giving a total sample volume of 4μL.

These sample droplets were analysed directly. The carrier ampholyte and urea in the IEF gel can often affect resolution in CE, but all of the bands can be clearly distinguished in the electropherogram (Figure 4-21). Lane 8 is the control (mixture containing all 5 proteins) and has 5 bands. The other gel lanes show 2results obtained from each combined sample droplet. Lane 1 covers the pH range from 3.7 to 4.4. There is no protein in this range. Lane 2 covers the pH range from 4.4 to 5.1, where the Trypsin Inhibitor can be found. β-Lactoglobullin A has a pI of 5.1, and appears in lane 3. Carbonic Anhydrase Isozyme II, Trypsin Inhibitor and Myoglobin appear in lane 4, 6, 7 respectively.

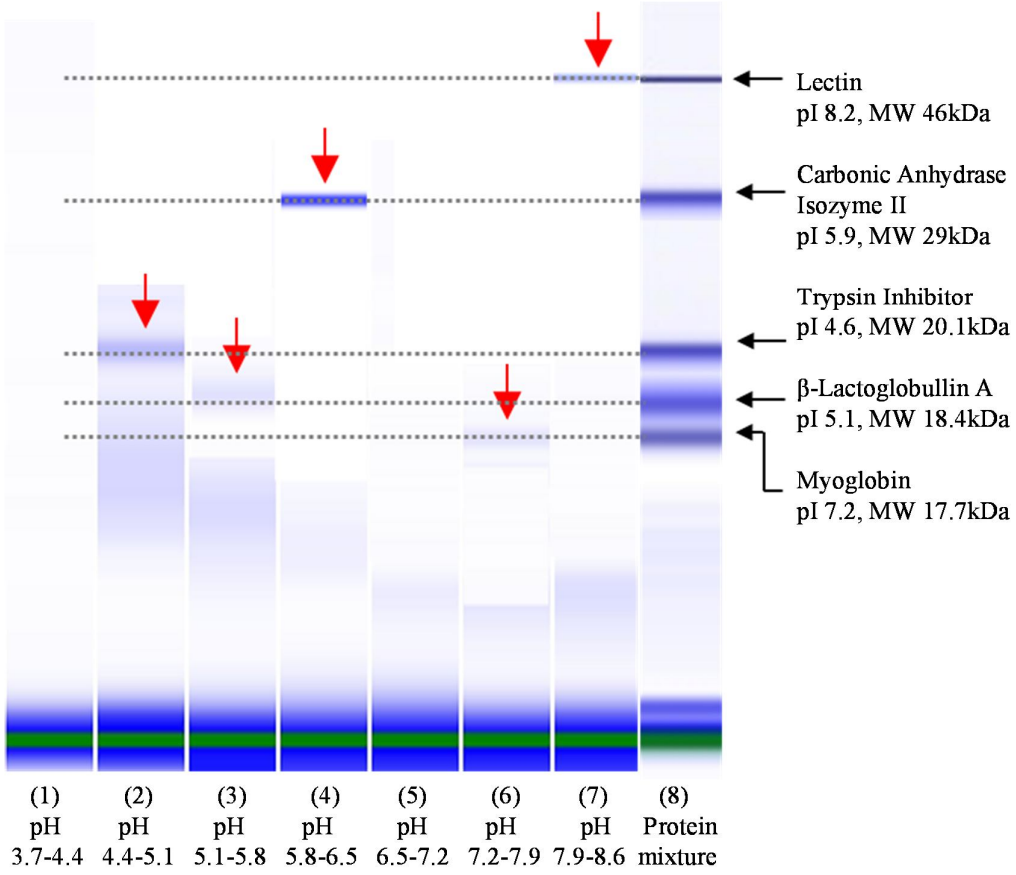

Figure 4-21: Gel electropherogram of collected droplets, processed with an Agilent 2100 Bioanalyzer. The sample contains five proteins with different pIs and molecular weights, as indicated on the right.

4.3.5 On-chip post-processing

The Slipchip IEF system is also capable of on-chip post-processing. As an example, the pH gradient can be calibrated by mixing separated sample droplets with universal pH indicator solution (Sigma-Aldrich, Dorset, UK) on-chip. Accurate pH gradient formation is a critical step in an IEF process. Previously, pH gradient calibration has been performed either by measuring the position of pI markers (Shimura *et al.*, 2002) or by premixing a pH indicator into the sample (Egatz-Gomez and Thormann, 2011, Weiss *et al.*, 2011). In the former method the pH values need

to be interpolated where markers are unavailable; in the later the pH indicator may influence sample and buffer conditions.

To perform on-chip indication, two channels for the pH indicator solution were made on both sides of the separation channel (schematic of which is shown in Figure 4-22). After IEF separation, by slipping the chip, both sample and indicator were compartmentalized into droplets in the wells. By aligning sample wells with indicator wells, the sample and pH indicator droplets in the different layers were merged and mixed.

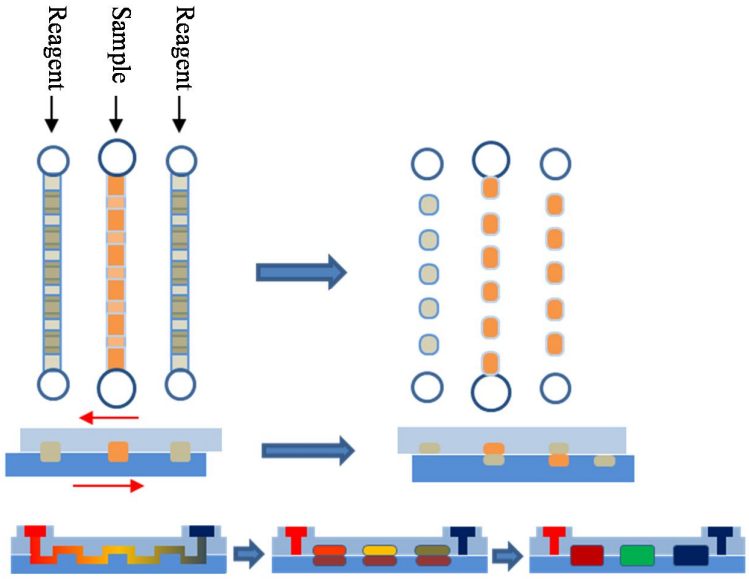

Figure 4-22: Schematic of on-chip post-processing. Two reagent channels are placed on each side of the sample channel. After separation, slipping the chip to align the reagent wells with sample wells, on-chip post-processing can be performed.

When the sample and indicator wells were aligned, the colour of this mixture started to change. After 10 minutes, the colour was stable. The chip was moved back to its original position, and a bright field microscope image of the entire channel taken, shown Figure 4-23. Four standard pH buffers (pH 4, 6, 7 and 10) were mixed on-chip with indicator in the same way, giving standard colours for comparison as shown in the inset of Figure 4-23. It was found that all the images show colorimetric similarity to their corresponding pH points, suggesting that a continuous and near linear pH gradient can be reliably established in Slipchip-based IEF device. It should be noted that this method of visual comparison is somewhat limited, and the resolution of the broadband

pH indicator solution is not high. Further efforts are required to calibrate an accurate pH gradient, such as using narrowband pH indicator to calibrate the pH in particular wells.

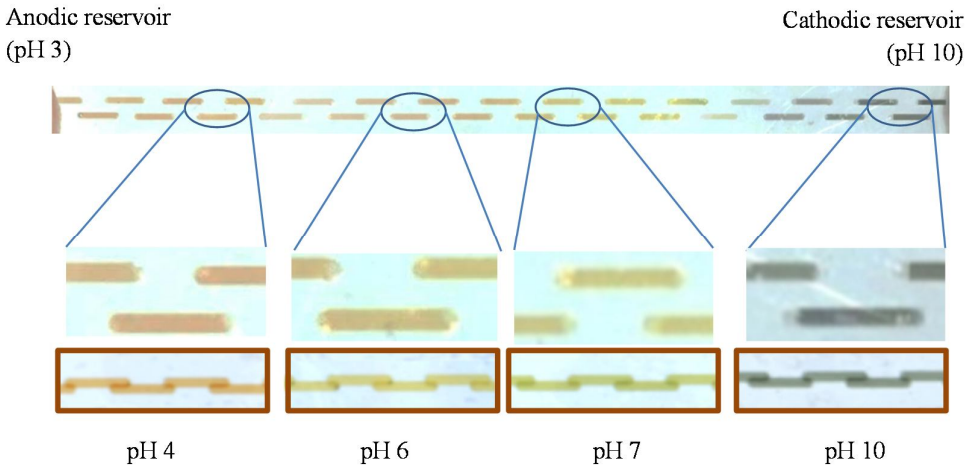

Figure 4-23: Colour image showing on-chip pH gradient calibration. Bottom panels show controls for each representative pH value.

4.4 Discussions and conclusions

This chapter presented the first application of a Slipchip for IEF separation of proteins followed by *in situ* compartmentalization. The Slipchip device was designed according to the discussion presented in section 3.2, and fabricated with micro milling. The design and fabrication processes further verified the Slipchip fast prototyping method. The UV transmission PMMA material was suitable for use of short-wavelength fluorescent dyes (e.g. DAPI) for on-chip detection. The droplet generation strategy presented in Chapter 3 was used for *in situ* sample compartmentalization after separation. Using the experimental platform described in Chapter 3, slipping can be precisely controlled to realise functions like sample loading, compartmentalization, droplet collection etc. Coating the device with Duxcoat prevented any leakage, but this surface treatment does not last very long and degraded after 5 experiments. However, the Duxcoat coating process is easy and device can be re-coated many times.

To prevent pH gradient compression and drift, 3% HPMC was added to the sample and electrolytes. It is noted that the focus position of the marker with low pI (4.0) is more stable than

that of the pI marker with a high pI (8.1), with a RSD of about 7%. This was attributed to isotachophoresis (ITP) (Righetti *et al.*, 2007b, Mack *et al.*, 2009, Xu *et al.*, 2010, Pager *et al.*, 2012). However, it still remains a problem in CA based IEF systems, so further effort is needed to optimise the chemical protocol to produce a more stable system, such as changing the concentration of electrolyte to optimise the boundary stability (Cao *et al.*, 2008). This thesis mainly focuses on the microfluidic system development; and optimisation of the chemical protocol was out of the scope of the work. The experimental test confirms that the positions of the pI markers fit with a linear distribution of pH gradient in the channel, and the IEF separation processes is relatively reproducible in the Slipchip, with an average RSD of 4.9%.

The *in situ* compartmentalization strategy does not mobilize the separated sample as in conventional methods, but it does eliminate re-mixing in the sample migration. Compartments can be collected and transferred to other analytical methods for further analysis. Two strategies; parallel collection and serial collection, have been described. Five standard proteins were separated and analysed downstream with gel electrophoresis using an Agilent 2100 Bioanalyzer. Such a compartmentalization strategy can also be hyphenated with the other analytical devices for multidimensional separation, such as CE, immunoseparation, or gel electrophoresis for protein or DNA/RNA analysis.

The compartmentalized droplets can also be post-processed on-chip, demonstrated using a universal pH indicator solution to show the pH gradient in the channel. Such functionality has not been demonstrated with other devices.

The high peak capacity of IEF can be achieved with long channel/capillary and high electric field. A suggestion for improvement is to increase the channel length and the electric field strength. The proposed Slipchip device is scalable and could support a longer (tens of centimetres) separation channel.

However, Joule heating will be a problem with a high electric field strength. Joule heating is generated when an electric current passes through a conductor. The power dissipated is given by:

$$Q \propto I^2 R = {}^{V^2}/_{R} \tag{4.6}$$

where Q is the amount of energy released, I is the current, V is the voltage and R is the resistance of the conductor. In the proposed system, Joule heating was simulated with COMSOL Multiphysics software (COMSOL, Inc., MA, US)(Figure 4-24), assuming a field of 100V/cm and

a steady state current of 180μA (the highest current in an IEF experiment). Simulation shows that the temperature of the sample in the separation channel stabilises at 64˚C in an external environment of 25˚C. In real life, the current in an IEF experiment drops to less than 30μA in 15 minutes, the temperature in this case is about 28.7˚C (COMSOL simulation). Experimentally, the IEF calibration and protein separation processes were not affected by heating. If the electric field strength is increased, extra cooling would be required such as the temperature control device used in FF-IEF system (Wen *et al.*, 2010b).

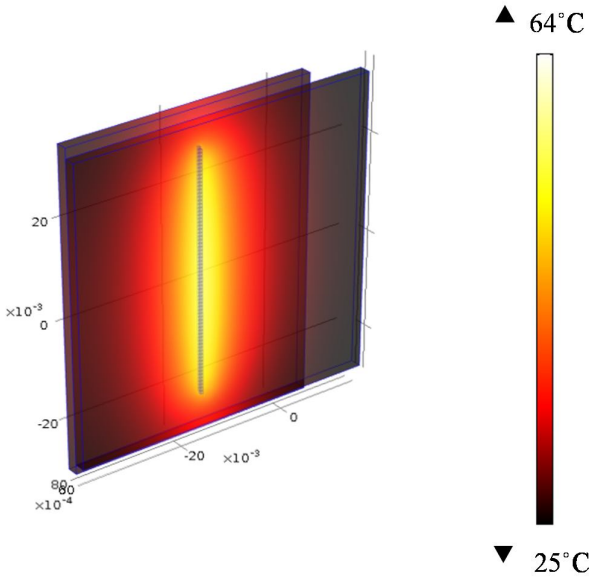

Figure 4-24: COMSOL simulation of the temperature of the Slipchip device during isoelectric focusing. The electric field is 100V/cm and current is 180μA, the ambient temperature is 25˚C. In this case, the channel has the highest temperature of 64˚C. A temperature gradient is visible from the channel to the edge of chip, this is because of the poor thermal conductivity of PMMA.

The resolution of compartmentalization depends on the well density of the Slipchip, which is limited by fabrication. The compartments are needed for downstream processes, so the well dimension (i.e. droplet size) should also consider the sample volume requirement of the downstream analysis method.

In conclusion, this chapter demonstrates the use of a re-engineered Slipchip to perform protein IEF separation. The *in situ* compartmentalization does not need the separated sample to be

immobilized, and the method solves a major problem faced by conventional methods. This concept could also be used for other chemical separation systems like CE.

Chapter 5

Droplet Microfluidic Chips for Cavity Ring Down Spectroscopy

5.1 Introduction

Chapter 4 described a Slipchip device for protein isoelectric focusing (IEF) and *in situ* compartmentalization after separation. Droplets were analysed downstream by capillary gel electrophoresis with an Agilent 2100 Bioanalyzer. This instrument detects protein bands with fluorescence after protein labelling with a fluorescence dye (Bousse *et al.*, 2001). As reviewed in Chapter 2, fluorescence detection has high sensitivity and has been widely used in microfluidics. However, fluorescence methods have limitations like photobleaching, which is the destruction of a fluorophore when excited. Absorption spectroscopy is a label-free technique and does not have such limitations but does suffer from limited sensitivity especially for short path length devices. Cavity Ring Down Spectroscopy (CRDS) (Okeefe and Deacon, 1988) is a direct absorption analytical method which has high sensitivity and has been commercialised for analysis of gas samples. Efforts are underway to use CRDS for liquid sample analysis (Bescherer *et al.*, 2013). In recent years, fibre-coupled CRDS microfluidic systems have been investigated (Waechter *et al.*, 2011, Neil *et al.*, 2011). However, many technology challenges exist when attempting to combine CRDS with microfluidics. For example, one big problem is how to easily and efficiently couple light into a microfluidic device.

CRDS is a sensitive analytical method, the high sensitivity relies on the high light coupling efficiency. This chapter investigates the interface of fibre-based CRDS system with droplet microfluidics.

5.1.1 Motivation

The previously reported CRDS and fluidic interfaces can be classified into two methods. First, in the device presented by Vallance and co-workers in University of Oxford UK (Neil *et al.*, 2011, James *et al.*, 2012), light coupling is achieved by aligning free space light beams with microfluidic channels. In this way, the CRDS and fluidic device are two separate systems so that the fluidic chips can be easily changed. But this is not a miniaturized device integration and the alignment of the light beam which microfluidic channel is a challenge. Therefore the channel is normally made quite wide to accommodate a big alignment tolerance. For example in the device presented by Neil *et al.*, the channel width is 1mm (Neil *et al.*, 2011). Devices with channel widths on the micrometre scale have not been reported.

The alternative approach is to integrate the optical cavity with the fluidic channel (or capillary), such as the device described by Loock and co-workers in Queen's University Canada, where a fibre loop was used to form an optical cavity (Tong *et al.*, 2004), and the fibre was cut to leave a gap for the liquid interface, and coupled with a capillary to detect a sample after capillary electrophoresis (Li *et al.*, 2006), or with a liquid core waveguide, which is a tubing filled with sample (Bescherer *et al.*, 2013). With this method, the optical cavity, i.e. fibre loop, is coupled directly with the fluidic channel via fibre grooves, and alignment is less of a problem. The fluidic channel can be made as small as the dimension of the optical fibre, such as the capillary channel with a diameter of 100μm (Li *et al.*, 2006). However, these devices can only perform off-line analysis, and not compatible with conventional microfluidic device like PDMS chip.

In this chapter, these two light coupling methods are re-engineered in an attempt to make an on-line CRDS-microfluidic analytical system. Two different chips are investigated for coupling a fibre-based CRDS system with a droplet microfluidic device; vertical coupling where the optical fibres are placed either side of a microfluidic chip (Figure 5-1A); and horizontal coupling where fibres are fixed into grooves in a PDMS droplet microfluidic chip (Figure 5-1B).

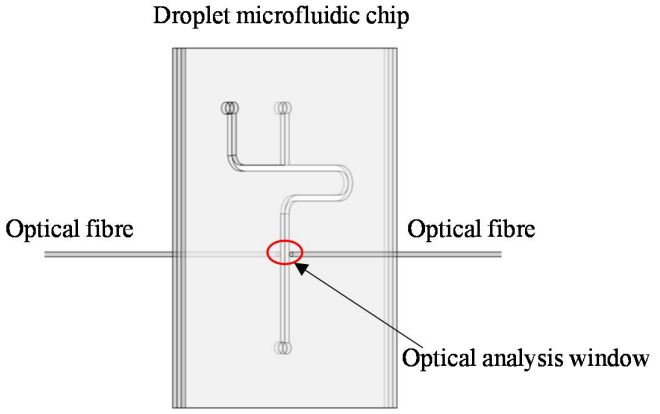

(A)

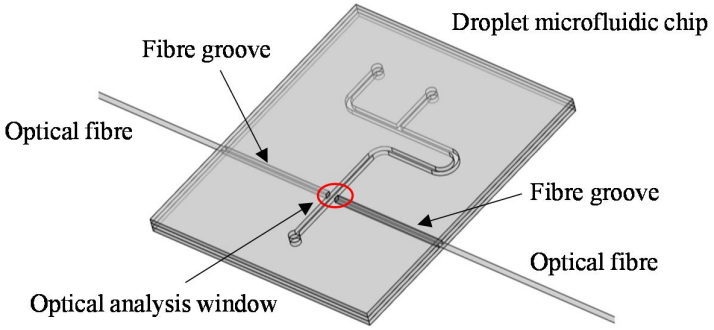

(B)

Figure 5-1: Schematic diagram of fibre-coupled microfluidic chips. (A) Vertically coupled chip, in which optical fibres are placed perpendicular (vertically) to the surface of a microfluidic chip, and aligned with a micro-channel through an optical window. (B) Horizontal coupling chip where optical fibres are aligned in the microfluidic chip using grooves.

5.2 CRDS setup

According to CRDS equation, as shown in (5.1) (Rushworth *et al.*, 2013)

$$\tau = \frac{d}{c(-\ln T_{tot} + \kappa l)} \tag{5.1}$$

where τ is ring-down time, d is cavity length, c is light speed, T_{tot} is the cavity sing round transmission ratio in the absence of sample. κl gives the sample absorption, where κ is the absorption per unit length and l is the light path length. $\kappa = \Delta C_{min} \cdot \alpha$, in which α is absorption coefficient of the sample, C is sample concentration. The detection resolution of sample absorption is (Rushworth *et al.*, 2013)

$$\Delta\kappa_{min} l = \frac{d\Delta\tau_{min}}{{\tau_0}^2} \tag{5.2}$$

in which $\Delta\tau_{min}$ is the smallest detection change of ring down time, and τ_0 is the baseline ring down time, which is the ring down time with the absence of sample. According to (5.1), (5.2) can be written as:

$$\Delta\kappa_{min} l = \frac{c \ln^2 T_{tot} \Delta\tau_{min}}{d} \tag{5.3}$$

It can be seen from (5.3), a low $\ln^2 T_{tot}$ and $\Delta\tau_{min}$ and high l and d will be helpful to realize a low $\Delta\kappa_{min} l$ detection. As shown in Table 5-1, the increasing of T_{tot} can greatly reduce the value of $\ln^2 T_{tot}$, which is a key point in CRDS system. In the mirror based CRDS system reported in (Rushworth *et al.*, 2013), the T_{tot} was 99.6%, corresponding to $\ln^2 T_{tot}$ of 1.61e-5. Xu *et al.* (2002) reported a system with T_{tot} of 99.97%, corresponding to $\ln^2 T_{tot}$ of 9e-8, nearly 200 times lower.

Table 5-1 The conventional table of $\boldsymbol{T_{tot}}$ to $\boldsymbol{\ln^2 T_{tot}}$.

T_{tot}	$\ln^2 T_{tot}$
97%	9.28E-04
98%	4.08E-04
99%	1.01E-04
99.50%	2.51E-05
99.90%	1.00E-06
99.95%	2.50E-07
99.99%	1.00E-08

For phase shift CRDS system, the phase shift $\emptyset$ follows equation (5.2) (Tong *et al.*, 2004)

$$\emptyset = \arctan(\Omega\tau) \tag{5.4}$$

in which the Ω is the angle modulation frequency. The smallest detectable phase shift $\Delta\emptyset_{min}$ determines the smallest detectable ring down time $\Delta\tau_{min}$, which can be calculated as:

$$\Delta\emptyset_{min} = (\emptyset_0 + \Delta\emptyset_{min}) - \emptyset_0 = \arctan\big(\Omega(\tau_0 + \Delta\tau_{min})\big) - \arctan(\Omega\tau_0)$$

$$= \arctan\left(\frac{\Omega(\tau_0+\Delta\tau_{min})-\Omega\tau_0}{1+\Omega\tau_0(\Omega(\tau_0+\Delta\tau_{min}))}\right) = \arctan\left(\frac{\Omega\Delta\tau_{min}}{1+\Omega^2{\tau_0}^2+\Omega^2\tau\Delta\tau_{min}}\right) \tag{5.5}$$

$\emptyset_0$ is the phase shift with absence of sample. So

$$\Delta\tau_{min} = \frac{(1+\Omega^2{\tau_0}^2)\tan\Delta\emptyset_{min}}{\Omega-\Omega^2\tau_0\tan\Delta\emptyset_{min}} = \frac{(1+\tan^2\emptyset_0)\tan\Delta\emptyset_{min}}{(1-\tan\emptyset_0\tan\Delta\emptyset_{min})\Omega} \tag{5.6}$$

It can be seen a higher frequency Ω and lower $\Delta\emptyset_{min}$ make a lower $\Delta\tau_{min}$.

The building of fibre-based CRDS system was collaborated with Dr. Vallance's group in University of Oxford, the setup shown in Figure 5-2 was built with standard commercial components with the help of Cathy Rushworth. It is a phase shift measurement system similar to that presented by Waechter *et al.* (Waechter *et al.*, 2011). The light source was a continuous 50mW 532nm frequency doubled Nd: YAG laser DPGL – 2050 (Photop Suwtech Inc., Shanghai, China) with controller model LDC – 1500 (Photop Suwtech Inc., Shanghai, China). A free space Electro-Optical Modulator (EOM) model EO-AM-NR-C4 (Thorlabs, NJ, US) driven by a high speed high voltage amplifier model WMA-300 (Falco System, Amsterdam, The Netherlands) was used to modulate the laser beam. The modulation signal was generated by an Agilent 33250A Function Generator (Agilent, CA, US).

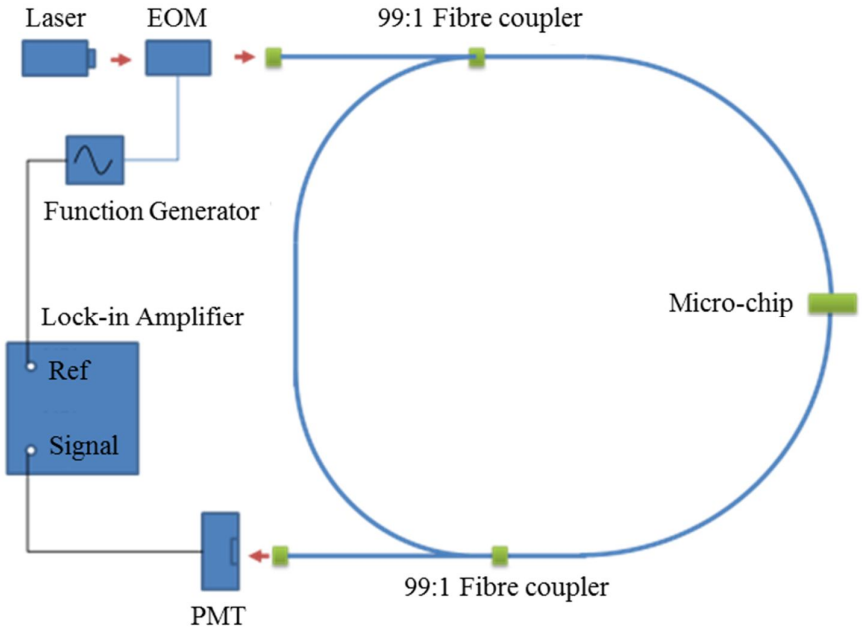

Figure 5-2: Schematic diagram of the fibre-based Phase Shift Ring-down system.

The fibre loop was formed from two 99:1 fibre couplers (Fibre Optic Network Technology Co., British Columbia, Canada) made of 400µm multimode fibre. The length of the fibre loop was 4m, The photon detector was a H9305 – 03 PhotoMultiplier Tube (PMT) from Hamamatsu Photonics UK Ltd. (Hertfordshire, UK). An amplifier model C9999 with bandwidth of 10MHz and conversion factor of 50mV/uA from Hamamatsu converted the current signal to voltage. A Lock-In Amplifier (Model SR844 RF Stanford Research System Inc. CA, US) with a phase resolution of 0.02 degree and a frequency range from 25kHz to 200MHz was used to measure phase shift. Control and data collection was performed using LabVIEW software (National Instruments Corporation (U.K.) Ltd., Berkshire, UK). The total single loop light transmission ratio of the system was measured at 96.7% (n=10, standard deviation =1.32%) was measurement, from (5.1) to (5.6), if the system was coupled with a micro-chip with no more light loss,

$$\Delta\tau_{min} = 3.49\ \text{ns} \tag{5.7}$$

and

$$\Delta\kappa_{min} l = 2.95 \times 10^{-4} \tag{5.8}$$

5.3 Vertical coupling chip

5.3.1 Chip design

The original idea of vertical coupling is from the free space CRDS system reported by Vallance's group (Neil *et al.*, 2011, James *et al.*, 2012), the free space laser system is replaced by optical fibre. The light from optical fibre can be coupled to the microfluidic channel and collected by another optical fibre,

Zemax optical simulation software (version 2007.11 EE, Radiant Zemax, LLC, WA, US) was used to simulate the system. The coupling efficiency of two 400µm fibres as a function of fibre distance was first simulated with Zemax. A schematic diagram is shown in Figure 5-3 and the simulation results plotted in Figure 5-4. It can be seen that the coupling efficiency decreases with the increase of fibre ends distance as expected. A coupling efficiency of 98% is possible when the fibres are 100µm apart, but for fibres separated by a distance of 1mm the light coupling efficiency dropt to only 75%.

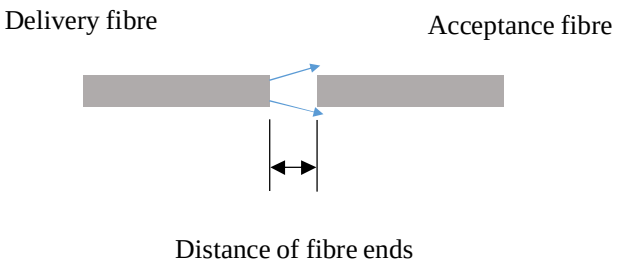

Figure 5-3: Schematic diagram of fibre coupling efficiency with different fibre end distances. The fibres are 400µm multi-mode fibre with NA of 0.22, the interface media is glass.

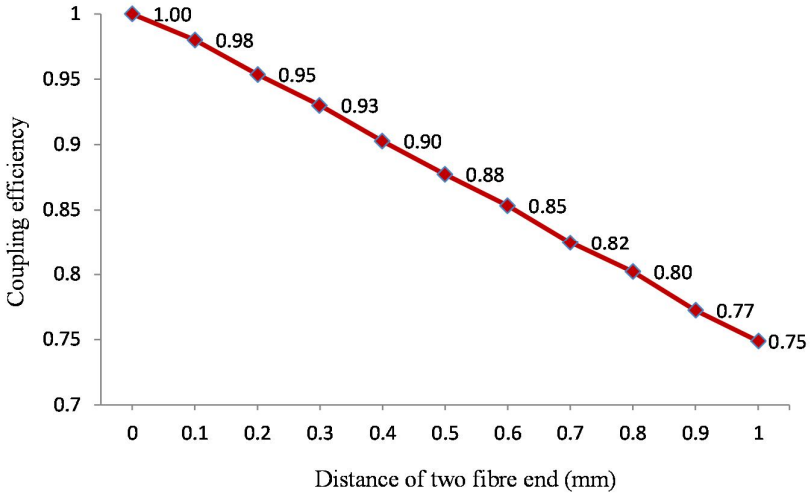

Figure 5-4: Fibre coupling efficiency vs distance simulated with Zemax optical simulation software. The fibre was a 400µm multimode silica fibre with NA of 0.22.

To increase the coupling efficiency, a thin chip structure is proposed. The microfluidic chip was formed from two 120µm thick glass cover slips, with a 100µm thick PDMS spacer. The microfluidic channel was patterned into this PDMS layer. The total thickness of the chip was 340µm and it was bonded to a holder with a 100µm thick PDMS membrane as shown in Figure 5-5.

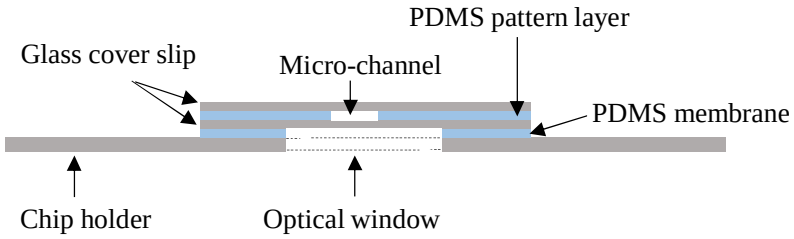

Figure 5-5: Schematic of the sandwich structure used for vertical coupling of the fibre. The device has five layers. The microfluidic chip was made of two 120µm thick glass cover slips and a 100µm thick PDMS layer which contained the microfluidic pattern. The total thickness of the microfluidic chip was 340µm. A holder was used to mount the chip onto the CRDS system. The chip to holder interface was made from a 100µm thick PDMS membrane. An optical window was made in the holder to mount the optical fibres.

The simulated coupling efficiency for two fibres with a 340µm distance is 91.9%. When the fibres are coupled with the 340µm thick microfluidic channel filled with water (Figure 5-6), the coupling efficiency is 87.3%. This is because the refractive index of water (1.33) is lower than glass (1.47) and such configuration expands the light beam from the delivery fibre as shown in Figure 5-6.

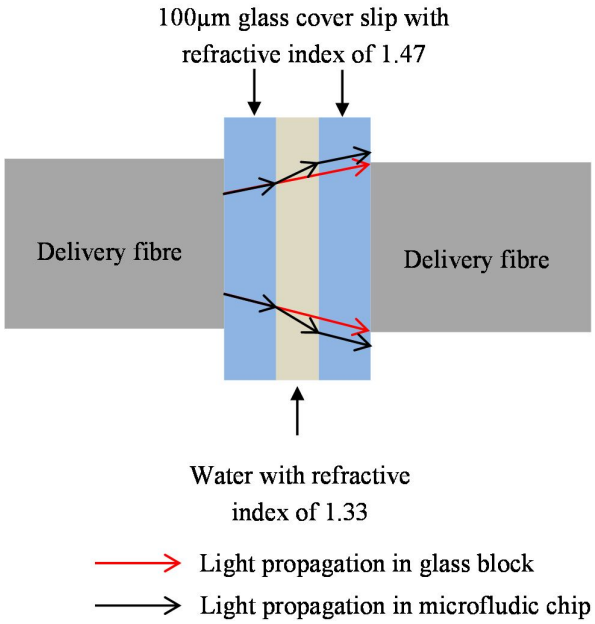

Figure 5-6: Schematic diagram of fibre coupling with 340µm thick microfluidic chip, which is formed from two 100µm thick glass cover slip with refractive index of 1.47, and the channel filled with water with refractive index of 1.33. The black arrows schematically show light propagation in the fibre-microfluidic interface. The water in the channel has a lower refractive index than glass, the light is refracted, shown by the red arrows.

The layout of the chip is shown in Figure 5-7. Sample droplet can be generated with a T-junction droplet generator, an optical window is placed in a zig-zag incubation area for CRDS analysis. The chip had dimensions of 22mm × 50mm. The width of the channel was 450µm, which can easily accommodate the 400µm diameter fibre.

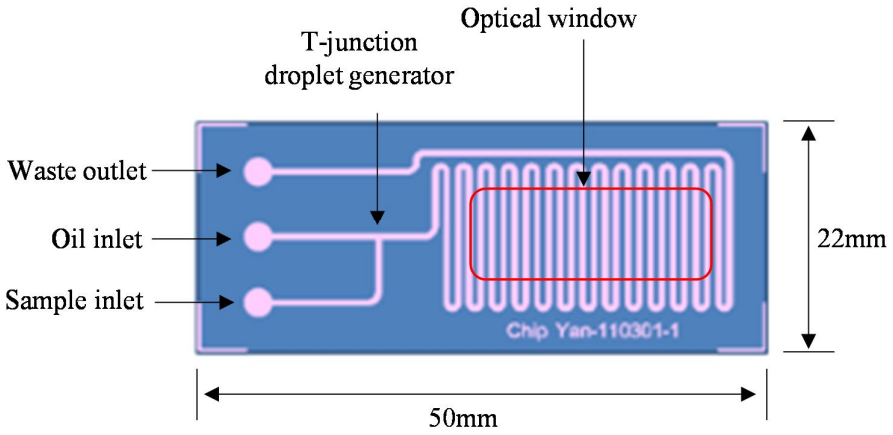

Figure 5-7: Layout of the microfluidic-optical interface chip. The chip dimension was 22mm × 50mm, with a channel width of 450µm. This chip was designed for droplet microfluidic and therefore had two inlets, one for sample and one for oil, and one waste outlet. These were placed on the top side of microfluidic chip; droplets were generated with a T-junction droplet generator. An optical window was used to position the optical fibres.

5.3.2 Fabrication

The fabrication of a thin chip is a challenge. The microfluidic pattern was drawn using mask design software (Clewin) and the photo mask was printed on polyester film (Microlitho Ltd., Essex, UK) at a resolution of 40,000dpi. A SU-8 master chip for moulding the PDMS channel was fabricated in the Southampton Nano Fabrication Centre. First. SU-8 50 negative photoresist (MICRO CHEM, MA, US) was spin coated on a 4 inch silicon wafer at a speed of 1200rpm for 60 seconds; then baked on a hotplate at 65˚C for 60 minutes. After 4 hours relaxing at room temperature, the wafer was exposed to UV light with an EVG-620TB mask aligner (EV Group, Austria) at an exposure dose of 1000mJ with an I-Line (365nm) filter. Post-baking was performed on a hotplate at 65°C for 30 minutes, and a slow ramp (5°C/min) was applied to cool the wafer to room temperature. The wafer was relaxed at room temperature for 24 hours, and subsequently developed in EC-Solvent (MICRO CHEM, MA, US) for 30 seconds in an ultrasonic bath, followed by rinsing with isopropyl alcohol (IPA) and MilliQ ultrapure water, and finally drying with nitrogen. Before moulding the PDMS, the wafer was processed by exposing it to oxygen

plasma using a PVA Tepla GIGABatch 310 plasma asher (PVA TePla AG, Wettenberg, Germany) at a power of 300W for 20 seconds. It was then placed in a vacuum desiccator for 30 minutes, together with a drop (5µL) of Trichloro (1H, 1H, 2H, 2H - perfluorooctyl) silane (Sigma-Aldrich, Dorset, UK) placed on a glass slide. In the desiccator, the silane evaporates and coats the surface of the wafer to make it non-sticky, preventing adhesion of the PDMS (Figure 5-8A).

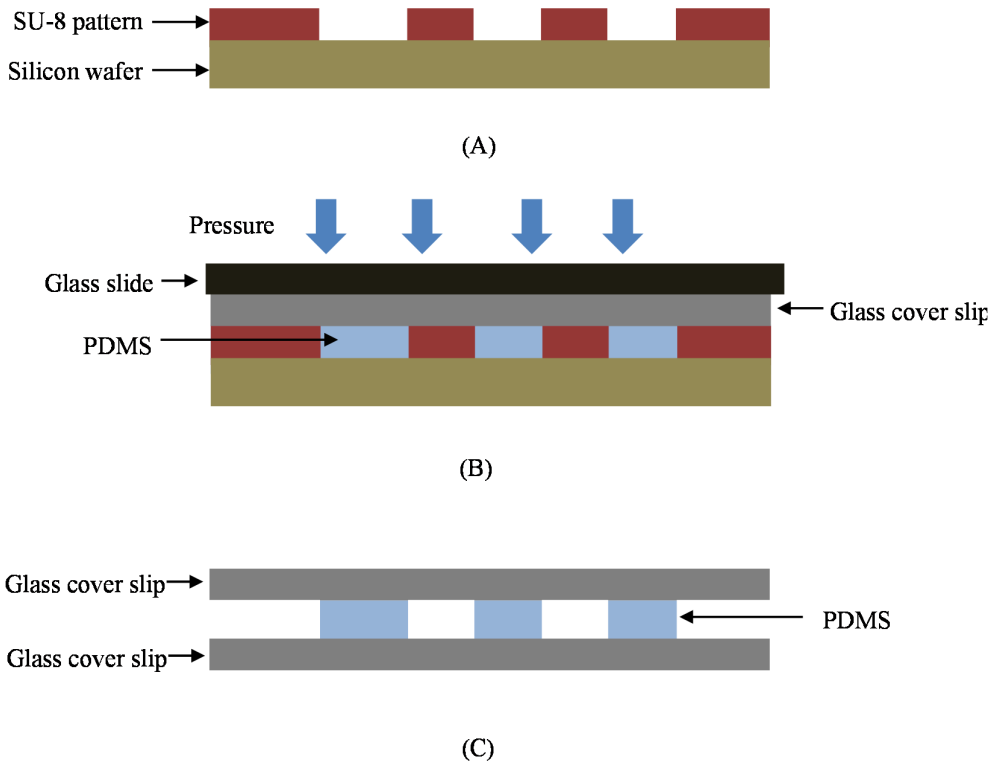

Figure 5-8: Fabrication of the vertically coupled fibre chip. (A) An SU-8 master was made with photolithography and then treated with Trichloro (1H, 1H, 2H, 2H - perfluorooctyl) silane to prevent PDMS adhesion. (B) Degassed PDMS was poured over the SU-8 master and covered with an oxygen plasma treated glass cover slip followed by a silanized glass slide. A pressure of 5 bars was applied to squeeze out the remaining PDMS. (C) After baking in an oven at 60°C for 6 hours, the PDMS was fully cured and bonded to the glass cover slip. The glass cover slip with PDMS was carefully peeled from the master, and bonded to another glass cover slip using oxygen plasma.

When the moulding master is ready, Sylgard® 184 Silicone Elastomer PDMS kit (Dow Corning, MI, US) was mixed in a ratio 10:1 (w/w) and degassed in a vacuum desiccator for 15 minutes. The degassed PDMS was poured onto the wafer, and then covered with an oxygen plasma treated glass cover slip and a glass slide. A pressure of 5 bar was applied using weights (Figure 5-8B). The chips was placed in an oven at 60°C for 6 hours, after which the PDMS was cured and bonded to the oxygen plasma treated glass cover slip. Due to the hydrophobic treatment on the master, the glass coverslip together with the cured PDMS could be peeled away. This must be very carefully as the glass cover slip is very fragile. After detachment chip was bonded to another glass cover slip by exposing the surface to oxygen plasma (Figure 5-8C). The final chip is very fragile and therefore a holder was made from a milled glass slide. This was bonded to the chip via a 100µm thick PDMS membrane using oxygen plasma treatment. The holder provides a solid base to the chip, with adequate fluid connections. A PDMS block punched with inlet/outlet holes was bonded on the holder; tubing can be inserted in the holes and connected to the micro-channel. A picture of the whole device is shown in Figure 5-9.

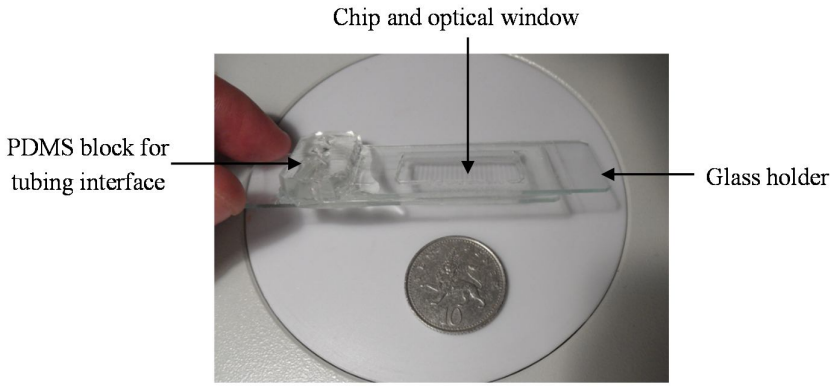

Figure 5-9: Photograph of the sandwich structure with glass holder. The chip and holder were bonded via a 100µm thick PDMS membrane with oxygen plasma.

5.3.3 Results and discussions

The quality of the moulding master is crucial in PDMS device fabrication. To assess this, the SU-8 pattern was analysed with a surface profiler. The thickness of the pattern was expected to be 100µm in all areas. It was found that in the centre of the master the pattern was 99µm thick, at

the edge the thickness was 101µm; the channel width was 449µm (±1µm). This small error is acceptable.

To generate droplets, two 500µl Hamilton glass syringes and Harward syringe pumps (Harvard Apparatus Ltd, Kent, UK) were used to load the food dye solution and FC-40 oil. With a flow rate for the dye of 5µL/min, and oil at 20µL/min, the volume of the each droplet was about 40nL (Figure 5-10).

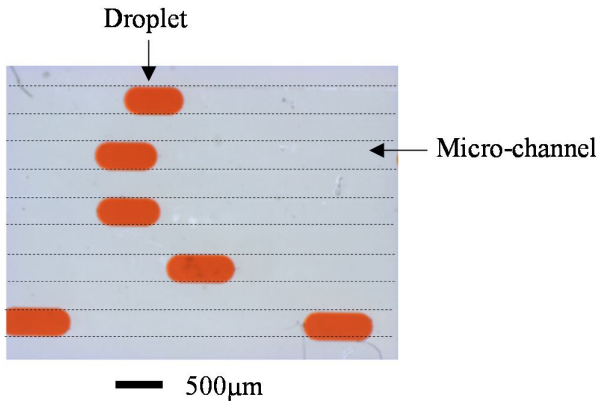

Figure 5-10: Microscope photograph of food dye droplets in the vertically coupled chip channel. The flow rate of dye was 5µL/min, and oil was 20µL/min, giving a volume for the each droplet of about 40nL.

The device was coupled with a fibre based CRDS setup, fibre coupling was performed with an optical alignment stage, and the fibre-chip interface was filled with index matching oil with refractive index of 1.47. When the channel was filled with water, a light coupling efficiency of 98.3% was measured, comparing well with the chips made by Rushworth and co-workers (Rushworth, 2012). This experimental result was 11% better than the Zemax simulation, which is partly because the limitation of the software. Zemax traces limited numbers of rays in the optical system (1 million rays in the simulations for this chapter), the coupling efficiency is calculated by counting the rays on detectors. In the software, the rays will disappear after passing several components or reflected several times (the default number is 10), but light propagation in real-life is much complex than software modelling. So the Zemax is strong in modelling the lens and ray path, but not accurate in modelling transmission efficiency on media interfaces.

5.4 Horizontal coupling chip

5.4.1 Chip design and fabrication

For vertically coupled chips, fibre alignment is performed using an optical alignment stage, it is not an integrated device. An alternative structure is the horizontal light coupling, the idea of which is integrating fibres with the microfluidic device using on-chip grooves. In which way the alignment accuracy defined by the tolerance of the micro-fabricated grooves, which can be achieved within 1μm as per micro-fabrication tolerance.

To make the chip compatible with conventional microfluidic method, it is proposed to be made with PDMS. The channel height is made 400μm to accommodate the 400μm optical fibre in CRDS system.

The fabrication of a 400μm thick SU-8 pattern is a challenge, the Thermal Expansion Coefficient (TEC) of SU-8 is 52 ppm/˚C (Lin *et al.*, 2002) and that of Silicon wafer is 2.6 ppm/˚C according to manufacturer's data sheet. This big difference of TEC may cause severe cracking in thick SU-8 (Lin *et al.*, 2002). In the fabrication process, double coating was used to form the 400μm thick SU-8. First, a layer of SU-8 100 was spin coated on a 4 inch silicon wafer at a speed of 1800rpm for 60 seconds, and baked on a hotplate at 60˚C for 60 minutes. After 10 minutes of relaxing at room temperature, the second layer of SU-8 100 was spin coated on the wafer at a speed of 2000rpm for 60 seconds; then baked at 60˚C for 90 minutes. The SU-8 was exposed using an EVG-620TB mask aligner at a dose of 2500mJ with I-line (365nm) filter. The wafer was post-baked at 50˚C for 4 hours and then slowly cooled to room temperature at a ramp rate of 1˚C/minute. The SU-8 post-baking is normally processed at 65˚C to 95˚C according to manufacturer's data sheet. For this 400μm thick SU-8 pattern, such a high temperature will induce significant thermal expansion of SU-8, and cause severe cracking of the pattern, and the SU-8 layer may detach from the wafer. The low baking temperature and low rate of ramping down can avoid such problems. After relaxing at room temperature for 24 hours (which helps to avoid cracks), the wafer was developed in EC-Solvent with an ultrasonic bath for 2 minutes, rinsed with isopropyl alcohol (IPA) and MilliQ ultrapure water, and dried with nitrogen gas. Then the mixed and degassed PDMS is poured on the SU-8 pattern and baked in 60˚C oven for 6 hours as described before.

It was noticed that due to the limitation of aspect ratio, the smallest width can be made on this 400µm thick PDMS pattern is 50µm. To make it comparable with vertical coupling device describe in the section 5.3, the chip design shown in Figure 5-11 was fabricated, which has 100µm wide channel, and the channel wall thickness is 120µm.

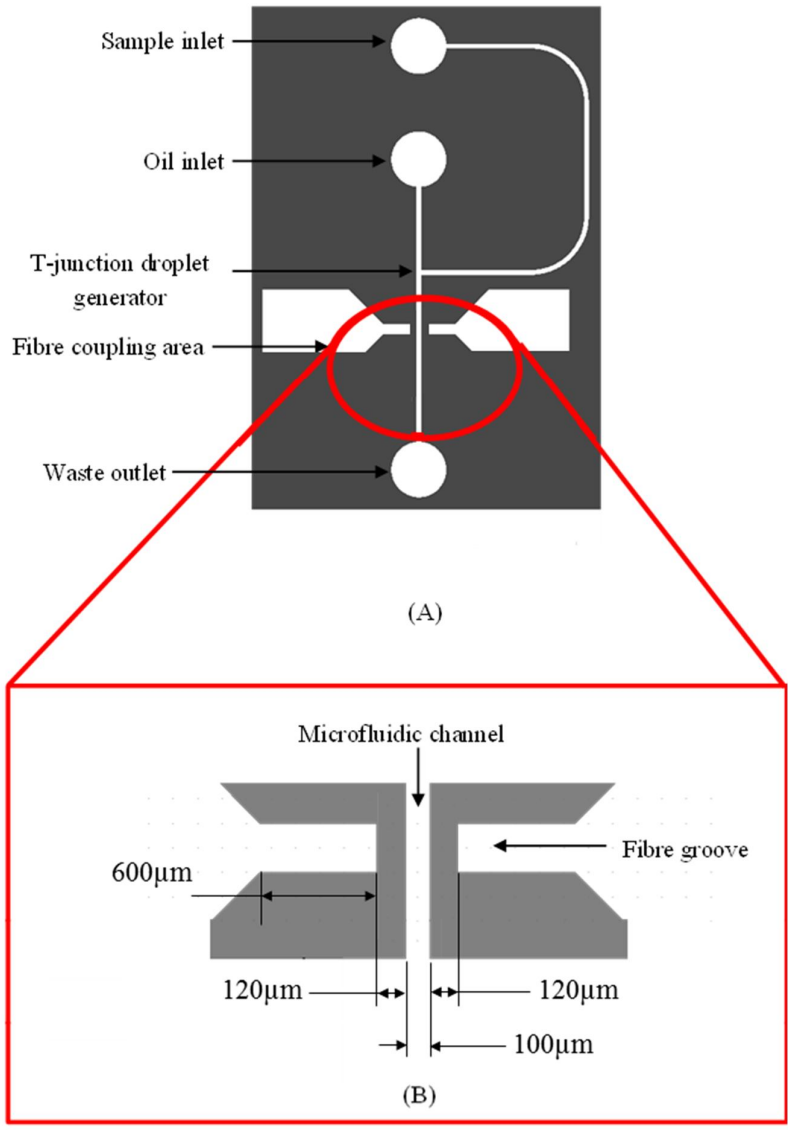

Figure 5-11: Design of the horizontal direct fibre coupling chip. T-junction is designed for generating sample droplets; the fibres are fixed in the 600µm long on-chip grooves; the width of microfluidic channel is 100µm and channel wall thickness is 120µm.

5.4.2 Results and discussions

Fabricating the SU-8 master at a low post-baking temperature is the critical point in making thick SU-8 pattern. It was noticed when the post-baking temperature is higher than 60˚C, cracks were clearly seen in the SU-8 pattern; when the post-baking temperature is higher than 75˚C, the SU-8 patterns were peeled off from silicon wafer due to thermal expansion. When the SU-8 master is developed, the 60˚C baking temperature for PDMS curing will not induce cracks to SU-8.

For measuring light coupling efficiency, the fibres were inserted into the grooves, index matching oil with refractive index of 1.47 was applied on the fibre-chip interface. The coupling efficiency was changed from 80.4% to 45.7% with average number of 60.9% (n=10, standard deviation = 11.8%). The bad coupling and poor reproducibility was because the grooves were made with soft PDMS and it was just 600μm long, the fibre can be easily moved in the grooves.

Two solutions for this problem, increasing the hardness of PDMS, and increasing the length of grooves. According to the manufacture's datasheet, increase the PDMS curing temperature can increase the hardness of PDMS. But when temperature is higher than 60˚C, the SU-8 master will crack, so the curing temperature cannot be increased. Another solution is increasing the length of fibre grooves, when it was increased to 10mm, coupling efficiency from 86.2% to 72.3% was measured with average number of 78.2% (n=10, standard deviation = 4.4%); when it was further increased to 20mm, the results were similar with 10mm grooves, so a 10mm groove was selected.

Three methods were considered to optimise the coupling efficiency. Firstly, reducing the surface roughness to increase the light transmission of the channel; secondly, using on-chip waveguide trapping the light; thirdly, using on-chip micro-lens to avoid light divergence. These three methods were studied in the following sections.

5.4.3 Surface treatments

The surface roughness is a crucial factor for any optical interface. The surface of the PDMS cylindrical lens was analysed with a Veeco Multimode V Atomic Force Microscope (AFM) (Bruker Corporation, MA, US). A scan was performed on an area of 20μm × 20μm area and the average surface roughness was found to be 115nm.

This surface roughness is an unacceptable level of for an optical interface. For plastic devices like PMMA and COC, the material can be reflowed with solvents to improve the surface property (Ogilvie *et al.*, 2010); for PDMS device, the SU-8 master defines the quality of PDMS device, but modifying a cross-linked SU-8 is recognised as very difficult or impossible. For PDMS modification, Jo *et al.* has shown the use of Reactive Ion Etch (RIE) with O_2 and CHF_3, to etch and modify the surface of PDMS devices (Jo *et al.*, 2000), and Ginn *et al.* reduced PDMS surface roughness after plasma treatment (Ginn and Steinbock, 2003). In this research, a Plasmalab 80 Plus RIE system (Oxford Instruments, Oxfordshire, UK) was used to improve the PDMS surface. The RF source frequency was 13.56MHz, the RF power, chamber pressure and the ratio of O_2 and CHF_3 were changed to find the best surface. Table 5-2 shows the measured surface roughness after 30 minutes etching for different conditions. From the table it can be seen that a low surface roughness is achieved with high chamber pressure and high RF power. The gas ratio does not affect the surface roughness. An RF power of 200W, a chamber pressure of 400mTorr and an O_2:CHF_3 gas ratio of 1:1 produced the lowest surface roughness of 32.3nm.

Table 5-2 Surface Roughness of PDMS device after 30 minutes RIE treatment.

Sample Number	Pressure (mTorr)	RF Power (W)	O_2 : CHF_3	Surface Roughness (nm) and standard deviation (SD) (n=4)
0	N/A	N/A	N/A	115 (SD=0.5)
1	400	200	25 : 75	41.2 (SD=1.7)
2	400	50	25 : 75	34.4 (SD=1.1)
3	400	200	50 : 50	32.3 (SD=0.9)
4	400	50	50 : 50	49.3 (SD=1.4)
5	400	200	75 : 25	38.6 (SD=1.0)
6	400	50	75 : 25	39.7 (SD=1.6)
5	30	200	25 : 75	67.6 (SD=2.5)
6	30	50	25 : 75	66.9 (SD=2.1)
7	30	200	50 : 50	43.9 (SD=2.0)
8	30	50	50 : 50	83.8 (SD=1.8)
9	30	200	75 : 25	44.0 (SD=1.0)
10	30	50	75 : 25	56.7 (SD=1.8)

Beside etching, surface coating can also be used to modify surface roughness, often to generate a super-hydrophobic surface (Miwa *et al.*, 2000). A method of coating with a thin (<10nm) PDMS layer has been proposed to form a smooth hydrophobic surface (Lee *et al.*, 2006a). To perform this, the PDMS device was first exposed to Oxygen plasma (generated with a PVA Tepla GIGABatch 310 plasma asher at power of 400W) for 10 seconds (Figure 5-12A), and then immersed in 0.5% (3-Aminopropyl) triethoxysilane (APTES) solution for 10 minutes (Figure 5-12B). Then monoglycidyl ether terminated Poly(dimethylsiloxane) was dropped onto the APTES silanized PDMS and the device was baked in oven at 80°C for 4 hours (Figure 5-12C), grafting a thin PDMS layer onto the device. The surface roughness of the original device was 115nm, after RIE etching it reduced to 32.3nm, and further reduced to 28.1nm (SD=0.7, n=4) after PDMS coating, measured with AFM. If the original device was coated directly with PDMS, the surface roughness was measured as 85nm (Figure 5-13), and after the same RIE process, the surface roughness was reduced to 31.6nm. In comparison, the etching-coating process can render a better surface. It is worth to note that although the surface roughness of the cylindrical lens was reduced dramatically from 115nm to 28.1nm after the aforementioned process, it is still not enough for an optical interface, for which an ideal roughness should be less than 15nm (Ogilvie *et al.*, 2010). The light coupling efficiency was 78.8% (n=10, standard deviation = 4.3%) after surface treatment, 0.6% higher than the original device.

5.4.4 Optical waveguide in microfluidics

Optical waveguide like optical fibre is used to control the transmission of light. The optical waveguide in PDMS microfluidic device has also been widely studied, such as Fleger *et al.* presented a PDMS chip integrated with micro-channel and PDMS waveguide for transmission spectrum analysis (Fleger and Neyer, 2006). In this section, a waveguide structure is investigated to reduce the light loss in this fibre-microfluidics-fibre system. As reported by Chang-Yen *et al.* (Chang-Yen *et al.*, 2005), the cured PDMS will have different optical refractive index, which is changing from 1.43 to 1.45 while curing at different temperature. Figure 5-14 shows a schematic drawing of the sandwiched PDMS optical waveguide, in which the middle PDMS layer has refractive index of 1.45, and the other layers have refractive index of 1.43. A Zemax simulation gives the coupling efficiency of this structure is 91.2%, 3.9% higher than the normal structure without waveguide previous shown in Figure 5-6.

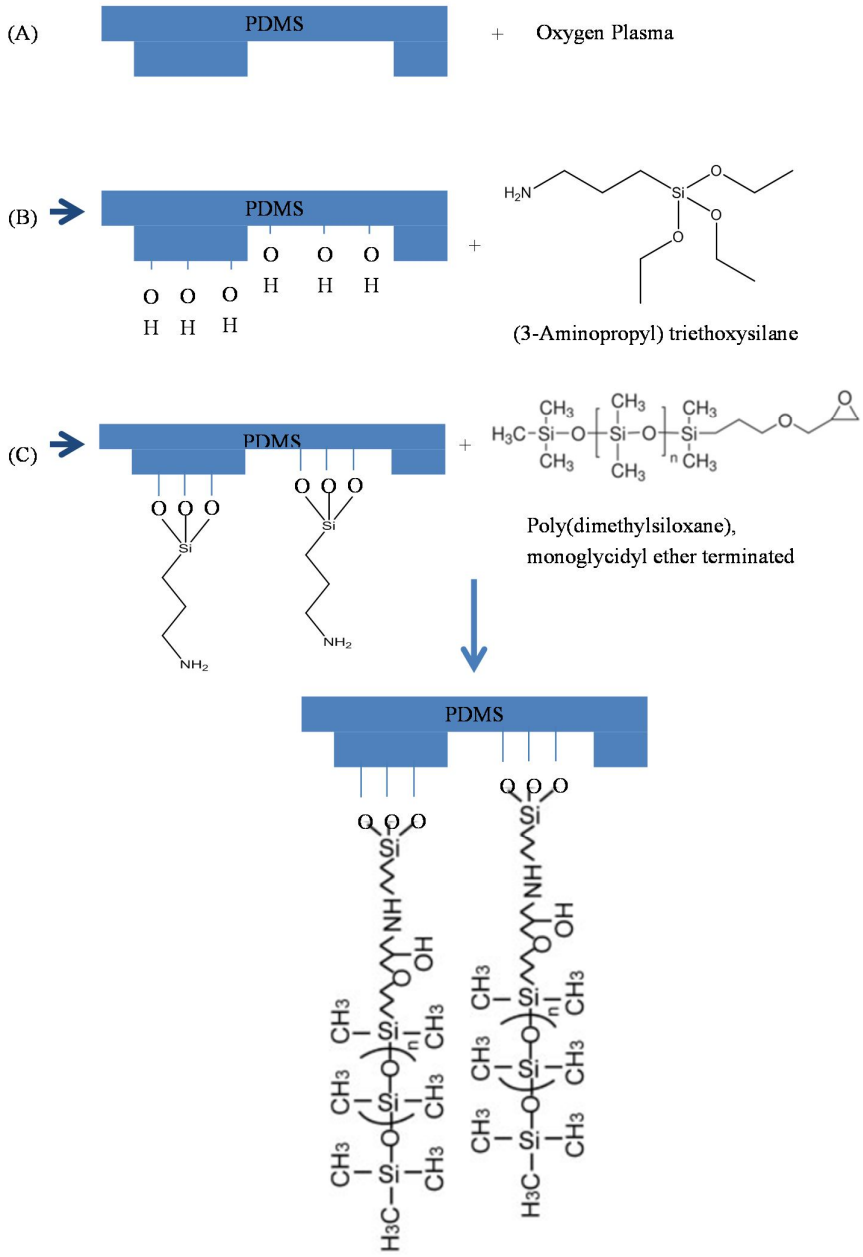

Figure 5-12: PDMS coating processing. (A) The PDMS device was treated with Oxygen plasma. (B) The plasma treated PDMS was immersed in (3-Aminopropyl)triethoxysilane (APTES) solution, the APTES molecules were grafted on the PDMS surface. (C) The Poly(dimethylsiloxane) monoglycidyl ether terminated was dropped on the silanized PDMS surface, it was reacted with the APTES and coated on the PDMS surface.

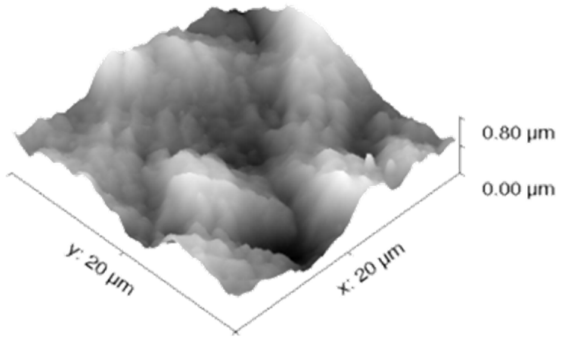

(A)

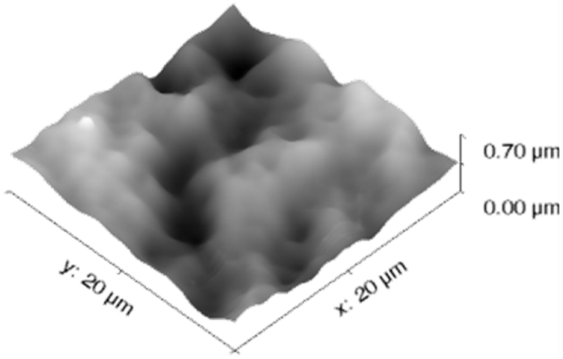

(B)

Figure 5-13: AFM images of PDMS cylindrical lens surface: (A) before modification, the surface roughness was 115nm; (B) after monoglycidyl ether terminated Poly(dimethylsiloxane) coating, the surface roughness was 85nm.

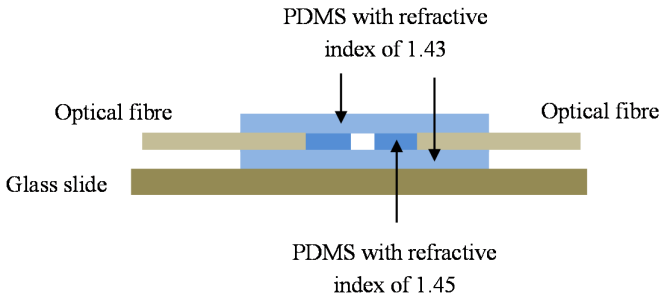

Figure 5-14: Schematic profile of the chip formed from three layers of PDMS. The middle layer was the waveguide core layer with refractive index of 1.45; the other two layers were cladding layers with refractive index of 1.43. The chip was bonded to a glass slide using oxygen plasma.

To fabricate the PDMS waveguide, a degassed PDMS mix (base to curing reagent ratio 10:1) was poured onto the SU-8 master and excess PDMS was scrapped off with a glass slide (Figure 5-15A). This layer was baked on a hotplate at 120°C for 2 hours (Figure 5-15B) to fully cure the PDMS. At this temperature the PMDS has a refractive index of 1.45 (Chang-Yen *et al.*, 2005). A second layer of PDMS was the poured over the wafer (Figure 5-15C), and the structure placed in a desiccator at room temperature for 48 hours to cure, giving a refractive index of 1.43 (Chang-Yen *et al.*, 2005). The fully cured PDMS was peeled off the wafer and bonded to a flat PDMS plate and cured at room temperature (Figure 5-15D). Finally, the PDMS device was bonded to a glass slide. The coupling efficiency results from experimental measurements was 79.1% (n=10, standard deviation = 3.0%), 0.9% higher than the original device.

5.4.5 Optical lens in microfluidics

In the work presented by Loock's group (Li *et al.*, 2006, Waechter *et al.*, 2011), a micro lens was made on the end of fibre to increase the coupling efficiency. In other microfluidic devices, micro-lens was also studied to increase the optical performance, such as Ogilvie *et al.* (2010) reported a PMMA on-chip lens for focusing the light for absorbance measurement; Camou *et al.* (Camou *et al.*, 2003) reported a PDMS on-chip lens. In this section, on-chip lens is investigated to optimise the light coupling efficiency.

As shown in Figure 5-16, two designs were made to use the on-chip micro lens. In design A (Figure 5-16A), two lens are used in the device, the light comes out from delivery fibre and collimated by the first micro lens. The collimated light passes through the microfluidic channel and focused by the second micro lens, then the focused light is collected by the acceptance fibre. In design B (Figure 5-16B), the light comes out from delivery fibre, and be collimated and focused by a micro lens pair. In the lens pair, the second micro lens, is connected with the micro-channel, the focused light goes directly into the microfluidic channel.

The micro lens was simulated using Zemax software. Considering the fabrication limits, the radius of the micro lens was 230μm, which considered the fabrication limitation. The lens distance in design A was 740μm, while in design B was 200μm. The coupling efficiency for design A was 81%, and for design B was 93% from the Zemax simulation. So design B was selected and fabricated, a coupling efficiency of 78.1% (n=10, standard deviation = 3.5%) was measured,

similar the optical fibre direct coupling efficiency. One big disadvantage of this micro lens design is the lack of anti-reflection coating, the reflection at the interface causes severe light loss.

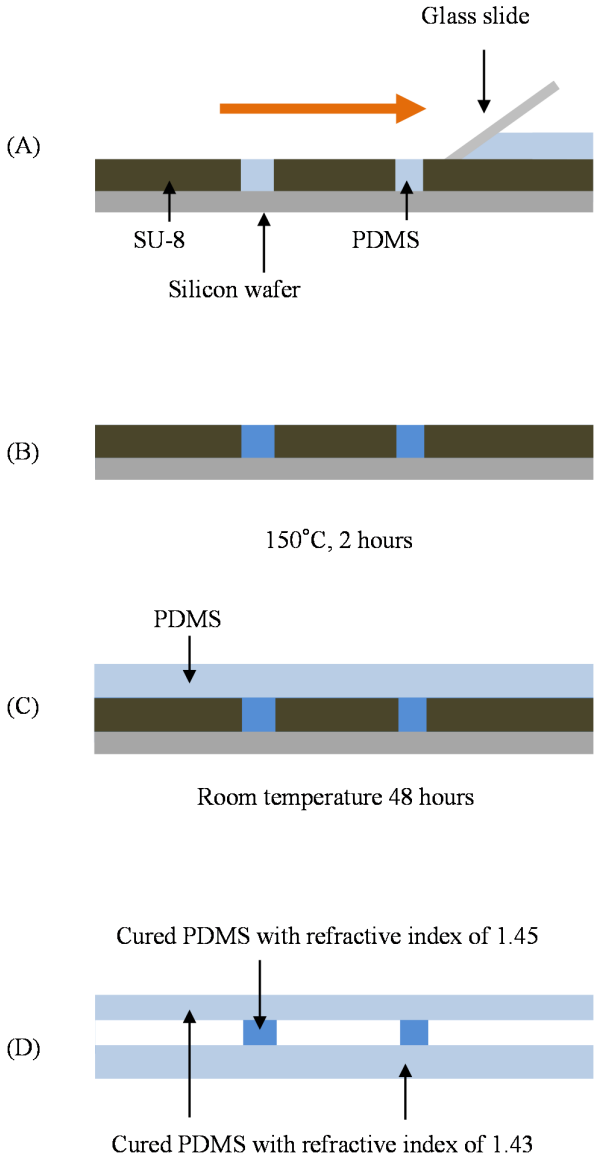

Figure 5-15: Fabrication of a PDMS waveguide. (A) Degassed PDMS was poured onto the SU-8 wafer, and scrapped with a glass slide. (B) Cured on a hotplate at 120℃ for 2 hours. (C) Fresh PDMS was poured again on the wafer, and cured at room temperature for 48 hours. (D) The PDMS device was oxygen plasma bonded to a PDMS plate and cured in room temperature.

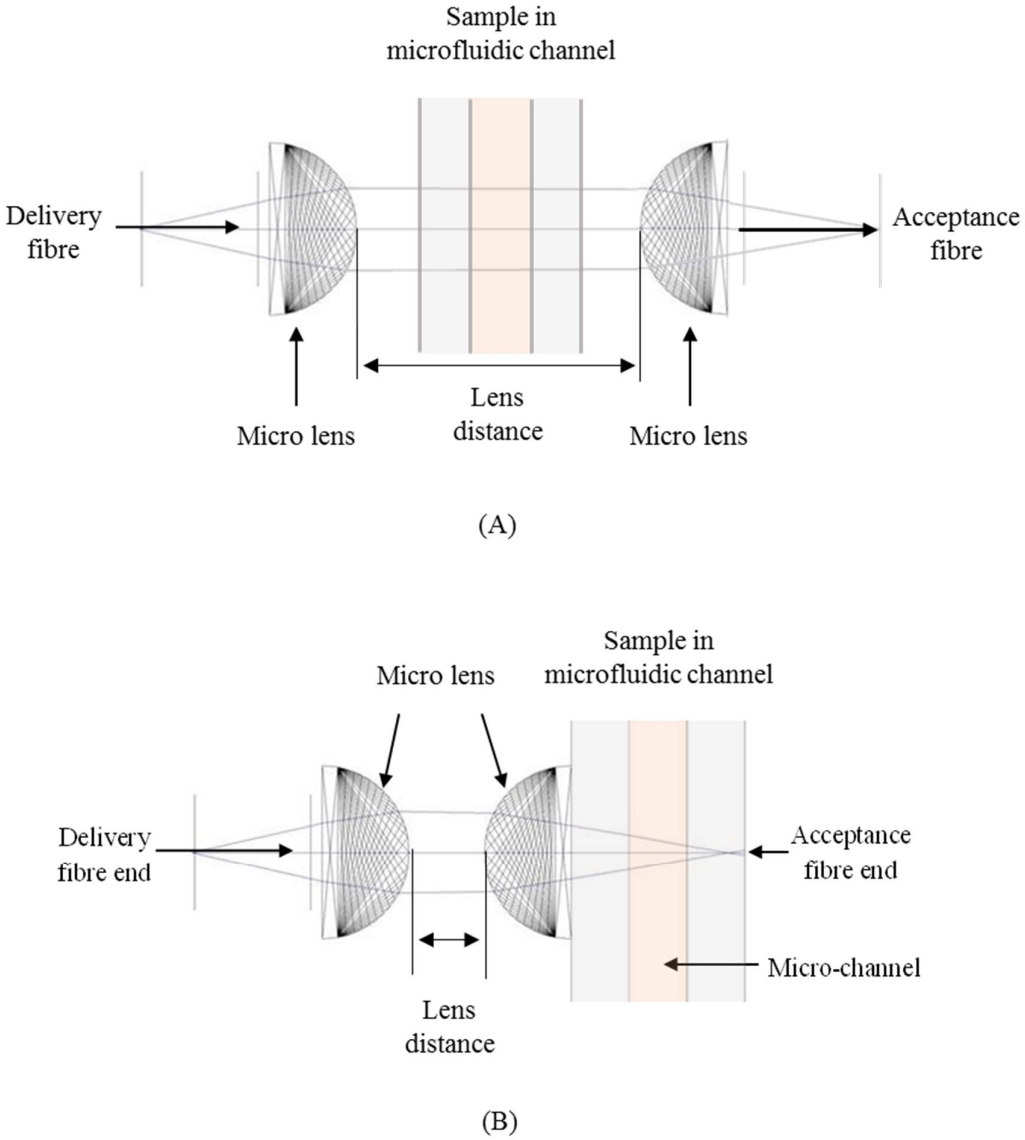

Figure 5-16: The schematic of on-chip micro lens. (A) The light comes out from delivery fibre and collimated by the first micro lens. The collimated light passes through the microfluidic channel and focused by the second micro lens, then the focused light is collected by the acceptance fibre. (B) The light comes out from delivery fibre, and be collimated and focused by two micro lens. The second micro lens, i.e. the focusing lens, is connected with the micro-channel, the focused light goes directly into the microfluidic channel.

5.5 CRDS-Microfluidic analysis

As discussed above, in vertical coupling chips, the fibre alignment has to be performed with a micro-movement stage on an optical table, it is not a system integration. So in the CRDS-microfluidics integration described in this section, the horizontal coupling chip was applied for nitrite detection with Griess reaction. The Griess reaction relies on the formation of an Azo dye from the reaction of sulphanilamide hydrochloride and N-(1-Naphthyl) ethylenediamine dihydrochloride (N.E.D.) with nitrite, and has been used for over a century (Moorcroft *et al.*, 2001). The reagent used for nitrite detection, also called the Griess reagent, was created by dissolving 0.5g sulphanilamide, 5mL of 37% hydrochloric acid and 0.05g N.E.D. in MilliQ ultrapure water to make total volume of 500mL (Sieben *et al.*, 2010).. For the assays, the nitrite solution was mixed with the Griess reagent in the same volume with a test tube. After 10 minutes incubation at room temperature, the solution was pumped into the micro-channel via the sample inlet with a syringe pump at a flow rate of 5μL/min, and FC-40 oil was loaded via the oil inlet at a flow rate of 20μL/min. The absorption coefficient for the azo dye product of the Griess reaction was measured as (96 400 ± 1600) $M^{-1}cm^{-1}$, which was reported in (Rushworth et al., 2013).

From (5.1) to (5.6), for the horizontal coupling chip, the light coupling efficiency was 78.1%, so the single loop light transmission ratio was 75.6%, corresponding to $\Delta\kappa_{min}l = 2.05 \times 10^{-2}$, which is the detection limit of light absorbance. The light path length $l = 0.1\text{mm}$, so the detection limit of nitrite concentration is expected to be 21.3μM.

From the nitrite detection results, the limit of detection (LOD) (mean signal value higher than three times the standard deviation) of 50μM were measured with the 0.1mm wide channel, corresponding to $\Delta\kappa_{min}l = 4.82 \times 10^{-2}$. In the work previously reported by Sieben *et al.*, where a nitrite detection limit of 14nM was achieved using a 25mm long single pass channel fabricated in black PMMA (Sieben *et al.*, 2010), corresponding to $\Delta\kappa_{min}l = 3.37 \times 10^{-3}$, the sensitivity of which is about 14 times of the horizontal coupling CRDS device. In the mirror-based CRDS system coupled to a 1mm path length flow cell reported in (Rushworth *et al.*, 2013), the light coupling efficiency was 99.75%, it achieved a LOD of 1.9nM nitrite, corresponding to $\Delta\kappa_{min}l = 1.83 \times 10^{-5}$, 2,600 times better than the horizontal device and 184 times better than Sieben's system, the comparison is shown in Table 5-3.

Table 5-3 Comparison of the system in this chapter with references.

System	Light coupling efficiency	Light path length	Limit of detection of nitrite concentration	Limit of detection of absorbance
This chapter	75.6%	0.1mm	50μM	4.82×10^{-2}
(Sieben *et al.*, 2010)	NA	25mm	14nM	3.37×10^{-3}
(Rushworth *et al.*, 2013)	99.75%	1mm	1.9nM	1.83×10^{-5}

The main problem of the proposed system is the high light loss. By calculating from (5.1) to (5.6), to achieve the same performance as reported in (Sieben *et al.*, 2010) and (Rushworth *et al.*, 2013), the total single loop light transmission ratio should be higher than 89% and 99.2% separately. The CRDS system used in this chapter induced 3.3% light loss, so to achieve the same performance with the Sieben's long light path device, the light coupling efficiency of microfluidic chip has to be higher than 92%; and the fibre loop CRDS system used in this chapter cannot achieve higher sensitivity detection than Rushworth's mirror based CRDS system.

5.6 Conclusions

Two fibre coupling methods were investigated for a fibre loop CRDS system. The system was designed to analyse droplet in a microfluidic device. For vertical coupling, a chip with thickness of 340μm was fabricated from two 120μm thick glass cover slips and a 100μm thick PDMS space layer. A 450μm wide channel was made to fit the 400μm fibre. A light coupling efficiency of 98.3% was achieved, comparing well with previous reported device (Rushworth, 2012).

In horizontal coupling, cylindrical lens coupling was investigated to increase the fibre coupling efficiency. This arrangement was designed and simulated with Zemax optical simulation software, and the device was made with PDMS. The surface roughness of the PDMS lens was 115nm, which was improved to 28.1nm by using RIE etching followed with PDMS coating. However, this is still much higher than required for a high performance optical components (< 15nm).. Experimental results from a Griess reaction show that the limit of detection of the fibre loop CRDS system was 50μM nitrite with a 100μm long light path. Therefore, a good light coupling

is critical for a high performance CRDS system, further investigation is still needed to increase light coupling efficiency of a CRDS-microfluidic integration.

Chapter 6

Conclusions and Future Direction

Discussions

6.1 Conclusions

In this thesis, I have developed a novel Slipchip device for isoelectric focusing separation of biomolecules and *in situ* compartmentalization of the separation samples into micro-droplets. I also investigated high sensitivity cavity ring down spectroscopic detection with droplet microfluidics.

A 3D plastic Slipchip platforms were proved to be easy to fabricate, and suitable for separation based biomolecule analysis. The process flow including laser ablation and micro milling of PMMA substrates. The prototyping time was reduced dramatically from original two weeks to two hours. A new UV transmission PMMA material with a cut-off wavelength of 260nm was used as the substitute for microfluidic devices for the first time. This PMMA device is suitable for DAPI fluorescence detection, whose excitation wavelength is 352-402nm, and emission wavelength is 417-477nm. The light transmission of the fabricated channel was improved by surface reflowing with chloroform vapour, giving a light transmission ratio up to 88.3%. In comparison, the laser ablated channel can only transmit 35.1% of light as observed by a bright field microscope. A modified Slipchip fabrication method was developed based on PMMA-tape-PMMA sandwich structures, using laser cut thin PMMA film bonded to another substrate with double sided tape. With this method, the light transmission ratio was improved to 91.3%. A versatile Slipchip operation platform was designed and fabricated, using magnets to clamp the

two halves of the Slipchip and a micro-meter drive to control the slipping. The maximum slipping distance is 10mm, and the alignment resolution is 10μm. Operation of the Slipchip is much easier and does not require special training.

With the proposed rapid prototyping method, a novel method of Slipchip based isoelectric focusing separation and sample collection was proposed and tested. IEF separation was performed in a zig-zag channel formed from wells in two halves of the chip, and the separated sample was compartmentalised *in situ* into droplets, which can be collected for downstream analysis. A uniform pH gradient was established in the zig-zag channel with average RSD of 4.9%. The peak capacity is 140, calibrated with commercial pI markers. A total of 141 wells in this device can effectively compartmentalise the focused peaks. Two droplet collection strategies, serial and parallel droplet collection, were described. For serial collection, the droplets were collected into tubing with the sequence of droplets maintained. For parallel collection, the droplets of interests were collected individually with a pipette; the collection efficiency was 91%. This device shows an effective way to covert sample from continuous to droplet. As a demonstration of the application, five standard proteins were separated with the device and the collected droplets analysed downstream by converting the droplet back into continuous with gel electrophoresis using an Agilent 2100 Bioanalyzer. The compartmentalized droplets can also be post-processed on-chip, demonstrated using universal pH indicator solution to show pH gradients in the channel.

A microfluidic interface was investigated for coupling fibre loop CRDS to droplet microfluidics. Two fibre coupling methods were studied. A glass-PDMS-glass structure chip was fabricated for a vertical (free space) interfacing method. The light loss of such method was measured at 1.7%, comparable with the literature available (Rushworth, 2012). For horizontal (integrated) fibre coupling method, cylindrical lens were used in an attempt to increase the light coupling efficiency. RIE etching and PDMS coating of the chip were used to reduce the surface roughness of the PDMS channel. AFM scanning shows that the surface treatment processes reduced the PDMS roughness from 115nm to 28.1nm. This device was used for nitrite detection giving a, the LOD of 50μM nitrite for a 100μm long light path length.

6.2 Future work

I would suggest the future work following this thesis from three areas. First, the Slipchip device developed in this research can achieve *in situ* continuous-flow/micro-droplet conversion of chemically separated samples; however the compartments were regenerated into continuous form for capillary gel electrophoresis in an Agilent 2100 Bioanalyzer. During the regeneration process, manual handling of liquid samples is still needed. A natural step forward would be performing micro-droplet/continuous-flow conversion within the same Slipchip, by combining CE channels and separation media to the chip. Such a device can directly perform continuous-flow/micro-droplet conversion and micro-droplet/continuous-flow conversion for two dimensional separation, which has the potential to significantly increase separation resolution. It also could avoid the interfacing challenges faced with the current 2D separation chip (for example, how to effectively transfer sample from the 1st dimension to the 2nd (Chen *et al.*, 2002)).

Second, the digitised droplets can be collected and stored serially in tubing, as described in section 4.3.3. These droplets can be spotted onto a plate for Matrix-Assisted Laser Desorption/Ionization (MALDI) Mass Spectrometry analysis as demonstrated by Pereira *et al.* (Pereira *et al.*, 2013), therefore achieving molecule identifications. The droplets can also be further analysed (for example, parallel immunoassays as demonstrated by Ismagilov's group (Liu *et al.*, 2010)). Therefore this device provides a facile interface between serial and parallel droplet manipulations.

I have prototyped a droplet trapping chip for converting the serial droplets into parallel as shown in Figure 6-1, which can convert the serial droplets, either be produced from the same Slipchip or collected from other sampling device like Dropix (Gielen *et al.*, 2013), into parallel. The chip was fabricated from a PMMA-tape-PMMA structure using the process and method developed in section 3.3.2. Initial testing showed that when the pre-produced droplets were injected into the trapping channel, they were trapped in the wells with inverse sequence (Figure 6-1 C-H and I). More quantitative characterizations are needed in the future to make a reliable droplet trapping system (such as droplet size, flow rate, surfactant etc.), which could have the potential of hyphenating closed channel based droplet microfluidics with the Slipchip format.

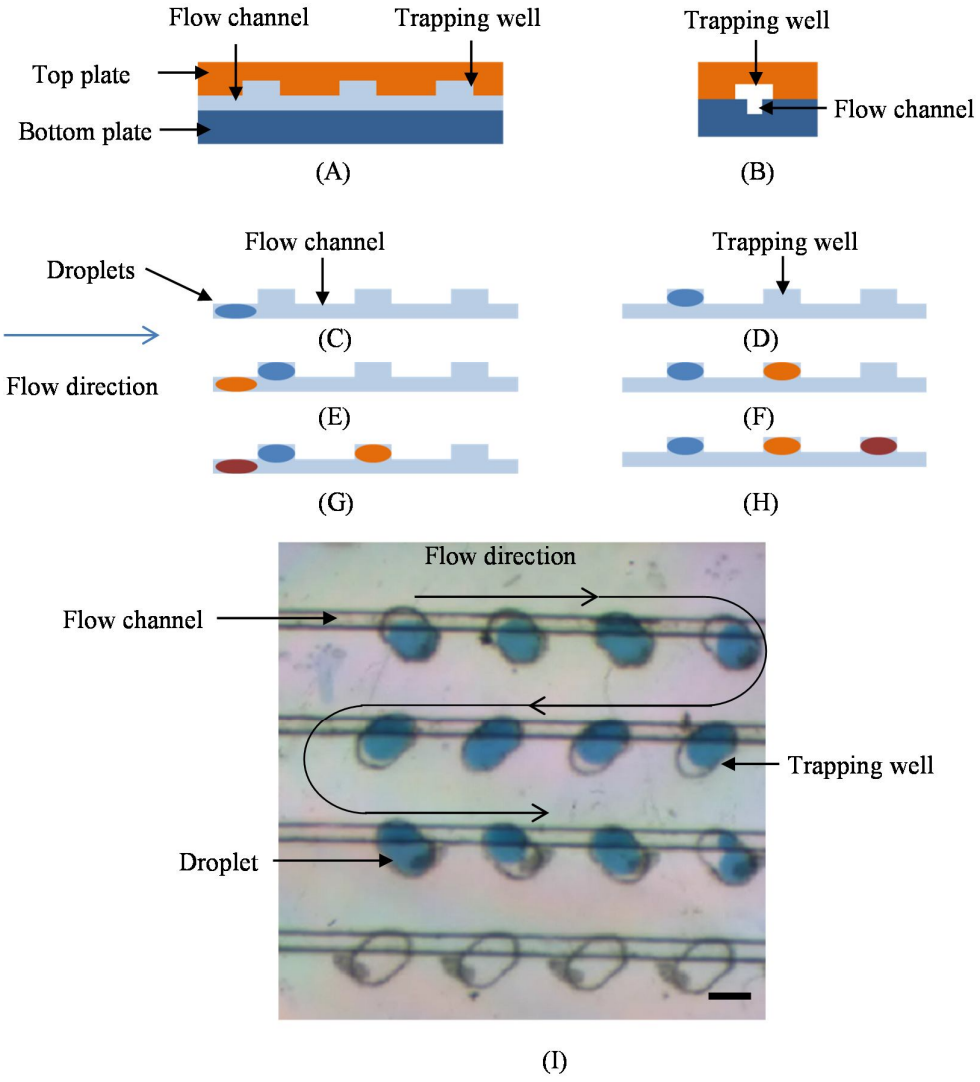

Figure 6-1: Droplet "serial" to "parallel" conversion in a Slipchip. (A) Side view of the channel. The flow channel and trapping well are on separate Slipchip plates. (B) The section view of the channel. The trapping wells are aligned with flow channel. (C)-(D) show that the first droplet (blue) comes from the left side can be trapped in the left well. (E)-(F) show the second droplet (orange) can be trapped in the middle well next to the first droplet. And (G)-(H) the third droplet (deep red) can be trapped in the right well next to the second droplet, so the droplet sequence will be inversed. (I) Bright field microscopy image of the droplet trapped in Slipchip wells from initial experiment. The scale bar is 1mm.

Third, the fibre loop CRDS may not be the best option for coupling with microfluidics, as shown in the studies in Chapter 5. The light loss in a fibre-microfluidic interface is much higher than a mirror-microfluidic interface, therefore a mirror based CRDS might be a more promising detection method for droplet microfluidics including Slipchip. A schematic design of such interface is shown in Figure 6-2. Metal electrodes can be patterned in droplet wells by metal deposition and patterning or via the PMMA-tape-PMMA sandwich method presented in section 3.3.2 (Figure 6-2A). The droplets in the wells on different plates could be merged by applying an electric field (Figure 6-2B) between the metal electrodes. The flat metal electrodes could also work as mirrors, forming an optical cavity for CRDS based detection of droplets (Figure 6-2C).

An initial test was performed based on this design, where a 530nm LED was used as the light source and a PMT for detector. The electrode mirror was coated with a 100nm thick Cr metallic coating. The mirror reflectivity was measured to be 0.54 – 0.78, which is comparable to (Billot *et al.*, 2008) with a reflectivity of 0.65. However, a commercial mirror can have a reflectivity of more than 0.99 (although not for droplet detection). Another problem is not transmission light was observed in the test, which means it cannot be used for a CRDS system. So fabricating a suitable mirror electrode is a critical step for the future work.

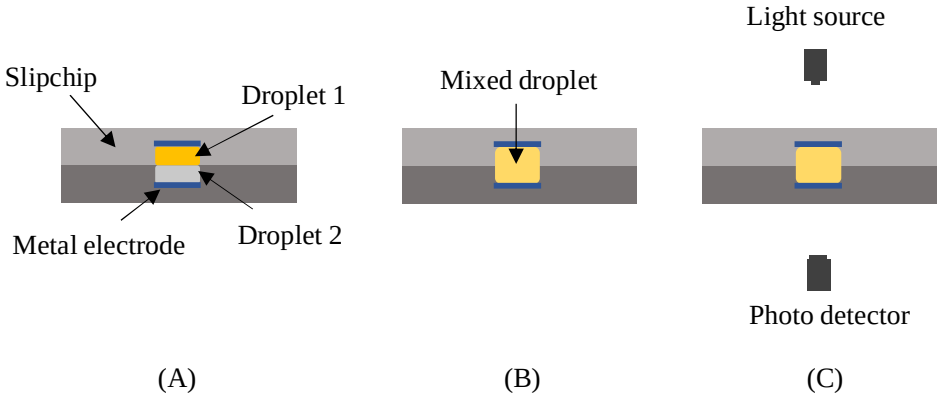

Figure 6-2: (A) Schematic of on-chip electrodes. (B) Merging of two droplets by applying an electric field between the electrodes. (C) The metal electrodes can also work as mirrors forming a cavity to perform on-line CRDS analysis of the droplet.

List of References

ABATE, A. R., THIELE, J. & WEITZ, D. A. 2011. One-step formation of multiple emulsions in microfluidics. *Lab on a Chip,* 11, 253-258.

ABATE, A. R. & WEITZ, D. A. 2009. High-Order Multiple Emulsions Formed in Poly(dimethylsiloxane) Microfluidics. *Small,* 5, 2030-2032.

ADAMSON, D. N., MUSTAFI, D., ZHANG, J. X. J., ZHENG, B. & ISMAGILOV, R. F. 2006. Production of arrays of chemically distinct nanolitre plugs via repeated splitting in microfluidic devices. *Lab on a Chip,* 6, 1178-1186.

AGRESTI, J. J., ANTIPOV, E., ABATE, A. R., AHN, K., ROWAT, A. C., BARET, J.-C., MARQUEZ, M., KLIBANOV, A. M., GRIFFITHS, A. D. & WEITZ, D. A. 2010. Ultrahigh-throughput screening in drop-based microfluidics for directed evolution. *Proceedings of the National Academy of Sciences,* 107, 4004-4009.

AHMED, R. & JONES, T. B. 2006. Dispensing picoliter droplets on substrates using dielectrophoresis. *Journal of Electrostatics,* 64, 543-549.

ANNA, S. L., BONTOUX, N. & STONE, H. A. 2003. Formation of dispersions using "flow focusing" in microchannels. *Applied Physics Letters,* 82, 364-366.

BEATTIE, J. K. 2006. The intrinsic charge on hydrophobic microfluidic substrates. *Lab on a Chip,* 6, 1409-1411.

BESCHERER, K., BARNES, J. A. & LOOCK, H. P. 2013. Absorption Measurements in Liquid Core Waveguides Using Cavity Ring-Down Spectroscopy. *Analytical Chemistry,* 85, 4328-4334.

BHATTACHARYA, S., DATTA, A., BERG, J. M. & GANGOPADHYAY, S. 2005. Studies on surface wettability of poly(dimethyl) siloxane (PDMS) and glass under oxygen-plasma treatment and correlation with bond strength. *Journal of Microelectromechanical Systems,* 14, 590-597.

BILLOT, L., PLECIS, A. & CHEN, Y. 2008. Multi-reflection based on chip label free molecules detection. *Microelectronic Engineering,* 85, 1269-1271.

BJELLQVIST, B., EK, K., RIGHETTI, P. G., GIANAZZA, E., GORG, A., WESTERMEIER, R. & POSTEL, W. 1982. Isoelectric-Focusing in Immobilized Ph Gradients - Principle,

Methodology and Some Applications. *Journal of Biochemical and Biophysical Methods,* 6, 317-339.

BOUSSE, L., MOURADIAN, S., MINALLA, A., YEE, H., WILLIAMS, K. & DUBROW, R. 2001. Protein sizing on a microchip. *Analytical Chemistry,* 73, 1207-1212.

BROUZES, E., MEDKOVA, M., SAVENELLI, N., MARRAN, D., TWARDOWSKI, M., HUTCHISON, J. B., ROTHBERG, J. M., LINK, D. R., PERRIMON, N. & SAMUELS, M. L. 2009. Droplet microfluidic technology for single-cell high-throughput screening. *Proceedings of the National Academy of Sciences of the United States of America,* 106, 14195-14200.

BROWN, L., KOERNER, T., HORTON, J. H. & OLESCHUK, R. D. 2006. Fabrication and characterization of poly(methylmethacrylate) microfluidic devices bonded using surface modifications and solvents. *Lab on a Chip,* 6, 66-73.

BU, M. Q., MELVIN, T., ENSELL, G. J., WILKINSON, J. S. & EVANS, A. G. R. 2004. A new masking technology for deep glass etching and its microfluidic application. *Sensors and Actuators a-Physical,* 115, 476-482.

CAMOU, S., FUJITA, H. & FUJII, T. 2003. PDMS 2D optical lens integrated with microfluidic channels: principle and characterization. *Lab on a Chip,* 3, 40-45.

CAO, C. X., FAN, L. Y. & ZHANG, W. 2008. Review on the theory of moving reaction boundary, electromigration reaction methods and applications in isoelectric focusing and sample pre-concentration. *The Analyst,* 133, 1139-1157.

CHAN, K. L. A., NIU, X., DEMELLO, A. J. & KAZARIAN, S. G. 2011. Generation of Chemical Movies: FT-IR Spectroscopic Imaging of Segmented Flows. *Analytical Chemistry,* 83, 3606-3609.

CHANG-YEN, D. A., EICH, R. K. & GALE, B. K. 2005. A monolithic PDMS waveguide system fabricated using soft-lithography techniques. *Journal of lightwave technology,* 23, 2088.

CHEN, H. & FAN, Z. H. 2009. Two-dimensional protein separation in microfluidic devices. *Electrophoresis,* 30, 758-765.

CHEN, X. X., WU, H. K., MAO, C. D. & WHITESIDES, G. M. 2002. A prototype two-dimensional capillary electrophoresis system fabricated in poly(dimethylsiloxane). *Analytical Chemistry,* 74, 1772-1778.

CHIU, C. P., CHEN, W. J. & FAN, S. K. 2007. Enhanced droplet mixer by LDEP on spiral microelectrodes. *2007 2nd IEEE International Conference on Nano/Micro Engineered and Molecular Systems, Vols 1-3,* 711-714.

CHIU, D. T. 2010. Interfacing droplet microfluidics with chemical separation for cellular analysis. *Analytical and Bioanalytical Chemistry,* 397, 3179-3183.

CHO, S. K., MOON, H. J. & KIM, C. J. 2003. Creating, transporting, cutting, and merging liquid droplets by electrowetting-based actuation for digital microfluidic circuits. *Journal of Microelectromechanical Systems,* 12, 70-80.

CHOBAN, E. R., MARKOSKI, L. J., WIECKOWSKI, A. & KENIS, P. J. A. 2004. Microfluidic fuel cell based on laminar flow. *Journal of Power Sources,* 128, 54-60.

CHURSKI, K., MICHALSKI, J. & GARSTECKI, P. 2010. Droplet on demand system utilizing a computer controlled microvalve integrated into a stiff polymeric microfluidic device. *Lab on a Chip,* 10, 512-518.

CRISTOBAL, G., ARBOUET, L., SARRAZIN, F., TALAGA, D., BRUNEEL, J. L., JOANICOT, M. & SERVANT, L. 2006. On-line laser Raman spectroscopic probing of droplets engineered in microfluidic devices. *Lab on a Chip,* 6, 1140-1146.

CUI, H. C., HORIUCHI, K., DUTTA, P. & IVORY, C. F. 2005a. Isoelectric focusing in a poly(dimethylsiloxane) microfluidic chip. *Analytical Chemistry,* 77, 1303-1309.

CUI, H. C., HORIUCHI, K., DUTTA, P. & IVORY, C. F. 2005b. Multistage isoelectric focusing in a polymeric microfluidic chip. *Analytical Chemistry,* 77, 7878-7886.

DAS, C., ZHANG, J., DENSLOW, N. D. & FAN, Z. H. 2007. Integration of isoelectric focusing with multi-channel gel electrophoresis by using microfluidic pseudo-valves. *Lab on a Chip,* 7, 1806-1812.

DENDUKURI, D. & DOYLE, P. S. 2009. The Synthesis and Assembly of Polymeric Microparticles Using Microfluidics. *Advanced Materials,* 21, 4071-4086.

DOLNIK, V. & LIU, S. R. 2005. Applications of capillary electrophoresis on microchip. *Journal of Separation Science,* 28, 1994-2009.

DRAPER, M. C., NIU, X. Z., CHO, S., JARNES, D. I. & EDEL, J. B. 2012. Compartmentalization of Electrophoretically Separated Analytes in a Multiphase Microfluidic Platform. *Analytical Chemistry,* 84, 5801-5808.

DU, W. B., LI, L., NICHOLS, K. P. & ISMAGILOV, R. F. 2009. SlipChip. *Lab on a chip,* 9, 2286-2292.

DUFFY, D. C., MCDONALD, J. C., SCHUELLER, O. J. A. & WHITESIDES, G. M. 1998. Rapid prototyping of microfluidic systems in poly(dimethylsiloxane). *Analytical Chemistry,* 70, 4974-4984.

DUGGAN, M. P., MCCREEDY, T. & AYLOTT, J. W. 2003. A non-invasive analysis method for on-chip spectrophotometric detection using liquid-core waveguiding within a 3D architecture. *Analyst,* 128, 1336-1340.

DUPIN, M. M., HALLIDAY, I. & CARE, C. M. 2006. Simulation of a microfluidic flow-focusing device. *Physical Review E,* 73.

EDDINGS, M. A., JOHNSON, M. A. & GALE, B. K. 2008. Determining the optimal PDMS-PDMS bonding technique for microfluidic devices. *Journal of Micromechanics and Microengineering,* 18.

EDGAR, J. S., MILNE, G., ZHAO, Y. Q., PABBATI, C. P., LIM, D. S. W. & CHIU, D. T. 2009. Compartmentalization of Chemically Separated Components into Droplets. *Angewandte Chemie-International Edition,* 48, 2719-2722.

EGATZ-GOMEZ, A. & THORMANN, W. 2011. Micropreparative isoelectric focusing protein separation in a suspended drop. *Electrophoresis,* 32, 1433-1437.

EMRICH, C. A., MEDINTZ, I. L., CHU, W. K. & MATHIES, R. A. 2007. Microfabricated two-dimensional electrophoresis device for differential protein expression profiling. *Analytical Chemistry,* 79, 7360-7366.

FLEGER, M. & NEYER, A. 2006. PDMS microfluidic chip with integrated waveguides for optical detection. *Microelectronic Engineering,* 83, 1291-1293.

FOWLER, J., MOON, H. J. & KIM, C. J. 2002. Enhancement of mixing by droplet-based microfluidics. *Fifteenth Ieee International Conference on Micro Electro Mechanical Systems, Technical Digest,* 97-100.

FRENZ, L., BLOUWOLFF, J., GRIFFITHS, A. D. & BARET, J. C. 2008. Microfluidic Production of Droplet Pairs. *Langmuir,* 24, 12073-12076.

GARSTECKI, P., FUERSTMAN, M. J., STONE, H. A. & WHITESIDES, G. M. 2006. Formation of droplets and bubbles in a microfluidic T-junction - scaling and mechanism of break-up. *Lab on a Chip,* 6, 437-446.

GAUDIOSO, J. & CRAIGHEAD, H. G. 2002. Characterizing electroosmotic flow in microfluidic devices. *Journal of Chromatography A,* 971, 249-253.

GEISER, L., VAEZZADEH, A. R., DESHUSSES, J. M. & HOCHSTRASSER, D. F. 2011. Shotgun proteomics: a qualitative approach applying isoelectric focusing on immobilized pH gradient and LC-MS/MS. *Methods Mol Biol,* 681, 449-58.

GHOSAL, S. 2004. Fluid mechanics of electroosmotic flow and its effect on band broadening in capillary electrophoresis. *Electrophoresis,* 25, 214-228.

GIANAZZA, E. & RIGHETTI, P. G. 2009. Immobilized pH gradients. *Electrophoresis,* 30, S112-S121.

GIELEN, F., VAN VLIET, L., KOPROWSKI, B. T., DEVENISH, S. R. A., FISCHLECHNER, M., EDEL, J. B., NIU, X. Z., DEMELLO, A. J. & HOLLFELDER, F. 2013. A Fully Unsupervised Compartment-on-Demand Platform for Precise Nanoliter Assays of Time-Dependent Steady-State Enzyme Kinetics and Inhibition. *Analytical Chemistry,* 85, 4761-4769.

GINN, B. T. & STEINBOCK, O. 2003. Polymer surface modification using microwave-oven-generated plasma. *Langmuir,* 19, 8117-8118.

GORG, A., BOGUTH, G., OBERMAIER, C. & WEISS, W. 1998. Two-dimensional electrophoresis of proteins in an immobilized pH 4-12 gradient. *Electrophoresis,* 19, 1516-1519.

GORG, A., DREWS, O., LUCK, C., WEILAND, F. & WEISS, W. 2009. 2-DE with IPGs. *Electrophoresis,* 30, S122-S132.

GORKIN, R., PARK, J., SIEGRIST, J., AMASIA, M., LEE, B. S., PARK, J. M., KIM, J., KIM, H., MADOU, M. & CHO, Y. K. 2010. Centrifugal microfluidics for biomedical applications. *Lab on a Chip,* 10, 1758-1773.

GUIJT, R. M., ARMSTRONG, J. P., CANDISH, E., LEFLEUR, V., PERCEY, W. J., SHABALA, S., HAUSER, P. C. & BREADMORE, M. C. 2011. Microfluidic chips for capillary electrophoresis with integrated electrodes for capacitively coupled conductivity detection based on printed circuit board technology. *Sensors and Actuators B-Chemical,* 159, 307-313.

GUO, F., LIU, K., JI, X. H., DING, H. J., ZHANG, M., ZENG, Q. A., LIU, W., GUO, S. S. & ZHAO, X. Z. 2010. Valve-based microfluidic device for droplet on-demand operation and static assay. *Applied Physics Letters,* 97.

GUO, M. T., ROTEM, A., HEYMAN, J. A. & WEITZ, D. A. 2012. Droplet microfluidics for high-throughput biological assays. *Lab on a Chip,* 12, 2146-2155.

HADWEN, B., BRODER, G. R., MORGANTI, D., JACOBS, A., BROWN, C., HECTOR, J. R., KUBOTA, Y. & MORGAN, H. 2012. Programmable large area digital microfluidic array with integrated droplet sensing for bioassays. *Lab on a chip,* 12, 3305-3313.

HALLOCK, A. J., BERMAN, E. S. F. & ZARE, R. N. 2003. Ultratrace kinetic measurements of the reduction of methylene blue. *Journal of the American Chemical Society,* 125, 1158-1159.

HARRISON, D. J., FLURI, K., SEILER, K., FAN, Z. H., EFFENHAUSER, C. S. & MANZ, A. 1993. Micromachining a Miniaturized Capillary Electrophoresis-Based Chemical-Analysis System on a Chip. *Science,* 261, 895-897.

HARRISON, D. J., MANZ, A., FAN, Z. H., LUDI, H. & WIDMER, H. M. 1992. Capillary Electrophoresis and Sample Injection Systems Integrated on a Planar Glass Chip. *Analytical Chemistry,* 64, 1926-1932.

HASHIMOTO, M., SHEVKOPLYAS, S. S., ZASONSKA, B., SZYMBORSKI, T., GARSTECKI, P. & WHITESIDES, G. M. 2008. Formation of Bubbles and Droplets in Parallel, Coupled Flow-Focusing Geometries. *Small,* 4, 1795-1805.

HERR, A. E., MOLHO, J. I., DROUVALAKIS, K. A., MIKKELSEN, J. C., UTZ, P. J., SANTIAGO, J. G. & KENNY, T. W. 2003. On-chip coupling of isoelectric focusing and free solution electrophoresis for multidimensional separations. *Analytical Chemistry,* 75, 1180-1187.

HOFMANN, O., CHE, D. P., CRUICKSHANK, K. A. & MULLER, U. R. 1999. Adaptation of capillary isoelectric focusing to microchannels on a glass chip. *Analytical Chemistry,* 71, 678-686.

HONG, T. F., JU, W. J., WU, M. C., TAI, C. H., TSAI, C. H. & FU, L. M. 2010. Rapid prototyping of PMMA microfluidic chips utilizing a CO2 laser. *Microfluidics and Nanofluidics,* 9, 1125-1133.

HUA, Y. M., KOSHEL, B. M. & WIRTH, M. J. 2010. Field-Free Remobilization of Proteins after Isoelectric Focusing in Packed Capillaries. *Analytical Chemistry,* 82, 8910-8915.

HUANG, T. L., SHIEH, P. C. H. & COOKE, N. 1994. Isoelectric-Focusing of Proteins in Capillary Electrophoresis with Pressure-Driven Mobilization. *Chromatographia,* 39, 543-548.

HUEBNER, A., BRATTON, D., WHYTE, G., YANG, M., DEMELLO, A. J., ABELL, C. & HOLLFELDER, F. 2009. Static microdroplet arrays: a microfluidic device for droplet trapping, incubation and release for enzymatic and cell-based assays. *Lab on a Chip,* 9, 692-698.

JAMES, D., OAG, B., RUSHWORTH, C. M., LEE, J. W. L., DAVIES, J., CABRAL, J. T. & VALLANCE, C. 2012. High-sensitivity online detection for microfluidics via cavity ringdown spectroscopy. *Rsc Advances,* 2, 5376-5384.

JENA, R. K., YUE, C. Y. & LAM, Y. C. 2012. Micro fabrication of cyclic olefin copolymer (COC) based microfluidic devices. *Microsystem Technologies-Micro-and Nanosystems-Information Storage and Processing Systems,* 18, 159-166.

JEZIERSKI, S., BELDER, D. & NAGL, S. 2013. Microfluidic free-flow electrophoresis chips with an integrated fluorescent sensor layer for real time pH imaging in isoelectric focusing. *Chemical Communications,* 49, 904-906.

JO, B. H., VAN LERBERGHE, L. M., MOTSEGOOD, K. M. & BEEBE, D. J. 2000. Three-dimensional micro-channel fabrication in polydimethylsiloxane (PDMS) elastomer. *Journal of Microelectromechanical Systems,* 9, 76-81.

JONES, T. B. 2001. Liquid dielectrophoresis on the microscale. *Journal of Electrostatics,* 51, 290-299.

JONES, T. B., GUNJI, M., WASHIZU, M. & FELDMAN, M. J. 2001. Dielectrophoretic liquid actuation and nanodroplet formation. *Journal of Applied Physics,* 89, 1441-1448.

JUNG, J. Y. & KWAK, H. Y. 2007. Separation of microparticles and biological cells inside an evaporating droplet using dielectrophoresis. *Analytical Chemistry,* 79, 5087-5092.

KIM, D. S., LEE, S. H., KWON, T. H. & AHN, C. H. 2005. A serpentine laminating micromixer combining splitting/recombination and advection. *Lab on a Chip,* 5, 739-747.

KIRBY, B. J. & HASSELBRINK, E. F. 2004. Zeta potential of microfluidic substrates: 1. Theory, experimental techniques, and effects on separations. *Electrophoresis,* 25, 187-202.

KLANK, H., KUTTER, J. P. & GESCHKE, O. 2002. CO2-laser micromachining and back-end processing for rapid production of PMMA-based microfluidic systems. *Lab on a Chip,* 2, 242-246.

KOHLHEYER, D., BESSELINK, G. A., SCHLAUTMANN, S. & SCHASFOORT, R. B. 2006. Free-flow zone electrophoresis and isoelectric focusing using a microfabricated glass device with ion permeable membranes. *Lab on a chip,* 6, 374-80.

KOHLHEYER, D., EIJKEL, J. C. T., SCHLAUTMANN, S., VAN DEN BERG, A. & SCHASFOORT, R. B. M. 2007. Microfluidic high-resolution free-flow isoelectric focusing. *Analytical Chemistry,* 79, 8190-8198.

KOLIN, A. 1955. ISOELECTRIC SPECTRA AND MOBILITY SPECTRA: A NEW APPROACH TO ELECTROPHORETIC SEPARATION. *Proceedings of the National Academy of Sciences,* 41, 101-110.

LEE, C. Y., CHANG, C. L., WANG, Y. N. & FU, L. M. 2011. Microfluidic Mixing: A Review. *International Journal of Molecular Sciences,* 12, 3263-3287.

LEE, G. B., CHEN, S. H., HUANG, G. R., SUNG, W. C. & LIN, Y. H. 2001. Microfabricated plastic chips by hot embossing methods and their applications for DNA separation and detection. *Sensors and Actuators B-Chemical,* 75, 142-148.

LEE, J., MOON, H., FOWLER, J., SCHOELLHAMMER, T. & KIM, C. J. 2002. Electrowetting and electrowetting-on-dielectric for microscale liquid handling. *Sensors and Actuators a-Physical,* 95, 259-268.

LEE, J. H., PETERSON, E. T. K., DAGANI, G. & PAPAUTSKY, I. 2005. Rapid prototyping of plastic microfluidic devices in cyclic olefin copolymer (COC). *Microfluidics, BioMEMS, and Medical Microsystems III,* 5718, 82-91.

LEE, M. J., LEE, N. Y., LIM, J. R., KIM, J. B., KIM, M., BAIK, H. K. & KIM, Y. S. 2006a. Antiadhesion surface treatments of molds for high-resolution unconventional lithography. *Advanced Materials,* 18, 3115-+.

LEE, S. W., KIM, D. S., LEE, S. S. & KWON, T. H. 2006b. A split and recombination micromixer fabricated in a PDMS three-dimensional structure. *Journal of Micromechanics and Microengineering,* 16, 1067-1072.

LEECH, P. W. 2009. Hot Embossing of Microchannels in Cyclic Olefin Copolymer. *Materials and Strategies for Lab-on-a-Chip - Biological Analysis, Cell-Material Interfaces and Fluidic Assembly of Nanostructures,* 1191, 17-22.

LI, L., DU, W. B. & ISMAGILOV, R. F. 2010a. Multiparameter Screening on SlipChip Used for Nanoliter Protein Crystallization Combining Free Interface Diffusion and Microbatch Methods. *Journal of the American Chemical Society,* 132, 112-119.

LI, L., DU, W. B. & ISMAGILOV, R. F. 2010b. User-Loaded SlipChip for Equipment-Free Multiplexed Nanoliter-Scale Experiments. *Journal of the American Chemical Society,* 132, 106-111.

LI, L. A., KARYMOV, M. A., NICHOLS, K. P. & ISMAGILOV, R. F. 2010c. Dead-End Filling of SlipChip Evaluated Theoretically and Experimentally as a Function of the Surface Chemistry and the Gap Size between the Plates for Lubricated and Dry SlipChips. *Langmuir : the ACS journal of surfaces and colloids,* 26, 12465-12471.

LI, R. K., LOOCK, H. P. & OLESCHUK, R. D. 2006. Capillary electrophoresis absorption detection using fiber-loop ring-down spectroscopy. *Analytical Chemistry,* 78, 5685-5692.

LIN, C. H., CHAO, C. H. & LAN, C. W. 2007. Low azeotropic solvent for bonding of PMMA microfluidic devices. *Sensors and Actuators B-Chemical,* 121, 698-705.

LIN, C. H., LEE, G. B., CHANG, B. W. & CHANG, G. L. 2002. A new fabrication process for ultra-thick microfluidic microstructures utilizing SU-8 photoresist. *Journal of Micromechanics and Microengineering,* 12, 590-597.

LIU, W. S., CHEN, D. L., DU, W. B., NICHOLS, K. P. & ISMAGILOV, R. F. 2010. Slip Chip for Immunoassays in Nanoliter Volumes. *Analytical Chemistry,* 82, 3276-3282.

LIU, Z. & PAWLISZYN, J. 2003. Capillary isoelectric focusing of proteins with liquid core waveguide laser-induced fluorescence whole column imaging detection. *Analytical Chemistry,* 75, 4887-4894.

LORENZ, R. M., EDGAR, J. S., JEFFRIES, G. D. M. & CHIU, D. T. 2006. Microfluidic and optical systems for the on-demand generation and manipulation of single femtoliter-volume aqueous droplets. *Analytical Chemistry,* 78, 6433-6439.

MACK, S., CRUZADO-PARK, I., CHAPMAN, J., RATNAYAKE, C. & VIGH, G. 2009. A systematic study in CIEF: Defining and optimizing experimental parameters critical to method reproducibility and robustness. *Electrophoresis,* 30, 4049-4058.

MANZ, A., EFFENHAUSER, C. S., BURGGRAF, N., HARRISON, D. J., SEILER, K. & FLURI, K. 1994. Electroosmotic Pumping and Electrophoretic Separations for Miniaturized Chemical-Analysis Systems. *Journal of Micromechanics and Microengineering,* 4, 257-265.

MAZUTIS, L., BARET, J. C. & GRIFFITHS, A. D. 2009. A fast and efficient microfluidic system for highly selective one-to-one droplet fusion. *Lab on a Chip,* 9, 2665-2672.

MAZUTIS, L., GILBERT, J., UNG, W. L., WEITZ, D. A., GRIFFITHS, A. D. & HEYMAN, J. A. 2013. Single-cell analysis and sorting using droplet-based microfluidics. *Nature Protocols,* 8, 870-891.

MCDONALD, J. C., DUFFY, D. C., ANDERSON, J. R., CHIU, D. T., WU, H. K., SCHUELLER, O. J. A. & WHITESIDES, G. M. 2000. Fabrication of microfluidic systems in poly(dimethylsiloxane). *Electrophoresis,* 21, 27-40.

MELLORS, J. S., BLACK, W. A., CHAMBERS, A. G., STARKEY, J. A., LACHER, N. A. & RAMSEY, J. M. 2013. Hybrid Capillary/Microfluidic System for Comprehensive Online Liquid Chromatography-Capillary Electrophoresis-Electrospray Ionization-Mass Spectrometry. *Analytical Chemistry,* 85, 4100-4106.

MIWA, M., NAKAJIMA, A., FUJISHIMA, A., HASHIMOTO, K. & WATANABE, T. 2000. Effects of the surface roughness on sliding angles of water droplets on superhydrophobic surfaces. *Langmuir,* 16, 5754-5760.

MOORCROFT, M. J., DAVIS, J. & COMPTON, R. G. 2001. Detection and determination of nitrate and nitrite: a review. *Talanta,* 54, 785-803.

MOSHER, R. A. & THORMANN, W. 1990. Experimental and Theoretical Dynamics of Isoelectric-Focusing .4. Cathodic, Anodic and Symmetrical Drifts of the Ph Gradient. *Electrophoresis,* 11, 717-723.

MOSHER, R. A., THORMANN, W. & BIER, M. 1988. Experimental and Theoretical Dynamics of Isoelectric-Focusing .2. Elucidation of the Impact of the Electrode Assembly. *Journal of Chromatography,* 436, 191-204.

NEIL, S. R. T., RUSHWORTH, C. M., VALLANCE, C. & MACKENZIE, S. R. 2011. Broadband cavity-enhanced absorption spectroscopy for real time, in situ spectral analysis of microfluidic droplets. *Lab on a Chip,* 11, 3953-3955.

NELSON, W. C. & KIM, C. J. 2012. Droplet Actuation by Electrowetting-on-Dielectric (EWOD): A Review. *Journal of Adhesion Science and Technology,* 26, 1747-1771.

NGUYEN, N. T. & WU, Z. G. 2005. Micromixers - a review. *Journal of Micromechanics and Microengineering,* 15, R1-R16.

NISISAKO, T., OKUSHIMA, S. & TORII, T. 2005. Controlled formulation of monodisperse double emulsions in a multiple-phase microfluidic system. *Soft Matter,* 1, 23-27.

NISISAKO, T., TORII, T. & HIGUCHI, T. 2002. Droplet formation in a microchannel network. *Lab on a Chip,* 2, 24-26.

NIU, X., PEREIRA, F., EDEL, J. B. & DE MELLO, A. J. 2013. Droplet-interfaced microchip and capillary electrophoretic separations. *Anal Chem,* 85, 8654-60.

NIU, X., ZHANG, M., PENG, S., WEN, W. & SHENG, P. 2007. Real-time detection, control, and sorting of microfluidic droplets. *Biomicrofluidics,* 1, 44101.

NIU, X. Z. & DEMELLO, A. J. 2012. Building droplet-based microfluidic systems for biological analysis. *Biochemical Society Transactions,* 40, 615-623.

NIU, X. Z., GIELEN, F., EDEL, J. B. & DEMELLO, A. J. 2011. A microdroplet dilutor for high-throughput screening. *Nature Chemistry,* 3, 437-442.

NIU, X. Z., ZHANG, B., MARSZALEK, R. T., CES, O., EDEL, J. B., KLUG, D. R. & DEMELLO, A. J. 2009. Droplet-based compartmentalization of chemically separated components in two-dimensional separations. *Chemical Communications,* 6159-6161.

OGILVIE, I. R. G., SIEBEN, V. J., FLOQUET, C. F. A., ZMIJAN, R., MOWLEM, M. C. & MORGAN, H. 2010. Reduction of surface roughness for optical quality microfluidic devices in PMMA and COC. *Journal of Micromechanics and Microengineering,* 20.

OKEEFE, A. & DEACON, D. A. G. 1988. Cavity Ring-down Optical Spectrometer for Absorption-Measurements Using Pulsed Laser Sources. *Review of Scientific Instruments,* 59, 2544-2551.

OKUSHIMA, S., NISISAKO, T., TORII, T. & HIGUCHI, T. 2004. Controlled production of monodisperse double emulsions by two-step droplet breakup in microfluidic devices. *Langmuir,* 20, 9905-9908.

PAGER, C., VARGOVA, A., TAKACSI-NAGY, A., DORNYEI, A. & KILAR, F. 2012. Effect of electrolyte pH on CIEF with narrow pH range ampholytes. *Electrophoresis,* 33, 3269-3275.

PARK, S. Y., WU, T. H., CHEN, Y., TEITELL, M. A. & CHIOU, P. Y. 2011. High-speed droplet generation on demand driven by pulse laser-induced cavitation. *Lab on a Chip,* 11, 1010-1012.

PEI, J. A., NIE, J. & KENNEDY, R. T. 2010. Parallel Electrophoretic Analysis of Segmented Samples On Chip for High-Throughput Determination of Enzyme Activities. *Analytical Chemistry,* 82, 9261-9267.

PEREIRA, F., NIU, X. & DEMELLO, A. J. 2013. A Nano LC-MALDI Mass Spectrometry Droplet Interface for the Analysis of Complex Protein Samples. *PLoS One,* 8, e63087.

POLLACK, M. G., FAIR, R. B. & SHENDEROV, A. D. 2000. Electrowetting-based actuation of liquid droplets for microfluidic applications. *Applied Physics Letters,* 77, 1725-1726.

QIN, D., XIA, Y. N. & WHITESIDES, G. M. 1996. Rapid prototyping of complex structures with feature sizes larger than 20 mu m. *Advanced Materials,* 8, 917-&.

RABILLOUD, T., CHEVALLET, M., LUCHE, S. & LELONG, C. 2010. Two-dimensional gel electrophoresis in proteomics: Past, present and future. *Journal of Proteomics,* 73, 2064-2077.

RAMSAY, L. M., DICKERSON, J. A. & DOVICHI, N. J. 2009. Attomole protein analysis by CIEF with LIF detection. *Electrophoresis,* 30, 297-302.

RENART, J., REISER, J. & STARK, G. R. 1979. Transfer of Proteins from Gels to Diazobenzyloxymethyl-Paper and Detection with Antisera - Method for Studying Antibody Specificity and Antigen Structure. *Proceedings of the National Academy of Sciences of the United States of America,* 76, 3116-3120.

REVELL, P. J. & GOLDSPINK, G. F. 1984. A Review of Reactive Ion-Beam Etching for Production. *Vacuum,* 34, 455-462.

RIGHETTI, P. G., CITTERIO, A. & GIRAULT, H. 2007a. Gel-free IEF in a membrane-sealed multicompartment cell for proteome prefractionation. *Electrophoresis,* 28, 1860-1866.

RIGHETTI, P. G., SEBASTIANO, R. & CITTERIO, A. 2013. Capillary electrophoresis and isoelectric focusing in peptide and protein analysis. *Proteomics,* 13, 325-340.

RIGHETTI, P. G., SIMO, C., SEBASTIANO, R. & CITTERIO, A. 2007b. Carrier ampholytes for IEF, on their fortieth anniversary (1967-2007), brought to trial in court: The verdict. *Electrophoresis,* 28, 3799-3810.

ROSSIER, J., REYMOND, F. & MICHEL, P. E. 2002. Polymer microfluidic chips for electrochemical and biochemical analyses. *Electrophoresis,* 23, 858-867.

RUSHWORTH, C. M. 2012. *Analysis of Small Volume Liquid Samples using Cavity Enhanced Absorption Spectroscopies.* Doctor of Philosophy, University of Oxford.

RUSHWORTH, C. M., YOGARAJAH, Y., ZHAO, Y., MORGAN, H. & VALLANCE, C. 2013. Sensitive analysis of trace water analytes using colourimetric cavity ringdown spectroscopy. *Analytical Methods,* 5, 239-247.

SALPLACHTA, J., KUBESOVA, A. & HORKA, M. 2012. Latest improvements in CIEF: From proteins to microorganisms. *Proteomics,* 12, 2927-2936.

SCHNEIDER, T., KREUTZ, J. & CHIU, D. T. 2013. The Potential Impact of Droplet Microfluidics in Biology. *Analytical Chemistry,* 85, 3476-3482.

SEILER, K., HARRISON, D. J. & MANZ, A. 1993. Planar Glass Chips for Capillary Electrophoresis - Repetitive Sample Injection, Quantitation, and Separation Efficiency. *Analytical Chemistry,* 65, 1481-1488.

SHEN, F., DU, W. B., KREUTZ, J. E., FOK, A. & ISMAGILOV, R. F. 2010. Digital PCR on a SlipChip. *Lab on a chip,* 10, 2666-2672.

SHI, W. W., QIN, J. H., YE, N. N. & LIN, B. C. 2008. Droplet-based microfluidic system for individual Caenorhabditis elegans assay. *Lab on a Chip,* 8, 1432-1435.

SHIMURA, K., KAMIYA, K., MATSUMOTO, H. & KASAI, K. 2002. Fluorescence-labeled peptide p1 markers for capillary isoelectric focusing. *Analytical Chemistry,* 74, 1046-1053.

SHIMURA, K., TAKAHASHI, K., KOYAMA, Y., SATO, K. & KITAMORI, T. 2008. Isoelectric focusing in a microfluidically defined electrophoresis channel. *Analytical Chemistry,* 80, 3818-3823.

SHIMURA, K., WANG, Z., MATSUMOTO, H. & KASAI, K. 2000. Synthetic oligopeptides as isoelectric point markers for capillary isoelectric focusing with ultraviolet absorption detection. *Electrophoresis,* 21, 603-610.

SIEBEN, V. J., FLOQUET, C. F. A., OGILVIE, I. R. G., MOWLEM, M. C. & MORGAN, H. 2010. Microfluidic colourimetric chemical analysis system: Application to nitrite detection. *Analytical Methods,* 2, 484-491.

SILVERTAND, L. H., TORANO, J. S., DE JONG, G. J. & VAN BENNEKOM, W. P. 2009. Development and characterization of cIEF-MALDI-TOF MS for protein analysis. *Electrophoresis,* 30, 1828-35.

SNYDER, K. L. & ZARE, R. N. 2003. Cavity ring-down spectroscopy as a detector for liquid chromatography. *Analytical Chemistry,* 75, 3086-3091.

SOBROVA, P., RYVOLOVA, M., ADAM, V. & KIZEK, R. 2012. Capillary electromigration based techniques in diagnostics of prion protein caused diseases. *Electrophoresis,* 33, 3644-3652.

SOLVAS, X. C. I. & DEMELLO, A. 2011. Droplet microfluidics: recent developments and future applications. *Chemical Communications,* 47, 1936-1942.

SQUIRES, T. M. & QUAKE, S. R. 2005. Microfluidics: Fluid physics at the nanoliter scale. *Reviews of Modern Physics,* 77, 977-1026.

STEIGERT, J., HAEBERLE, S., BRENNER, T., MULLER, C., STEINERT, C. P., KOLTAY, P., GOTTSCHLICH, N., REINECKE, H., RUHE, J., ZENGERLE, R. & DUCREE, J. 2007. Rapid prototyping of microfluidic chips in COC. *Journal of Micromechanics and Microengineering,* 17, 333-341.

STONE, H. A., STROOCK, A. D. & AJDARI, A. 2004. Engineering flows in small devices: Microfluidics toward a lab-on-a-chip. *Annual Review of Fluid Mechanics,* 36, 381-411.

STROOCK, A. D., DERTINGER, S. K. W., AJDARI, A., MEZIC, I., STONE, H. A. & WHITESIDES, G. M. 2002. Chaotic mixer for microchannels. *Science,* 295, 647-651.

STROOCK, A. D., WECK, M., CHIU, D. T., HUCK, W. T. S., KENIS, P. J. A., ISMAGILOV, R. F. & WHITESIDES, G. M. 2000. Patterning electro-osmotic flow with patterned surface charge. *Physical Review Letters,* 84, 3314-3317.

SUN, T. & MORGAN, H. 2010. Single-cell microfluidic impedance cytometry: a review. *Microfluidics and Nanofluidics,* 8, 423-443.

SUN, Y. & KWOK, Y. C. 2006. Polymeric microfluidic system for DNA analysis. *Anal Chim Acta,* 556, 80-96.

TAKEUCHI, S., GARSTECKI, P., WEIBEL, D. B. & WHITESIDES, G. M. 2005. An axisymmetric flow-focusing microfluidic device. *Advanced Materials,* 17, 1067-+.

TAN, W., FAN, Z. H., QIU, C. X., RICCO, A. J. & GIBBONS, I. 2002. Miniaturized capillary isoelectric focusing in plastic microfluidic devices. *Electrophoresis,* 23, 3638-3645.

TAN, Y. C., FISHER, J. S., LEE, A. I., CRISTINI, V. & LEE, A. P. 2004. Design of microfluidic channel geometries for the control of droplet volume, chemical concentration, and sorting. *Lab on a Chip,* 4, 292-298.

TANDON, V., BHAGAVATULA, S. K., NELSON, W. C. & KIRBY, B. J. 2008. zeta potential and electroosmotic mobility in microfluidic devices fabricated from hydrophobic polymers: 1. The origins of charge. *Electrophoresis,* 29, 1092-1101.

TEH, S. Y., LIN, R., HUNG, L. H. & LEE, A. P. 2008. Droplet microfluidics. *Lab on a chip,* 8, 198-220.

TERRAY, A., OAKEY, J. & MARR, D. W. M. 2002. Microfluidic control using colloidal devices. *Science,* 296, 1841-1844.

THEBERGE, A. B., COURTOIS, F., SCHAERLI, Y., FISCHLECHNER, M., ABELL, C., HOLLFELDER, F. & HUCK, W. T. S. 2010. Microdroplets in Microfluidics: An Evolving Platform for Discoveries in Chemistry and Biology. *Angewandte Chemie-International Edition,* 49, 5846-5868.

THORSEN, T., MAERKL, S. J. & QUAKE, S. R. 2002. Microfluidic large-scale integration. *Science,* 298, 580-584.

THORSEN, T., ROBERTS, R. W., ARNOLD, F. H. & QUAKE, S. R. 2001. Dynamic pattern formation in a vesicle-generating microfluidic device. *Physical Review Letters,* 86, 4163-4166.

TONG, Z. G., WRIGHT, A., MCCORMICK, T., LI, R. K., OLESCHUK, R. D. & LOOCK, H. P. 2004. Phase-shift fiber-loop ring-down spectroscopy. *Analytical Chemistry,* 76, 6594-6599.

TOWBIN, H., STAEHELIN, T. & GORDON, J. 1979. Electrophoretic Transfer of Proteins from Polyacrylamide Gels to Nitrocellulose Sheets - Procedure and Some Applications. *Proceedings of the National Academy of Sciences of the United States of America,* 76, 4350-4354.

TSALOGLOU, M. N., WATSON, R. J., RUSHWORTH, C. M., ZHAO, Y., NIU, X., SUTTON, J. M. & MORGAN, H. 2015. Real-time microfluidic recombinase polymerase

amplification for the toxin B gene of Clostridium difficile on a SlipChip platform. *Analyst,* 140, 258-264.

TSAO, C. W. & DEVOE, D. L. 2009. Bonding of thermoplastic polymer microfluidics. *Microfluidics and Nanofluidics,* 6, 1-16.

TSAO, C. W., HROMADA, L., LIU, J., KUMAR, P. & DEVOE, D. L. 2007. Low temperature bonding of PMMA and COC microfluidic substrates using UV/ozone surface treatment. *Lab on a Chip,* 7, 499-505.

UNGER, M. A., CHOU, H. P., THORSEN, T., SCHERER, A. & QUAKE, S. R. 2000. Monolithic microfabricated valves and pumps by multilayer soft lithography. *Science,* 288, 113-116.

UTADA, A. S., LORENCEAU, E., LINK, D. R., KAPLAN, P. D., STONE, H. A. & WEITZ, D. A. 2005. Monodisperse double emulsions generated from a microcapillary device. *Science,* 308, 537-541.

VERPOORTE, E., MANZ, A., LUDI, H., BRUNO, A. E., MAYSTRE, F., KRATTIGER, B., WIDMER, H. M., VANDERSCHOOT, B. H. & DEROOIJ, N. F. 1992. A Silicon Flow Cell for Optical-Detection in Miniaturized Total Chemical-Analysis Systems. *Sensors and Actuators B-Chemical,* 6, 66-70.

VERTESSY, B. G., PEREIRA, F., NIU, X. & DEMELLO, A. J. 2013. A Nano LC-MALDI Mass Spectrometry Droplet Interface for the Analysis of Complex Protein Samples. *Plos One,* 8, e63087.

WAECHTER, H., MUNZKE, D., JANG, A. & LOOCK, H. P. 2011. Simultaneous and Continuous Multiple Wavelength Absorption Spectroscopy on Nanoliter Volumes Based on Frequency-Division Multiplexing Fiber-Loop Cavity Ring-Down Spectroscopy. *Analytical Chemistry,* 83, 2719-2725.

WANG, H. & HANASH, S. 2003. Multi-dimensional liquid phase based separations in proteomics. *Journal of Chromatography B-Analytical Technologies in the Biomedical and Life Sciences,* 787, 11-18.

WANG, T. S., AIKEN, J. H., HUIE, C. W. & HARTWICK, R. A. 1991. Nanoliter-Scale Multireflection Cell for Absorption Detection in Capillary Electrophoresis. *Analytical Chemistry,* 63, 1372-1376.

WANG, W., LU, J. J., GU, C., ZHOU, L. & LIU, S. 2013. Performing isoelectric focusing and simultaneous fractionation of proteins on a rotary valve followed by sodium dodecyl-polyacrylamide gel electrophoresis. *Anal Chem,* 85, 6603-7.

WEHKING, J. D., GABANY, M., CHEW, L. & KUMAR, R. 2014. Effects of viscosity, interfacial tension, and flow geometry on droplet formation in a microfluidic T-junction. *Microfluidics and Nanofluidics,* 16, 441-453.

WEISS, N. G., HAYES, M. A., GARCIA, A. A. & ANSARI, R. R. 2011. Isoelectric focusing in a drop. *Langmuir : the ACS journal of surfaces and colloids,* 27, 494-8.

WEISS, N. G., ZWICK, N. L. & HAYES, M. A. 2010. Capillary isoelectric focusing coupled offline to matrix assisted laser desorption/ionization mass spectrometry. *Journal of chromatography. A,* 1217, 179-82.

WEN, J., WILKER, E. W., YAFFE, M. B. & JENSEN, K. F. 2010a. Microfluidic Preparative Free-Flow Isoelectric Focusing: System Optimization for Protein Complex Separation. *Analytical Chemistry,* 82, 1253-1260.

WEN, J. A., ALBRECHT, J. W. & JENSEN, K. F. 2010b. Microfluidic preparative free-flow isoelectric focusing in a triangular channel: System development and characterization. *Electrophoresis,* 31, 1606-1614.

WHEELER, M. D., NEWMAN, S. M., ORR-EWING, A. J. & ASHFOLD, M. N. R. 1998. Cavity ring-down spectroscopy. *Journal of the Chemical Society-Faraday Transactions,* 94, 337-351.

WHITESIDES, G. M. 2006. The origins and the future of microfluidics. *Nature,* 442, 368-373.

XIE, J., MIAO, Y. N., SHIH, J., TAI, Y. C. & LEE, T. D. 2005. Microfluidic platform for liquid chromatography-tandem mass spectrometry analyses of complex peptide mixtures. *Analytical Chemistry,* 77, 6947-6953.

XU, J. H., LI, S. W., TAN, J., WANG, Y. J. & LUO, G. S. 2006. Preparation of highly monodisperse droplet in a T-junction microfluidic device. *Aiche Journal,* 52, 3005-3010.

XU, L. F., LEE, H., PANCHAPAKESAN, R. & OH, K. W. 2012. Fusion and sorting of two parallel trains of droplets using a railroad-like channel network and guiding tracks. *Lab on a Chip,* 12, 3936-3942.

XU, S., NIE, Z., SEO, M., LEWIS, P., KUMACHEVA, E., STONE, H. A., GARSTECKI, P., WEIBEL, D. B., GITLIN, I. & WHITESIDES, G. M. 2005. Generation of monodisperse particles by using microfluidics: Control over size, shape, and composition (vol 44, pg 724, 2005). *Angewandte Chemie-International Edition,* 44, 3799-3799.

XU, Z. Q., OKABE, N., ARAI, A. & HIROKAWA, T. 2010. Investigation of the pH gradient formation and cathodic drift in microchip isoelectric focusing with imaged UV detection. *Electrophoresis,* 31, 3558-3565.

YOBAS, L., MARTENS, S., ONG, W. L. & RANGANATHAN, N. 2006. High-performance flow-focusing geometry for spontaneous generation of monodispersed droplets. *Lab on a Chip,* 6, 1073-1079.

YU, W. J., LI, Y., DENG, C. H. & ZHANG, X. M. 2006. Comprehensive two-dimensional separation in coupling of reversed-phase chromatography with capillary isoelectric focusing followed by MALDI-MS identification using on-target digestion for intact protein analysis. *Electrophoresis,* 27, 2100-2110.

ZENG, J. & KORSMEYER, T. 2004. Principles of droplet electrohydrodynamics for lab-on-a-chip. *Lab on a Chip,* 4, 265-277.

ZHONG, Q., BHATTACHARYA, S., KOTSOPOULOS, S., OLSON, J., TALY, V., GRIFFITHS, A. D., LINK, D. R. & LARSON, J. W. 2011a. Multiplex digital PCR: breaking the one target per color barrier of quantitative PCR. *Lab on a Chip,* 11, 2167-2174.

ZHONG, X. F., MAXWELL, E. J., RATNAYAKE, C., MACK, S. & CHEN, D. D. Y. 2011b. Flow-Through Microvial Facilitating Interface of Capillary Isoelectric Focusing and Electrospray Ionization Mass Spectrometry. *Analytical Chemistry,* 83, 8748-8755.

ZHU, X. L., LIU, G., GUO, Y. H. & TIAN, Y. C. 2007. Study of PMMA thermal bonding. *Microsystem Technologies-Micro-and Nanosystems-Information Storage and Processing Systems,* 13, 403-407.

ZHU, Y. & FANG, Q. 2013. Analytical detection techniques for droplet microfluidics-A review. *Analytica Chimica Acta,* 787, 24-35.